Managing Groundwater for Environmental Stream Temperature

By

CHRISTINA RENE BUCK
B.S. (University of California, Davis) 2007
M.S. (University of California, Davis) 2009

DISSERTATION

Submitted in partial satisfaction of the requirements for the degree of

DOCTOR OF PHILOSOPHY

in

Hydrologic Sciences

in the

OFFICE OF GRADUATE STUDIES

of the

UNIVERSITY OF CALIFORNIA

DAVIS

Approved:

_____

Dr. Jay R. Lund, Chair

_____

Dr. Thomas Harter

_____

Dr. Graham E. Fogg

Committee in Charge

2013

Abstract

This research explores the benefits of conjunctively managed surface and groundwater resources in a volcanic aquifer system to reduce stream temperatures while valuing agricultural deliveries. The example problem involves advancing the understanding of flows, stream temperature, and groundwater dynamics in the Shasta Valley of Northern California. Three levels of interaction are explored from field data, to regional simulation, to regional management optimization. Stream temperature processes are explored using Distributed Temperature Sensing (DTS) data from the Shasta River and recalibrating an existing physically-based heat balance flow and temperature model of the Shasta River. DTS technology can collect abundant high resolution river temperature data over space and time to improve development and performance of modeled river temperatures. These data also identify and quantify thermal variability of micro-habitat that temperature modeling and standard temperature sampling do not capture. This helps bracket uncertainty of daily temperature variation in reaches, pools, side channels, and from cool or warm surface or subsurface inflows. The application highlights the influence of air temperature on stream temperatures, and indicates that physically-based numerical temperature models, using a heat balance approach as opposed to statistical models, may under-represent this important stream temperature driver. The utility of DTS to improve model performance and detailed evaluation of hydrologic processes is demonstrated.

Second, development and calibration of a numerical groundwater model of the Pluto's Cave basalt aquifer and Parks Creek valley area in the eastern portion of Shasta Valley helps quantify and organize the current conceptual model of this Cascade fracture flow dominated aquifer. Model development provides insight on system dynamics, helps identify important and influential components of the system, and highlights additional data needs. The objective of this model development is to reasonably represent regional groundwater flow and to explore the interaction between Mount Shasta recharge, pumping, and Big Springs flow. The model organizes and incorporates available data from a wide variety of sources and presents approaches to quantify the major flow paths and fluxes. Major water balance components are estimated for 2008-2011. Sensitivity analysis assesses the degree to which uncertainty in boundary flow affects model results, particularly spring flow.

Finally, this work uses optimization to explore coordinated hourly surface and groundwater operations to benefit Shasta River stream temperatures upstream of its confluence with Parks Creek. The management strategy coordinates reservoir releases and diversions to irrigated pasture adjacent to the river and it supplements river flows with pumped cool groundwater from a nearby well. A basic problem formulation is presented with results, sensitivity analysis, and insights. The problem is also formulated for the Shasta River application. Optimized results for a week in July suggest daily maximum and minimum stream temperatures can be reduced with strategic operation of the water supply portfolio. These temperature benefits nevertheless have significant costs from reduced irrigation diversions. Increased irrigation efficiency would reduce warm tail water discharges to the river instead of reducing diversions. With increased efficiency, diversions increase and shortage costs decrease. Tradeoffs and sensitivity of model inputs are explored and results discussed.

Acknowledgements

Special thanks to The Nature Conservancy for funding and supporting this research and to Dr. Maurice Hall, Chris Babcock, and others who facilitated field work and data gathering.

I am full of gratitude for my major professor, Dr. Jay Lund, and his part in making graduate school wonderful, challenging, and growth-filled years. Your guidance, enthusiasm, insightful problem solving, willingness to always be available to your students, and ability to lead a research group of varied interests and projects makes you a truly exceptional advisor. Special thanks also to Dr. Thomas Harter for helping get the Shasta Valley groundwater modeling from concept to reality and problem solving along the way. I've learned a tremendous amount from our conversations. Thanks to Dr. Graham Fogg for your thoughtful review and input that improved this work. Also to the other members of my qualifying exam committee, Dr. Jeffrey Mount and Dr. Timothy Ginn, thank you for your input and guidance in the early stages and encouragement to get this thing done.

This dissertation builds on the field work, data collection and expertise of a number of people for whom I'm grateful for the many conversations, email responses, and in some cases tromping around in the field: Carson Jeffres, Drew Nichols, Dr. Christine Hatch and Dr. Scott Tyler with CTEMPS, Jeff Davids, Dr. Mike Deas, Dave Webb and others. And special thanks to Dr. Sarah Null for your guidance and valuable contributions. To Dr. Josue Medellin-Azuara for your abundant willingness to give a hand and contribute your skills and expertise. To you and the many others I shared the office with and those who dropped by for a chat (Heidi, Gugu, Matt, Kaveh, Eric, Marcelo, Rachel, Will, Eleanor, Nate, Sachi), what good times and some long hours we shared.

A number of wonderful communities of friends have provided love and support throughout this journey. First thanks to my lovely Davis UCC friends who shared life together: Kristen and Lewis Waha, Jen and Carlos Canales, Nidhi and Deepak Lal, Kevin Lee, and the Threshold crew. And to Tierrasanta life group in San Diego who welcomed me with open arms, I love you and thank you for walking with me as I worked on this from afar. A special shout out to my girls: Laura Scott, Abby Nguyen, Lisa Di Fiore, Autumn Ross, and Kat Prus and to Jennifer Johnson and Kristen Secora, you were my cheerleaders through the ups and downs. For your dear friendships I am so grateful, and look forward to visiting you in sunny SD! Thanks for spurring me on. In the final months, thanks to our Chico group that listened and encouraged to the very end. I'm excited to say yes more and live life with you! And lest I forget two of my best friends, Amy Eleazarian and Nicole Baroldy who have walked with me through this from the beginning. You're awesome!

For all the couches I crashed on and their owners' hospitality as I traveled monthly to Davis from San Diego for almost two years, thank you!! Jenna Christophersen, Kathy Keilman and Andrea Hanson, Wahas, Mockfords, Lals, Canales…thanks for a warm and friendly place to stay, a home away from home. I couldn't have done it without you.

To the Buck family, I love you and am so blessed to be part of your family. To my brother, Stephen, and your sweet family, thanks for making me stronger and for having two of the cutest boys around. To my dear parents, Joe and Rene Connell, thank you for your abundant love and support, listening ear and for equipping me to take on life's greatest joys and challenges, including this PhD work. You each inspire me to work hard and love well. And most of all, to the most loving, patient, and amazing hubby, Steve, thank you for loving me well through the ups and downs and for helping me not take life too seriously and making me laugh often. I'm so thankful to have you to do life with.

And to my Lord and God, to you be the glory. The joy and peace in my life is from you.

Table of Contents

Abstract ii
Acknowledgements iii
Table of Figures vi
Table of Tables ix
Chapter 1: Introduction 1
The Shasta River and Pluto's Cave basalt aquifer 2
Outline of chapters 3
References 4
Chapter 2: Modeling Insights from Distributed Temperature Sensing Data- Shasta River 6
Abstract 6
Introduction 6
Site description 7
Methods 11
Measurements 11
Stream temperature model 12
Calibration 12
Results and discussion 13
Calibration process 13
Calibration results 15
Measured temperature results 16
Daily thermal variability 19
Longitudinal rate of heating 21
Limitations 23
Conclusions 23
Acknowledgements 24
References 24
Chapter 3: Understanding Shasta Valley Groundwater through Numerical Simulation Modeling 27
Abstract 27
Background 27
Cascade hydrogeology 27
Study area hydrogeology 29
Surface water and groundwater sources 31
Existing water budget 32
Conceptual model 32
Modeling approaches 32
Data sources 33
Model description 34
Lake Shastina – constant head 35

Parks Creek and Shasta River – river boundary 36
Mount Shasta recharge – constant flux boundary 37
No flow boundaries 41
General head boundaries 42
Model properties and components 44
Spring flow representation- drain package 44
Groundwater pumping 47
Canal leakage 50
Local recharge: applied water and precipitation on the valley floor 52
Model calibration 55
Targets: observed water levels 55
Targets: spring flow 57
Calibration parameters 58
Model scenarios 59
Results 60
Measured v. modeled heads and fluxes 62
Model water budget 66
Sensitivity analysis 67
Discussion 69
Assessment of data needs 72
Limitations 73
Conclusions 73
References 75
Chapter 4: Conjunctive operation of groundwater pumping, surface water diversions, and Lake Shastina releases for stream temperature 79
Abstract 79
Introduction 79
Basic problem formulation 80
Objective function 80
Estimating stream temperature change (ΔT_t) 81
Constraints 82
Sensitivity analysis 83
Results and insights from the basic problem 86
Case study- Shasta River application 89
Current operations 90
Problem formulation 92
Objective function and inputs 93
Estimating temperature change for the Shasta River 94
Constraints 97

Solver 98
Results 98
Current operations 98
Optimization results 99
Sensitivity analysis 101
Discussion 102
Conclusions 103
References 104
Chapter 5: Conclusions 106
Methodological conclusions 106
Case study conclusions 107
Appendix A 108
Additional recharge estimated 108
Northern boundary revisited 109
Eastern boundary revisited 110
Additional modeling, initial calibration, and results 110
References 113

Table of Figures

Figure 1. Study area- Shasta River watershed 2
Figure 2. Shasta River watershed 8
Figure 3. Shasta River mean daily discharge (m^3s^{-1}) at USGS 11517500 gauge near Yreka 9
Figure 4. a) Shasta River DTS study area b) descriptions of river kilometer locations (RMS is River Modeling System) 11
Figure 5. Modeled and measured river temperature for node 4 with modeled temperature largely overlapping measured temperature except at the peaks and the troughs 15
Figure 6. a) Mean temperature and temperature range at each meter for measured period of record. b) Mean daily temperature indicated by color ramp at meter increments along DTS cable for period of record. 17
Figure 7. Mean weekly maximum and minimum stream temperatures at each location for the hottest and coolest week 18
Figure 8. Daily thermal variability of stream temperature (daily max-min) from DTS measured and modeled results for the week of August 22 19
Figure 9. Measured maximum daily air and water temperature for model period 20
Figure 10. Maximum and minimum modeled and measured temperatures in mixing zone of Parks Creek Overflow and mainstem Shasta River 21
Figure 11. a) Hourly downstream rate of longitudinal heating (node 8 – node 1) with hourly solar radiation. b) Hourly downstream rate of longitudinal heating (node 8 – node1) with hourly air temperature 22
Figure 12. Areal geology of Shasta Valley area, Department of Water Resources (adapted from Ward and Eaves 2008) 28
Figure 13. Shasta Valley geology and major features of interest 30
Figure 14. DWR Geology cross-section A' (adapted from Ward and Eaves 2008) 30
Figure 15. Study area geology and model boundary conditions 35
Figure 16. Average daily Lake Shastina elevation (meters). Breaks indicate missing or questionable data. 36
Figure 17. Mount Shasta recharge zone 37
Figure 18. GAP land cover ecosystems in recharge zone 38
Figure 19. General head boundary with 1954 water level elevation contours from Mack (1960) 43
Figure 20. Hydraulic conductivity (K) zones 44
Figure 21. a) Big Springs complex: Big Springs Lake and alcove springs in Big Springs Creek b) Springs modeled as drains 46
Figure 22. Landuse map within model domain. Green polygons are groundwater irrigated agricultural lands with irrigation district boundaries overlain 47
Figure 23. District irrigation canals in model area overlying soils layer 51
Figure 24. Groundwater head targets for 2008 56
Figure 25. Groundwater level contours (blue) for three model scenarios: HIGH, MODERATE, and LOW. Red cells are 'wells' (injection wells for canals and Mt. Shasta recharge boundary; extraction wells for pumping), Blue is Lake Shastina, Green cells are Parks Creek and Shasta River, Purple cells are where ground surface is below water surface elevation, gray area is no flow (outside active model domain) .. 61
Figure 26. Observed vs. modeled groundwater surface elevation (meters) at targets compared with one-to-one line 65
Figure 27. Percentage of inflow and outflow for major flow paths for each realization. 67
Figure 28. Mass Balance for MODERATE scenario with approximate flows in million cubic meters (MCM) 69
Figure 29. Schematic for basic problem with flows (Q) and temperatures (T) 80
Figure 30. Effect of changing q_{out} on objective value, costs, and temperatures for 24 hour period 83
Figure 31. Sensitivity of alpha on objective function components and average temperature 84
Figure 32. Tradeoff between average temperature and total pumping cost as a function of lift (meters) .. 85
Figure 33. Total diversion (TCM) and daily average temperature tradeoff curve for varied marginal shortage cost ($/TCM) 86
Figure 34. Fractions of source waters for the 24 hour period 87
Figure 35. Hourly flow decisions with specified and calculated temperatures for 24 hour period 88

Figure 36. Effect of T_{cold} on average downstream temperature ($T_{ave,}$ T_{min}) and volume of cold water pumped over 24 hours 89
Figure 37. Overview map with nodes defining optimization model reaches and key inflow and diversion points along the Shasta River 91
Figure 38. Shasta River application schematic with RMS node numbering 93
Figure 39. Stream temperature at node 65 from 2001 RMS model and spreadsheet model using regression, July-August 96
Figure 40. Optimized Shasta River temperature at node 65 compared to Current Operations and Input temperature from Shastina releases 100
Figure 41. Optimized flows for Shastina releases, SLD well releases, and diversions at HIGPMP 101
Figure 42. Tradeoff curve between average temperature and cost (alpha in $/^{o}C) 102
Figure 43. Additional recharge zones (1-4) with labeled estimated recharge volume (MCM) for 2008. . 109
Figure 44. Same K zones as original calibration (Figure 20). New fixed flux boundaries on the northern and eastern boundaries and increased flux from the Mount Shasta Recharge zone (southern boundary, also extended). Figure A shows results with calibrated K values from the MODERATE realization; B results from newly calibrated K values. Purple cells are flooded, i.e. head is above the ground surface elevation. Blue and Red circles are targets, color and size indicative of residual. 111

Table of Tables

Table 1. RQUAL Parameters evaluated during calibration 14
Table 2. Calibration statistics at each node (n = 1201 for all nodes) 16
Table 3. Mack estimate of groundwater discharge from Shasta Valley in Million Cubic Meters (MCM), 1953 water year (Mack 1960, p. 65) 32
Table 4. Data types and sources 34
Table 5. Lake Shastina annual average lake elevation, 2008-2011 36
Table 6. River package inputs 37
Table 7. GAP ecological systems with vegetation within the recharge zone 39
Table 8. Sublimation rates in the literature 40
Table 9. Mount Shasta recharge zone precipitation, estimated ET, sublimation, total upper and lower bound recharge volume and groundwater flow rates (modeled as injection pumping rate, MCM) per model cell on the southeastern constant flux boundary 41
Table 10. Land use codes assigned to model elements (cropland and non-cropland) and associated % ground cover and area 47
Table 11. Inputs to BIS program 49
Table 12. Irrigation method and efficiency 50
Table 13. Conveyance recharge (MCM) 52
Table 14. Shasta Valley ECOWAT inputs 53
Table 15. Annual recharge from precipitation for different amounts of native vegetation (NV) ground cover 54
Table 16. Total recharge summary (from applied water (AW) and precipitation) for cropland, agricultural zones 1-8 (MCM) 55
Table 17. Target groundwater surface elevation (m) 57
Table 18. Parks Creek valley spring flow targets (MCM) 58
Table 19. Parameter ranges for hydraulic conductivity (m/d) for calibration 59
Table 20. Minimum, Maximum and Range of K (m/d) considered for each reach during calibration (See Figure 19 and Figure 20 for reach locations) 62
Table 21. Calibrated K values for river conductance, GHB conductance, and aquifer K zones. NA indicates reaches that are set as no flow boundaries to define the three different scenarios with remaining K values calibrated. (See Figure 19 and Figure 20 for reach locations) 63
Table 22. Calibration statistics and residuals (measured minus modeled water level) (Figure 24) 64
Table 23. Detailed modeled flow results (MCM) for surface water features, general head boundaries (GHB) and spring flows. Note: Positive value is flow into groundwater, Negative value is flow out of groundwater. 66
Table 24. Mass balance of model inflows and outflows (MCM/year) for the three model scenarios: HIGH, MODERATE, and LOW. 67
Table 25. Percent change in flow with a 30% increase in Mount Shasta recharge rate 68
Table 26. Percent change in flow with a 30% increase in agricultural pumping rate 68
Table 27. Percent change in flow with 30% increased local recharge (deep percolation of applied water and precipitation and canal leakage rates) 69
Table 28. Mass balance summary based on estimates for model inputs. Closure term represents net boundary flows and stream-groundwater interaction. 70
Table 29. Given model parameters for basic problem 81
Table 30. Evapotranspiration of Applied Water (ETAW) for July and August as estimated in 2010 (TCM) and irrigation efficiency for the three fields (Davids Engineering 2011a) 92
Table 31. Shasta River model parameters 94
Table 32. Regression coefficients for July-August estimate of ΔT_t (^oC) 95
Table 33. Mean Weekly Maximum and Mean Weekly Minimum Temperatures for weeks July-August from the 2001 RMS and spreadsheet regression-based model for RMS node 65 96
Table 34. Capacity constraint for Lake Shastina releases, pumping rate from SLD well, diversions HGGV and HGPMP, and all three return flows 97
Table 35. Mean Weekly Maximum Temperature and Mean Weekly Minimum Temperature (^oC) for the nine weeks spanning July-August for temperatures at node 65 simulated with the spreadsheet-based model 99

Table 36. Comparison of weekly costs ($) and temperatures (^{o}C) at node 65 for Current Operations and Optimized results 100
Table 37. Irrigation efficiency effects on shortage cost, pumping cost and the temperature component of the objective function 102
Table 38. Estimated precipitation, evapotranspiration (ET) and resulting recharge from additional recharge zones in million cubic meters (MCM) 109
Table 39. Hydraulic Conductivity (K) in meters per day for new model runs 111
Table 40. Calibration statistics and residuals for new runs (meters) 111
Table 41. Annual spring flow results for new model runs (MCM) 112

Chapter 1: Introduction

It is widely understood by hydrologists and water managers that surface water and groundwater are an interconnected resource rather than two distinct water supplies. However, California state law has long ignored that reality by having separate laws for surface water and groundwater (Sax 2002). This can be problematic as water managers and policy makers manage an increasingly scarce resource with competing demands by urban, agricultural, and environmental uses. Though the law ignores their physical connection, water and ecosystem management should not.

Many aquatic species rely directly or indirectly on groundwater for flow and temperature moderation. Surface water flow and quality is often directly influenced by groundwater's characteristics, use, and sources, and it has a profound and measurable effect on stream temperatures. Groundwater influences fish migration, spawning, rearing, productivity, distribution and behavior (McCarthy et al. 2009; Power et al. 1999). Therefore, strategic management of groundwater is often necessary, but overlooked, for sustaining habitat needed for fish survival.

This dependence on groundwater conditions can be especially important for salmon in some Western rivers. The importance of groundwater contribution to stream flow has been demonstrated in the literature. For example, the decline of fall flows in the Cosumnes River has degraded Chinook salmon's ability to migrate and spawn in this undammed river. Extensive pumping has lowered the water table, causing the stream to become dry during the early fall when salmon would normally migrate upstream (Fleckenstein et al. 2004). This and other studies (Kondolf et al. 1987) demonstrate the connection between surface and aquifer processes and their importance for providing sufficient flows for fish migration and spawning.

In addition to flow requirements, many aquatic species are sensitive to temperature. Warming surface water due to decreased flows, loss of riparian shading, warm tail water returns or decreased groundwater inflows can be lethal to fish and exclude otherwise suitable habitat. Groundwater inflow is important for stream temperatures (Gaffield et al. 2005; Power et al. 1999). This is true for the Shasta River in northern California which receives significant inflows from cold water springs, namely the Big Springs complex, and other smaller sources including Clear Springs, Hole in the Ground, Little Springs and smaller seeps along the river banks (Figure 1).

Management of water resources for ecosystem health and environmental purposes has largely focused on securing flows for healthy aquatic habitats (Kendy and Bredehoeft 2006). With population growth in California and extensive agricultural water use, maintaining flow for environmental benefits at sufficient quantities and with proper timing is challenging and is expected to become more difficult as water becomes managed more tightly for increasing and diversifying demands. Creative management strategies are needed to stretch limited resources amongst growing demands. Such strategies have included water use efficiency, conjunctive use, water recycling, water banks, water markets and others (DWR 2009). Water use efficiency for environmental flows was explored by Null (2008) for making the most of water made available for environmental purposes. Part of doing so includes managing flows for temperature. In hydrologic systems dominated by cool groundwater inflows, this becomes a matter of understanding how surface and groundwater interact and considering groundwater use in conjunction with surface water diversions and operation. It can also mean recognizing groundwater, as part of the water supply portfolio, could serve as a cold water source to benefit in-stream temperatures in some cases.

Conjunctive use is the coordinated management of surface and groundwater resources. As stated in Common Waters, Diverging Streams, "conjunctive management is intended to reduce exposure to drought and flooding, maximize water availability, improve the efficiency of water distribution, protect water quality, and sustain ecological needs…"(Blomquist et al. 2004). This has traditionally related to magnitude of flow in space and time - having enough water to meet agricultural, urban, and environmental demands for water quantity. However, the quality of water supporting environmental benefits can be as, or more, important (NRC 2004). Specifically, water temperatures can be the most

significant factor determining presence or absence of fish species under many circumstances (Power et al. 1999).

Although the connection between groundwater and surface water is recognized, these sources are often managed as if they were separate. This can threaten efforts to restore fish habitat. This study's goal is to advance understanding of stream temperature and groundwater processes and methods used to model them to explore new management alternatives that might help support salmon habitat and agricultural water demands. Benefiting stream temperature explicitly in optimization is a novel goal for conjunctive management. Previous work has optimized groundwater and surface water use to minimize pumping effects on stream flow, maximize aquifer yield, meet urban and agricultural water demands, maximize economic benefit, or minimize net operating costs (Barlow et al. 2003; Basagaoglu and Marino 1999; Louie et al. 1984; Peralta et al. 1995; Pulido-Velazquez et al. 2006). A search of the literature has not found a study in which coordinated management of surface and groundwater resources was done to minimize in-stream temperatures.

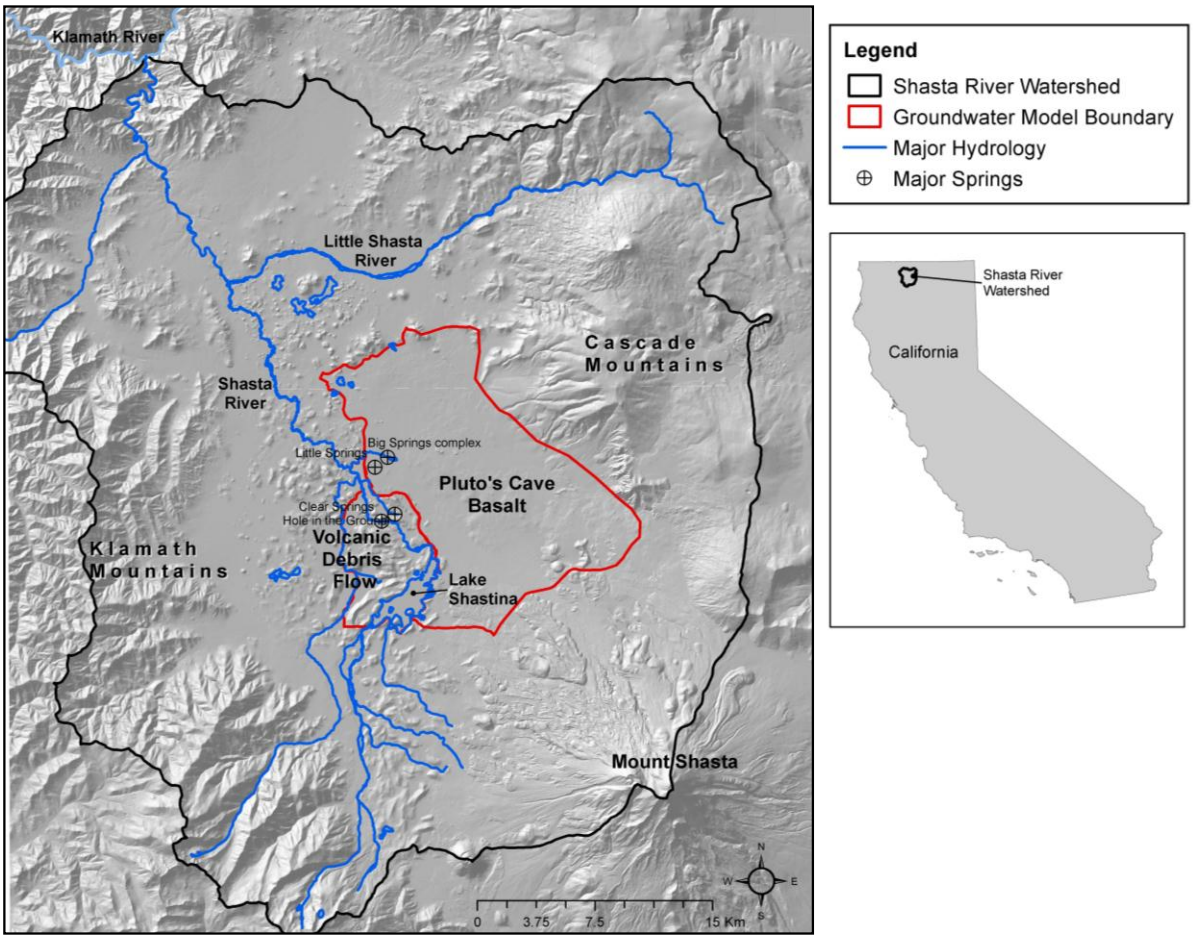

Figure 1. Study area- Shasta River watershed

The Shasta River and Pluto's Cave basalt aquifer

The Shasta River in rural Northern California, just north of Mount Shasta and tributary to the Klamath (Figure 1), is an interesting place to optimize surface and groundwater use for stream temperatures. Here the connection between surface and groundwater is explicit and environmentally important. Characteristic of the Cascades, its volcanic aquifers are dominated by preferential flow paths and numerous springs directly feeding and, in some areas, originating rivers at their source. Like other basins in the Cascades, it contains a river once swarming with salmon. Reportedly one of the most productive

salmon streams in California, run of Chinook salmon in the Shasta River exceeded 80,000 returning adults in the 1930s (NRC 2004). Historically, the river supported populations of fall-run and spring-run Chinook, Coho salmon, and steelhead trout. Coho salmon, steelhead trout, and fall-run Chinook are still present in the river but their numbers are drastically reduced (Ward and Eaves 2008).

Geologically the watershed is a mix of coastal range alluvial valley, volcanic debris flow, and basalt flows. The Pluto's Cave basalt conducts large volumes of water presumably recharging from snowfall and spring and stream discharge from the Cascade Mountains and Mount Shasta (Ward and Eaves 2008). The volcanic geology of the Pluto's Cave basalt aquifer is a highly porous fracture flow system littered with spring complexes that feed surface waters (Mack 1960). Previous work suggests the spring water is slightly thermal and likely interacts with marine sediments at depth giving it elevated levels of nitrate, phosphate, chloride and sulfate (McClain 2008; Nathenson et al. 2003). With sufficient quantities of nitrogen and phosphorus available, primary productivity is appreciable and creates a unique aquatic ecosystem supporting a productive and complicated food web. Food is not biologically limiting in this system. Instead, limits primarily come from inadequate flows and water temperature (Jeffres et al. 2009).

Outline of chapters

With the theme of coordinated management of surface and groundwater for stream temperature benefits, this research has three independent but related pieces.

1. Chapter 2 presents the results of Distributed Temperature Sensing (DTS) technology deployed in the Shasta River to observe the temperature effects of small groundwater seeps and irrigation tail water inflow from a side channel. The high resolution DTS data (temperature measured in meter increments at least every 15 minutes) is used to recalibrate an existing physically-based stream temperature simulation model. The measured stream temperatures and comparison to model results demonstrates the utility of DTS data in identifying and quantifying thermal variability of micro-habitats such as pools, side channels, or a result of cool or warm inflows. This has value for post-processing existing simulation model results that generally do not capture these areas of greater thermal variability.
2. Chapter 3 describes the Pluto's Cave basalt aquifer and develops a steady state groundwater MODFLOW model for this area of Shasta Valley including Parks Creek Valley (Figure 1). This modeling effort helps quantify and organize the current conceptual model of the fracture flow dominated aquifer and provides a tool with which to explore system dynamics on a regional scale. The interaction of recharge, pumping, and spring flow is explored for three model scenarios that vary the degree of groundwater flow across the north and western boundaries of the model domain.
3. Chapter 4 presents a method for optimizing surface water and groundwater ranch operations for the benefit of stream temperature while penalizing water shortage to agricultural deliveries. An optimization model for a basic problem encompassing the major components of the system (reservoir releases, groundwater pumping, diversions, tail water return flow and simulated stream temperature) is developed to first explore the initial tradeoffs and demonstrate the approach. Then an optimization model for the Shasta Springs Ranch decision variables for reservoir releases, groundwater pumping, and diversions is developed for the Shasta River upstream of its confluence with Parks Creek to minimize stream temperatures and maintain temperatures below an upper bound temperature target. Stream temperature is directly incorporated into the optimization using a regression-based model to warm/cool water over specified river reaches. Optimal operations and tradeoffs are presented.

To conjunctively manage groundwater and surface water effectively for stream temperature, understanding stream temperature and groundwater dynamics is essential. This dissertation takes an in depth look at stream temperature dynamics using high resolution DTS data and demonstrates how this data can be valuable in improving the development, performance, and post-processing of physically-based heat balance stream temperature simulation models. Better understanding hydrologic and thermal processes in rivers will improve efforts to incorporate stream temperature directly into optimization modeling. Likewise, understanding groundwater dynamics and stream-aquifer interaction is crucial for

coordinated management. Thus a piece of this research also advances the understanding of the Pluto's Cave basalt aquifer system in the Shasta Valley and Cascade hydrogeology.

References

Barlow, P. M., Ahlfeld, D. P., ASCE, M., and Dickerman, D. C. (2003). "Conjunctive-Management Models for Sustained Yield of Stream-Aquifer Systems." *Journal of Water Resources Planning and Management*, 129(1), 35-48.

Basagaoglu, H., and Marino, M. A. (1999). "Joint management of surface and ground water supplies." *Ground Water*, 37(2), 214-222.

Blomquist, W., Schlager, E., and Heikkila, T. (2004). *Common Waters, Diverging Streams* Resources for the Future, Washington D.C.

DWR. (2009). "Water Plan Update 2009." Department of Water Resources, http://www.waterplan.water.ca.gov/cwpu2009/index.cfm.

Fleckenstein, J., Anderson, M., Fogg, G., and Mount, J. (2004). "Managing Surface Water-Groundwater to Restore Fall Flows in the Cosumnes River." *Journal of Water Resources Planning and Management* 130(4), 301-31.

Gaffield, S. J., Potter, K. W., and Wang, L. (2005). "Predicting the Summer Temperature of Small Streams in Southwestern Wisconsin." *Journal of the American Water Resources Association*, 41(1), 25-36.

Jeffres, C., Dahlgren, R., Kiernan, J., King, A., Lusardi, R., Nichols, A., Null, S., Tanaka, S., and Willis, A. (2009). "Baseline Assessment of Physical and Biological Conditions Within Waterways on Big Springs Ranch, Siskiyou County, California." Report Prepared for: California State Water Resources Control Board.

Kendy, E., and Bredehoeft, J. D. (2006). "Transient effects of groundwater pumping and surface-water-irrigation returns on streamflow." *Water Resources Research*, 42, W08415, doi:10.1029/2005WR004792.

Kondolf, G. M., Maloney, L. M., and Williams, J. G. (1987). "Effects of bank storage and well pumping on base flow, Carmel River, Monterey, California." *Journal of Hydrology*, 91, 351-369.

Louie, P. W. F., Yeh, W. W. G., and Hsu, N. S. (1984). "Multiobjective Water-Resources Management Planning." *Journal of Water Resources Planning and Management-Asce*, 110(1), 39-56.

Mack, S. (1960). "Geology and ground-water features of Shasta Valley, Siskiyou County California." California Division of Water Resources.

McCarthy, S. G., Duda, J. J., Emlen, J. M., Hodgson, G. R., and Beauchamp, D. A. (2009). "Linking Habitat Quality with Trophic Performance of Steelhead along Forest Gradients in the South Fork Trinity River Watershed, California." *Transactions of the American Fisheries Society*, 138(3), 506-521.

McClain, C. (2008). "Provenance and Pathways: A geochemical and isotope analysis of Mt. Shasta groundwater," University of California, Davis.

Nathenson, M., Thompson, J. M., and White, L. D. (2003). "Slightly thermal springs and non-thermal springs at Mount Shasta, California: Chemistry and recharge elevations." *Journal of Volcanology and Geothermal Research*, 121, 137-153.

NRC. (2004). "Endangered and Threatened Fishes in the Klamath River Basin Causes of Decline and Strategies for Recovery." N. R. Council, ed., National Academies Press, Washington DC.

Null, S. (2008). "Improving Managed Environmental Water Use: Shasta River Flow and Temperature Modeling," University of California, Davis.

Peralta, R. C., Cantiller, R. R. A., and Terry, J. E. (1995). "Optimal Large-Scale Conjunctive Water-Use Planning - Case-Study." *Journal of Water Resources Planning and Management-Asce*, 121(6), 471-478.

Power, G., Brown, R. S., and Imhof, J. G. (1999). "Groundwater and fish- insights from northern North America." *Hydrological Processes*, 13, 401-422.

Pulido-Velazquez, M., Andreu, J., and Sahuquillo, A. (2006). "Economic optimization of conjunctive use of surface water and groundwater at the basin scale." *Journal of Water Resources Planning and Management-Asce*, 132(6), 454-467.

Sax, J. L. (2002). "Review of the laws establishing the SWRCB's permitting authority over appropriations of groundwater classified as subterranean streams and the SWRCB's implementation of those laws." Final Report SWRCB No. 0-076-300-0.

Ward, M., and Eaves, N. (2008). "Groundwater Data Needs Assessment." California Department of Water Resources.

Chapter 2: Modeling Insights from Distributed Temperature Sensing Data- Shasta River

Abstract

Distributed Temperature Sensing (DTS) technology can collect abundant high resolution river temperature data over space and time to improve development and performance of modeled river temperatures. These data can also identify and quantify thermal variability of micro-habitat that temperature modeling and standard temperature sampling do not capture. This allows one to bracket uncertainty of daily maximum and minimum temperature that may occur in pools, side channels, or as a result of cool or warm inflows. This is demonstrated in a reach of the Shasta River in Northern California that receives irrigation runoff and inflow from small groundwater seeps. This approach highlights the influence of air temperature on stream temperatures, and indicates that physically-based numerical models may under-represent this important stream temperature driver. This work suggests DTS datasets improve efforts to simulate stream temperatures and demonstrates the utility of DTS to improve model performance and enhance detailed evaluation of hydrologic processes.

Introduction

Advances in instrumentation and monitoring techniques have made collecting temperature data easier and more robust. This has provided opportunities to explore hydrological processes in greater detail and model them in new ways (Macfarlane et al. 2002; Moffett et al. 2008; Selker et al. 2006a; Tyler et al. 2009; Westhoff et al. 2011; Westhoff et al. 2007). Recent applications of Distributed Temperature Sensing (DTS) technology to hydrologic studies have opened up an exciting and rapidly expanding area of field research. DTS methods allow for temperature measurement that has high spatial resolution (1 m spatial resolution for up to a 1000 m cable) and temporal resolution (fractions of a minute) (Selker et al. 2006a; Tyler et al. 2009). Fiber optic cables can be up to 30 km (kilometers) in length.

DTS technology has a variety of applications for environmental science, including soil moisture research (Steele-Dunne et al. 2010), exploration of snow thermal processes (Tyler et al. 2008), analysis of temperature anomalies in a saltmarsh tidal channel system (Moffett et al. 2008), deployment in a fumarolic ice cave to estimate flank degassing rates (Curtis and Kyle 2011), leakage detection in sewer-storm water systems and dikes (Hoes et al. 2009; Khan et al.), lake hydrology (Vercauteren et al.), deployment in deep well boreholes for characterization of aquifer dynamics (Macfarlane et al. 2002; Yamano and Shusaku 2005), atmospheric study of the stable boundary layer (Keller et al. 2011), and multiple applications in rivers to explore and quantify groundwater-surface water interactions (Fleckenstein et al. 2010; Lowry et al. 2007; Selker et al. 2006b; Slater et al. 2010; Vogt et al. 2010; Westhoff et al. 2011).

The potential to obtain stream temperature measurements continuously - from mainstem conditions to side channel or micro-habitat areas - provides opportunities to improve field and modeling studies, and it can be useful to collect these data prior to or following simulation modeling. DTS data can help improve stream temperature modeling by providing high quality input and calibration data, and by identifying mixing zones where model nodes should be located at more frequent intervals. DTS can also be used to post-process model results to explore heating processes and temperature variability of micro-habitats relative to the mainstem. High-resolution measured data builds on previous modeling efforts by more accurately quantifying the range of measured thermal variability, estimating the rate of longitudinal heating as water moves downstream, or identifying thermal refugia from small springs or other inflows.

Only a few studies in the literature use DTS data to improve stream temperature model calibration, although obtaining temperature data with spatial resolution of less than 1 m and temperature resolution of +/- 0.01^{o}C provides abundant data (Selker et al. 2006a; Tyler et al. 2009). Westhoff et al (2007) use DTS data as input and to calibrate an energy-based temperature model of a first order stream in central Luxembourg. The temperature model is based on a series of well-mixed two meter length reservoirs and simulates seven days in April 2006. Model simulation of stream temperatures is compared to DTS temperature data. DTS measurements from this first order stream were used in two other studies to

calibrate, improve, or expand the energy balance model by adding instream rock clasts as heat storage zones and describing hyporheic exchange (Westhoff et al. 2010; Westhoff et al. 2011). Roth et al (2010) used Westhoff et al's energy balance modeling approach, comparing modeled temperatures against measured DTS data to explore effects of varying riparian vegetation conditions on stream temperatures. Their application is in the Boiron de Morges River in southwest Switzerland over a three day period in August 2007.

The objective of this study is to show the utility and value of DTS data in recalibrating an existing temperature model for river temperatures over a multiple week study period, and to provide insights on hydrologic processes that can enhance model development and interpretation of modeled results. Our hypothesis is that DTS input data will improve model result accuracy. To date, studies have focused on short-term experiments exploring in-stream processes over a period of a week or less. The DTS dataset for the Shasta River in Northern California used in this study extends from mid-August to mid-October 2010. This period of time spans the transition from the irrigation season to non-irrigation season and captures atmospheric changes that occur as summer transitions into fall. This research contributes to the literature by demonstrating the value of long-term DTS observations for model calibration and increased confidence in simulated temperatures. The methods and findings developed here can be applied to river management and assessment of habitat suitability by deploying DTS in reaches of interest for restoration or reaches with more complex temperature dynamics due to pools or inflows. DTS data also could be used with existing simulation results to post-process a more realistic range of variability in stream temperature not captured in simulation results.

We show the value of post-processing existing modeled stream temperature results to quantify micro-habitat and the range of variability in stream temperatures that are not captured by modeling. This has widespread applications because models do not have to be rerun. In fact, simulation results can be used to highlight promising locations for restoration or other changes, and DTS can be deployed to better measure temperatures or monitor changes. In this way, we show that DTS technology complements simulation modeling and can provide much greater benefit than simulation modeling with standard temperature logger protocols. This research uses a case-study on California's Shasta River to assess the role of measuring stream temperatures with DTS to improve model calibration and post-process thermal variability from existing stream temperature simulation results.

Site description

The Shasta River is the last tributary on the Klamath River before Iron Gate Dam, the lowest dam on the Klamath River (Figure 2). Native salmonid populations in the Klamath Basin have declined due to low flow conditions, warm stream temperatures, and barriers to migration (NRC 2004). Restoring the Shasta River for native trout and salmon is a no-regrets action to ameliorate current poor in-stream conditions and future dam decommissioning activities on the Klamath River (Null et al. 2010). Three species of salmonids, coho salmon (*Oncorhynchus kisutch*), fall-run Chinook salmon (*O. tshawytscha*), and steelhead trout (*O. giardneri*) are present in the Shasta River (spring-run Chinook trout were extirpated with construction of Dwinnell Dam at RK 65 (Moyle 2002). Klamath Basin coho salmon belong to the Southern Oregon/Northern California Coast evolutionarily significant unit, which was listed as federally threatened by the National Marine Fisheries Service in 1997 (NMFS 1997). Coho salmon are the only listed salmonid species, although all trout and salmon fish populations have been drastically reduced compared to historical populations that reportedly exceeded 80,000 returning adults in the 1930s (NRC 2004; Ward and Eaves 2008). Stream temperatures are one of the major factors limiting salmonid survival in the Shasta River (NRC 2004).

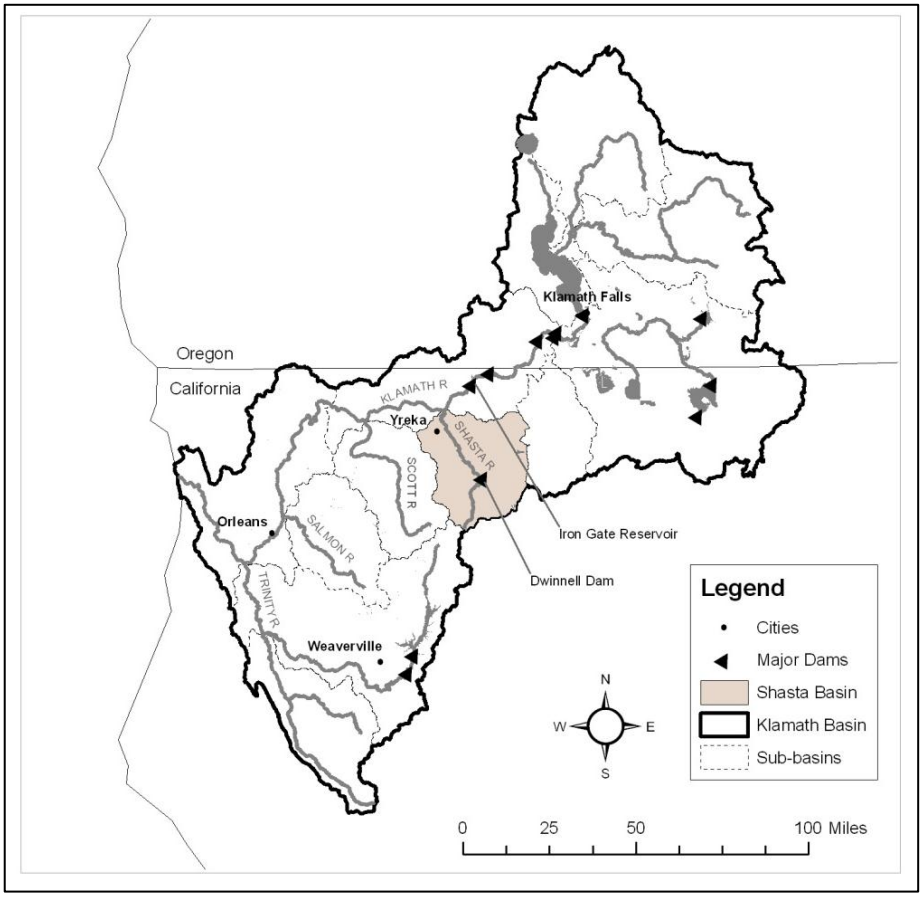

Figure 2. Shasta River watershed

The Shasta River originates in the Eddies Mountains of rural northern California and flows across the Shasta Valley for approximately 95 km northwestward to the Klamath River, with a catchment area of 2070 km^2. The valley is bounded by the Scott Mountains to the west, Siskiyou Mountains to the north, and the Cascade Range to the south and east. In the rain shadow of Mount Shasta, the valley is a high desert environment with hot, dry summers and cool winters. Mean annual air temperature for 2010 was 11.3^oC. Annual mean precipitation varies considerably with elevation with a minimum of 33 to 38 cm in the low elevation areas of the valley (Ward and Eaves 2008). The diverse geology of the area influences the region's complex hydrology. Volcanic deposits make up much of the valley floor's surficial deposits and most prolific groundwater aquifers (Ward and Eaves 2008). Mount Shasta, an active Cascade volcano, contributes recharge to a highly productive aquifer characterized by preferential flow paths through basalt flows. Volcanic debris flow material (older than the basalt flows) is the result of a debris avalanche from Mount Shasta. It is composed of a block and matrix facies of volcanic rocks and fine sandy ash-rich material, respectively. Its chaotic deposition leads to a lack of internal structure and low permeability and is understood to serve as a boundary impeding groundwater flow from the basalt, therefore giving rise to numerous springs along the contact between the formations (Ward and Eaves 2008).

The lower Shasta River is sustained by significant baseflows from springs, most notably, the Big Springs complex, which joins the mainstem at river kilometer (RK) 54.246 (Figure 4A) and contributes approximately 2.5 m^3s^{-1} to the Shasta River during the non-irrigation season and about 1.7 m^3s^{-1} during the irrigation season. Groundwater springs are an important source of cold water (12-14^oC) to the Shasta River, which is otherwise subject to atmospheric heating and cooling. During spring and summer, river temperatures exceed 20^oC (Null et al. 2010), which surpasses the thermal tolerance for salmonid species (Myrick and Cech Jr. 2001).

Mean annual discharge (years 1934-2010) near the mouth of the Shasta River (at USGS Yreka gauging station) is 5.18 m^3s^{-1}, with a range of 2.21-10.3 m^3s^{-1}. Mean daily discharge for 2010 exemplifies the pattern of peak snowmelt runoff and subsequently reduced flows during the irrigation season from April through September (Figure 3).

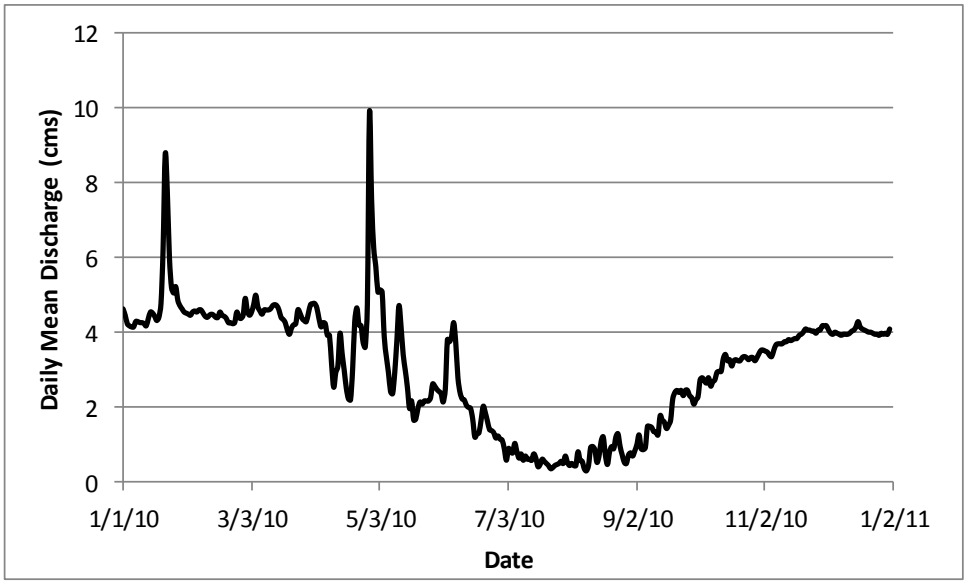

Figure 3. Shasta River mean daily discharge (m^3s^{-1}) at USGS 11517500 gauge near Yreka

Our study site is approximately 0.8 km of the mainstem Shasta River downstream of Dwinnell Dam and upstream of the confluence with Big Springs Creek (Figure 4), RK 54.898-55.699. This stretch has an average slope of 0.0028 m/m. Most stream flow in this stretch originates from snowmelt runoff and groundwater accretion upstream and small seeps along the course of the mainstem. Summertime flows are on the order of 0.71 m^3s^{-1} or less during the irrigation season. The course of the river in this area runs along the base of the debris flow and averages a width of 11.3 meters. Basalt outcrops are dispersed along the Shasta River and several small groundwater seeps contribute small amounts of cold (~14°C) water. The flow rate, size, and prevalence of these seeps have not been quantified.

The complex spring hydrology and prevalence of coldwater seeps makes better measuring, simulating, and characterizing the thermal diversity of the Shasta River a priority. Previous simulation modeling has indicated that restoration could enhance coldwater habitat in this river (Null et al. 2010). While it is generally known that coldwater springs and seeps exist in this system and that they play a role in maintaining a stable thermal regime, it is not well understood how exactly they influence stream temperatures or the role they play for thermal refugia. High resolution temperature monitoring in the Shasta River can help to fill these information gaps and also provide better input data for stream temperature simulation modeling.

A

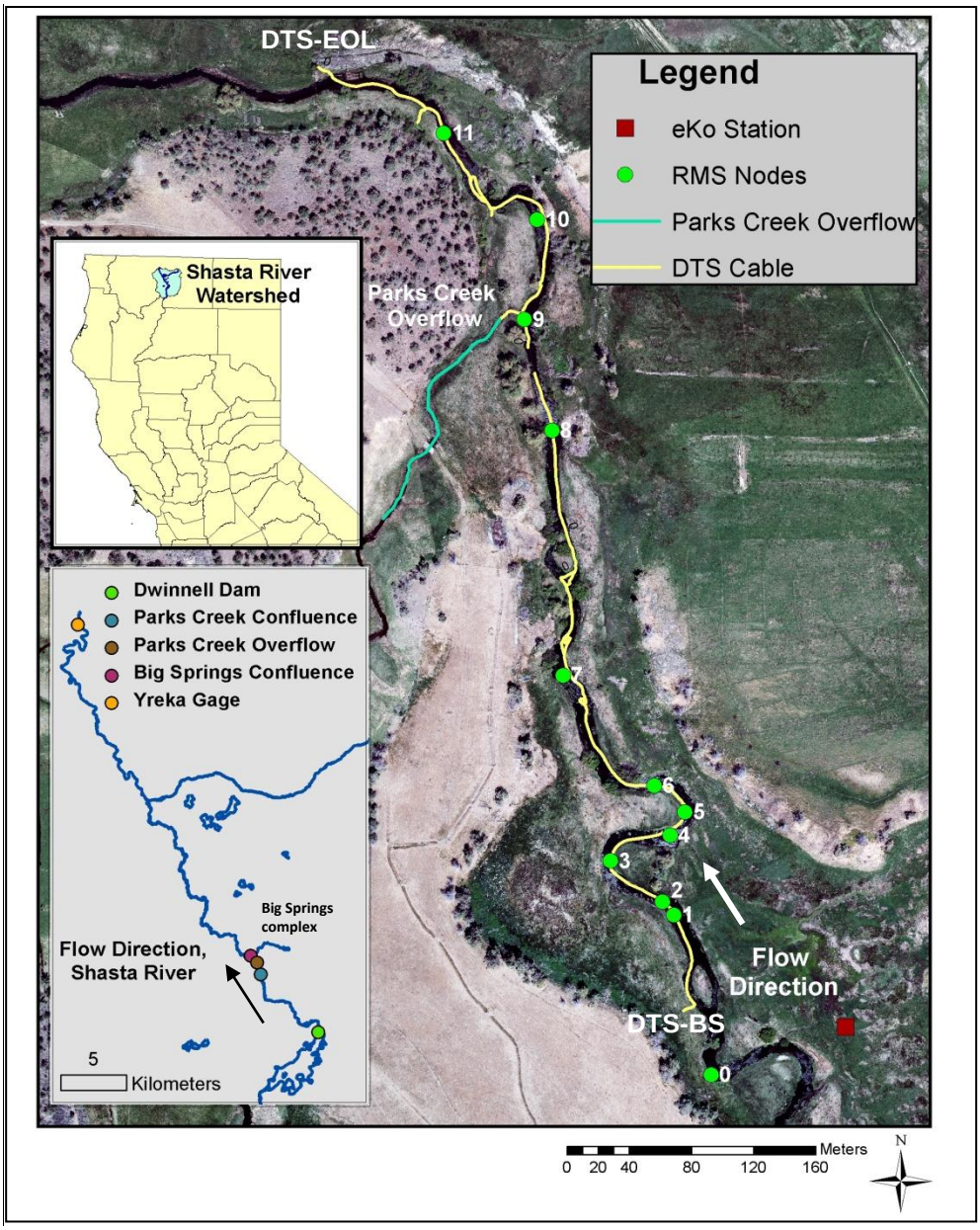

B

River Kilometer	Approximate Distance from Upstream node (m)	Description
65.372		Dwinnell Dam
56.229		Parks Creek Confluence
55.699		RMS node 0, Upstream Boundary Condition
55.659	40	Hobo logger for boundary condition temperature
55.649	50	DTS cable enters river, near Base Station
55.579	120	DTS-BS flow cross section and stream gauge

55.587	112	RMS node 1
55.571	16	RMS node 2
55.538	33	RMS node 3
55.506	32	RMS node 4
55.49	16	RMS node 5
55.474	16	RMS node 6
55.361	113	RMS node 7
55.232	129	Below Basalt Outcrop flow cross section
55.2	161	RMS node 8
55.136	64	RMS node 9, Parks Creek Overflow Lateral
55.13	6	Parks Creek Overflow
55.117	19	Below Parks flow cross section
55.056	80	RMS node 10
55.038	18	Groundwater seep2
54.975	81	RMS node 11
54.96	15	Groundwater seep1
54.898	77	DTS- End of the Line (EOL), cable secured on fence post
54.888	87	EOL stream gauge and flow cross section
54.246	729	Big Springs Confluence
Average distance between RMS nodes (m)		66

Figure 4. a) Shasta River DTS study area b) descriptions of river kilometer locations (RMS is River Modeling System)

Methods

Measurements

A 4 channel Sensornet Oryx DTS was deployed to measure stream temperatures. DTS systems send a laser light down an optical fiber and measure the Raman backscatter, whose intensity is related to the temperature of the optical fiber (Selker et al. 2006a; Tyler et al. 2009). The DTS data storage system is enclosed in a weather proof shelter with a 3G compatible cell phone data link. 200 Watt solar panels with two 70 amp-hour deep discharge batteries provide power. In our application, the DTS recorded water temperature every meter along a 1 km cable every 5 minutes August 17-September 6 and then every 15 minutes September 6 thru October 12 because quarter hour resolution is sufficient for the purposes of this study and reduces excessive data storage and transmittal. The location of the DTS system at the upstream end of the cable is hereafter referred to as the DTS Base Station (DTS-BS) (Figure 4). The cable was secured with fence posts or rocks and typically rested a few inches above the river bed. Abundant macrophyte growth in the Shasta River (Jeffres et al. 2009) made the cable difficult to see. Instrumentation also included an eKo-brand remote weather station with precipitation, solar radiation, wind speed, temperature and relative humidity sensors. This weather station was located in the middle of an open damp grassy area 30 m east of the river and recorded atmospheric data every 15 minutes.

An ice bath, periodically maintained over the study period, and ambient bath were located at the DTS-BS and another ambient bath was at the end of the cable. These calibration baths housed 20-30 meters of coiled fiber optic cable situated such that the cable did not touch the sides of the bath. A Hobo temperature logger with accuracy of +/- 0.2°C for the 0^{o}-50^{o}C temperature range and a high resolution temperature probe from the DTS system was placed in the middle of the coil for cable calibration to account for signal attenuation and temperature offset (Tyler 2009). The cable was deployed August 17,

2010 and removed October 12, 2010 in the mainstem Shasta River from approximately RK 55.649 to 54.898, the side channel of Parks Creek Overflow (PCO), and two sources of groundwater seeps on river left (Figure 4). The cable was placed in PCO and the groundwater seeps to quantify thermal differences between them and the mainstem Shasta River.

Stream temperature model

The Tennessee Valley Authority's River Modeling System (TVA-RMS v.4) was used to simulate flow and stream temperature in the Shasta River for August 21 through October 9, 2010 with an hourly time step. RMS is a one-dimensional longitudinal, physically-based numerical model composed of a hydrodynamics module (ADYN) and a water quality module (RQUAL) (Hauser and Schohl 2002). ADYN solves equations for conservation of mass and momentum (St. Venant equations) using a four point implicit finite difference scheme with weighted spatial derivatives outputting velocity and depth at each node. Required inputs include channel geometry, roughness coefficients, upstream and lateral inflows, and initial conditions specified as either flow or water surface elevation (Hauser and Schohl 2002). The dynamic water quality model (RQUAL) solves the mass transport equation using the Holly-Priessmann numerical scheme and can simulate time varying temperature, dissolved oxygen, carbonaceous BODu, and nitrogenous BODu at multiple locations (nodes) along a river reach. Modeling temperature was the focus of this study, and the other water quality aspects were not simulated. Model inputs for RQUAL include velocity and water surface elevation from ADYN, meteorological data (air temperature, dew point temperature, wind speed, cloud cover, barometric pressure, and solar radiation), temperatures of inflow sources, and initial stream temperatures (Hauser and Schohl 2002).

The temperature component of the water quality module uses a heat budget approach estimating heat fluxes for net solar radiation adjusted by a shading factor, atmospheric long-wave radiation, channel bed heat flux, back radiation from the river, evaporative heat loss, and conductive heat transfer (Hauser and Schohl 2002). Changes to the RMS code to represent riparian shading were made by Abbot (2002) allowing for a separate shading fraction for the left and right bank of a river.

Meteorology input data for RQUAL (dry bulb temperature, atmospheric pressure, wind speed, solar radiation and relative humidity) were obtained from the eKo-brand weather station located near the river. Dew point temperature was calculated from dry bulb temperature and relative humidity. Cloud cover was estimated using measured short wave solar radiation.

Modeling efforts for this study began with a previously developed RMS model of the Shasta River simulating temperatures from Dwinnell Dam to the confluence with the Klamath for 2001 (Null et al. 2010). That model represented the Shasta River with 999 unevenly-spaced nodes over a modeled length of 65.4 km. Meandering reaches, as in the currently modeled section, have a higher density of nodes than straighter reaches (Figure 4). The approximately 0.8 km fiber optic cable placed in the mainstem in summer 2010 corresponds to eleven of the nodes from the 2001 model. A five-point channel cross-sectional geometry defines each node. The new Shasta River model for 2010 has a boundary condition node and 11 nodes modeling stream temperature, representing approximately 0.72 km.

The most upstream RMS node (node 0) is assigned boundary condition temperature and flow inputs and in the 2010 model is located upstream of the DTS stretch (Figure 4). A Hobo temperature logger located about 40 m downstream of the boundary condition node (node 0) but upstream of the DTS cable provided hourly upstream boundary condition temperature data.

Calibration

Modeled water temperature was compared to DTS measured data averaged over 15-50 m upstream and downstream of each node. This was done rather than taking temperature at a single point closest to the model node to avoid capturing localized temperature conditions of the cable at a single location. Averaging measured temperature over space better represents water temperature conditions corresponding to each modeled reach.

Mean bias is calculated for each node by averaging the difference between hourly modeled and measured temperature for the model period, August 21 to October 9. A positive mean bias indicates overestimation by the model. Similarly, the root mean square error (RMSE) is calculated for the same

hourly time series by averaging the squared residuals (absolute value of modeled minus measured) and taking the square root.

Results and discussion

This section describes the model calibration process and results followed by DTS temperature results. Daily thermal variability of measured and modeled stream temperatures are also presented and discussed. Finally an examination of longitudinal rates of heating for measured versus modeled results explores the roles of solar radiation and air temperature in influencing stream temperatures.

Calibration process

Calibration explored the sensitivity of stream temperatures to the upstream flow boundary condition, as well as the inflow of Parks Creek Overflow (PCO) since these presented a data gap in our field measurements. Overall, temperatures were not highly sensitive to the upstream flow boundary condition. The order of change to modeled stream temperatures was thousandths of a degree (°C) and the largest improvement from one model run to another was a mean bias of 0.039^{o}C. Changing the upstream inflow within its likely flow range has negligible effects on river temperature. A new lateral (not included in the 2001 RMS model) was added at node 9 to represent the inflow of PCO. PCO may be an abandoned channel of Parks Creek, but now is a narrow, rocky channel with dense vegetation that mostly conveys tail water return flow from flood-irrigated pasture. Flow data for this lateral was unavailable, but was estimated to be 0.05 to 0.11 m^3s^{-1} based on five flow measurements taken above and below the inlet. In reality, we believe the inflow of PCO varies based on irrigation events. During calibration, models were run with uniform daily flows of 0.06 to 0.14 m^3s^{-1}. Based on model performance and knowledge of the river system, a uniform daily flow rate of approximately 0.11 m^3s^{-1} was assigned to PCO lateral. Lack of flow data for this inflow is a limitation and may affect downstream temperatures. For nodes 10-11, changes in the lateral flow from 0.06 to 0.14 m^3s^{-1} affects the mean bias on the order of a tenth of a degree (^{o}C) and the RMSE as much as 0.058^{o}C. Boundary condition inflow temperatures for PCO were an average of temperatures along 15 m of DTS cable looped into the side channel.

A number of inputs were adjusted slightly from 2001 RMS model values for model calibration (Table 1). These included bank width, the wind coefficient in wind-driven evaporative cooling (AA), thermal diffusivity of bed material (DIF), and bed albedo (BEDALB). The bank width is an input to RQUAL defined as the distance from the water's edge to trees or an effective barrier at each node (Hauser and Schohl 2002). This was set to 0 for the entire river in the 2001 RMS model. Using high resolution aerial photographs and observations from the field, this parameter was adjusted to better reflect riparian vegetation setback from the river and to capture a ridge along RKM 55.4-55.7 that may provide topographic shading in early morning or late afternoon. The new bank width varies from 0.0 to 71.9 m. Transmittance of solar radiation through riparian vegetation for both banks was also adjusted to better represent shading conditions in this stretch.

Table 1. RQUAL Parameters evaluated during calibration

Parameter	Recommended Range (Hauser and Schohl 2002)	2001 RMS (Null et al. 2010)	Current Value
AA	0E-09 - 4E-09 m^3/mb/s	0.5E-09 m3/mb/s	0.2E-09 m3/mb/s
BB	1E-09 - 3E-09 m^2/mb	1.5E-09 m2/mb	1.5E-09 m2/mb
DIF	25 - 50 cm^2/hr	25 cm2/hr	50 cm2/hr
XL	5-50 cm	15 cm	15 cm
EXCO	0.05 for clean water	0.1 (1/m)	0.1 (1/m)
	0.30 for turbid water		
CV	0.4-0.7 cal/cm^{3o}C	0.68	0.68
BEDALB	0.1-0.5 (unitless)	0.25	0.3

AA wind coefficient in wind-driven evaporative cooling
BB wind exponent in wind-driven evaporative cooling
DIF thermal diffusivity of bed material
XL effective channel bed thickness of upper layer for bed heat conduction
EXCO light extinction coefficient
CV bed heat storage capacity
BEDALB albedo of bed material

Sensitivity of other heat flux parameters in RQUAL was explored during calibration. The wind coefficient in wind-driven evaporative cooling (AA) is positively related to evaporative heat flux and increases simulated temperatures as it is decreased. For the current study, AA was slightly reduced to 0.2E-09 from the 2001 RMS value of 0.5E-09 (Table 1). This increased temperatures by 0.01^{o}C in 13% of the time periods which improved model performance for all nodes.

Mainstem channel bed material is primarily saturated sands and gravels with a few short reaches with cobbles and boulders. Saturated sand has higher thermal diffusivity compared to silt or clays (GeoReports 2011). Increasing the thermal diffusivity of bed material parameter (DIF) generally increases thermal variability in the model. DIF was increased to 50.0 cm^2/hr, the upper end of its recommended range. Bed albedo (BEDALB) affects the channel bed heat transfer and was increased from 0.25 to 0.30.

During calibration of the 2001 RMS model, the geometry of cross sections in the current reach of interest were narrowed to 60% of the previously defined width (Null 2008). Based on estimates of stream width in the study area, the wider cross sections were restored for the current modeling and calibration. This affected simulated stream temperatures on the order of 0.02^{o}C.

The sensitivity of Manning's n was also explored during calibration. A reasonable range of estimated Manning's n values based on USGS supply Paper 2339 (Arcement Jr. and Schneider 1989) for the RMS nodes is 0.053-0.09. Model runs with varying values of Manning's n indicate that simulated temperatures are not sensitive to changes in this parameter of this magnitude. Manning's n was left at its 2001 RMS model value of 0.05 for each node.

In addition, the latitude and longitude in the 2001 RMS model corresponded to the confluence of the Shasta River with the Klamath. Latitude and longitude in the current input file was updated to 41.587 and 122.433, which is located just downstream of the meander in the DTS reach of the Upper Shasta River.

Other parameters, including bed heat storage capacity, effective channel bed thickness of the upper layer for bed heat conduction, wind exponent in wind-driven evaporative cooling, and the light extinction coefficient, were tested but either had little or no effect on modeled temperatures or worsened model performance.

Calibration results

Overall, modeled data represented stream temperatures in the Shasta River well. Modeled stream temperatures were compared with measured data (Figure 5) and mean bias, root mean square error (RMSE), and mean absolute error (MAE) statistics were calculated for each node. Mean absolute error (MAE) is less than 0.3^{o}C for all nodes and mean bias for all nodes is -0.04^{o}C. 2001 RMS model results had MAE of 1.48 and 1.90^{o}C for nearby reaches (Parks Creek and Louie Road) (Table 2). Using DTS as input data and for calibration improved model performance considerably for this short reach with a decrease of the RMSE from 2.00^{o}C to 0.35^{o}C from the earlier 2001 RMS model to the newly calibrated model. A couple degrees (^{o}C) can be significant when evaluating the suitability of temperature conditions for fish habitat or ranking ecosystem management alternatives. Using DTS for initial stream temperature and boundary conditions helped improve model accuracy.

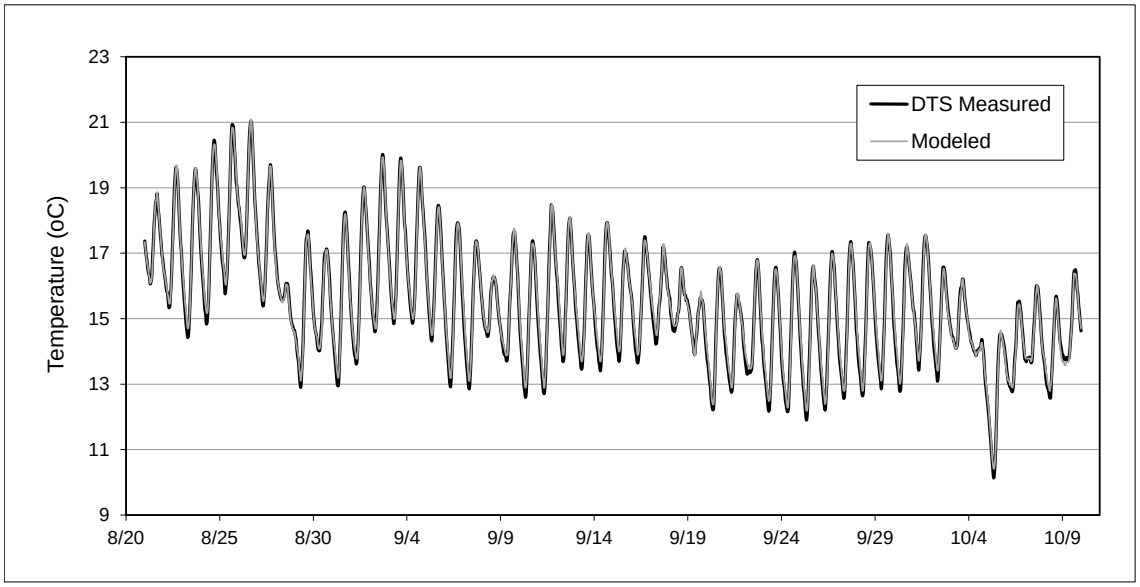

Figure 5. Modeled and measured river temperature for node 4 with modeled temperature largely overlapping measured temperature except at the peaks and the troughs

Table 2. Calibration statistics at each node (n = 1201 for all nodes)

Node	Mean bias (^{o}C)	RMSE (^{o}C)	MAE (^{o}C)
1	0.04	0.14	0.11
2	0.03	0.15	0.12
3	0.05	0.14	0.11
4	0.02	0.15	0.12
5	0.00	0.15	0.13
6	-0.02	0.17	0.14
7	-0.06	0.18	0.15
8	-0.11	0.21	0.17
9	-0.16	0.24	0.19
10	-0.10	0.30	0.24
11	-0.16	0.35	0.29
Average	***-0.04***	***0.20***	***0.16***
Earlier 2001 RMS Model Results			
Parks Creek	-0.96	2.00	1.48
Louie Road	-0.09	2.27	1.90

Measured and modeled river temperatures at node 4 are included for visual corroboration of results (Figure 5). Daily minimum modeled temperatures of nodes 1-9 tend to be warmer than measured temperatures by approximately 0.2^{o}C. In other words, not enough cooling occurs at nighttime in model results. Modeled daily maximum temperatures for nodes 1-9 are warmer than measured temperatures about half the days by an average of 0.05-0.09^{o}C and cooler than measured temperatures by an average of 0.05-0.14^{o}C. Temperatures downstream of PCO (nodes 10 and 11) are strongly influenced by the inflow of that lateral and therefore are less accurate since flow volumes are uncertain (Table 2). Modeled maximum daily temperatures are warmer than measured temperatures at node 10 and 11 by approximately 0.3^{o}C, which occurs about 80% of the days.

Measured temperature results

The DTS data show local thermal variability that was not evident from temperature simulation or from previous stream temperature measurements using thermistors located tens of kilometers apart. PCO and the two measured cold water seeps contribute water noticeably warmer and cooler, respectively, than the mainstem temperature (Figure 6). The measured temperature range, calculated as the difference between maximum and minimum temperature for each meter along the cable over the period of record,

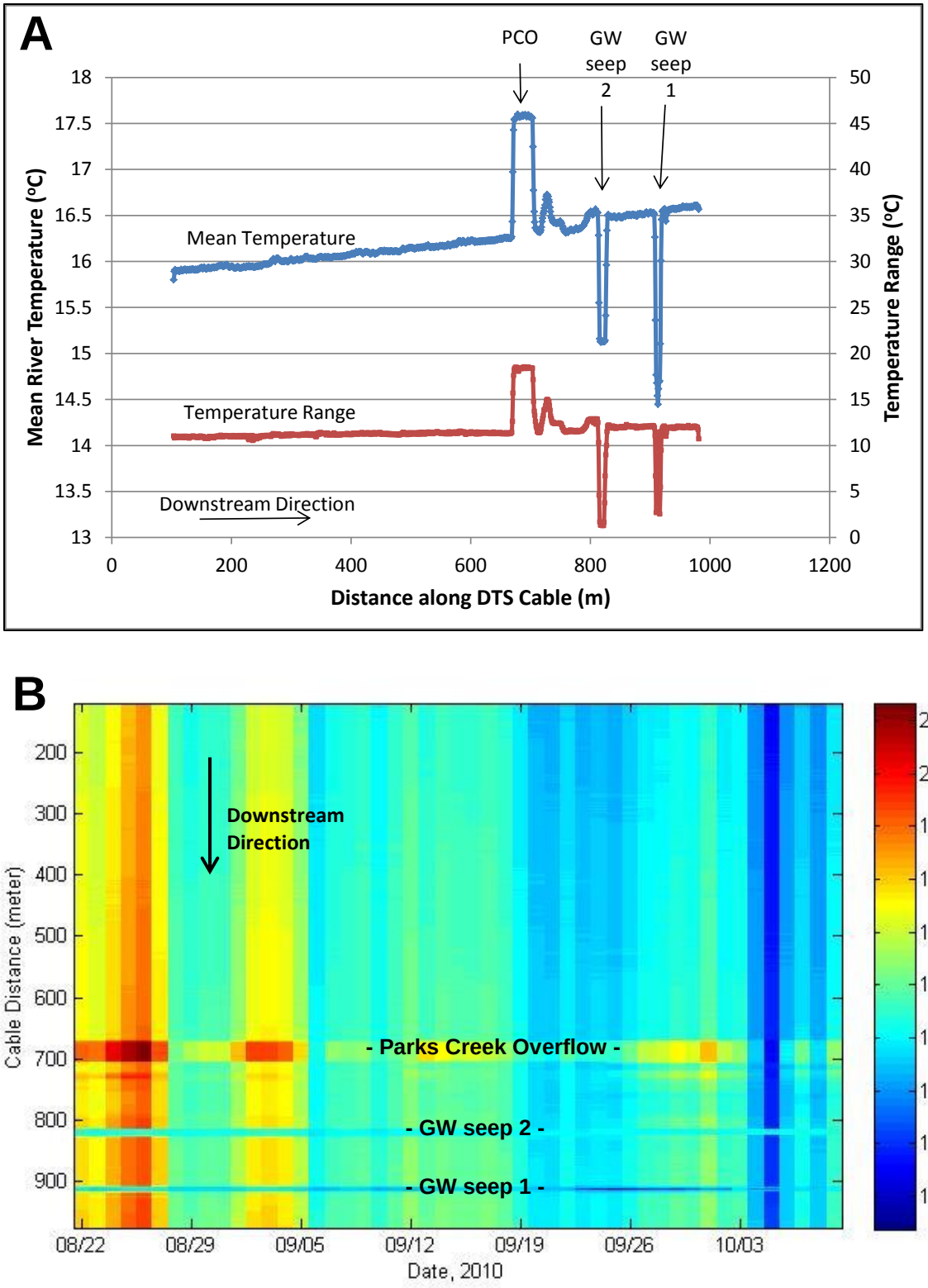

Figure 6. a) Mean temperature and temperature range at each meter for measured period of record. b) Mean daily temperature indicated by color ramp at meter increments along DTS cable for period of record.

shows sites with high and low temperature variability (Figure 6A). Namely, the groundwater seeps are both consistently about 15.2°C and 14.4°C. Though significantly colder than the mainstem, these seeps do not contribute enough flow to affect mainstem temperatures significantly; although they could provide very localized thermal refugia for coldwater species. PCO is shallower than the mainstem with less thermal mass, and thus is colder than the mainstem at night and warmer during the day, with higher temperatures than the mainstem on average. Examining the range of temperature for each location along the cable is one way to identify groundwater inflows as they dampen diurnal temperature fluctuations. Aside from the two seeps, previously discussed, the dataset does not reveal significant groundwater inflows. Temperature affects from other seeps and any diffuse baseflow that may be occurring along the reach is not great enough or near enough to the DTS cable to influence the measured temperature. The warmer temperatures just downstream of PCO indicates a mixing zone where the PCO mixes with the mainstem and persists for about 40 meters downstream of the PCO channel (Figure 6). The length of the mixing zone would be expected to change with flow volume of both the mainstem and side channel. With DTS, we were able to specify stream temperatures, coldwater seeps, and thermal variability of a side channel, and quantify the size of mixing zones in the Shasta River from the PCO return flow channel. This is useful for evaluating potentially beneficial thermal features or thermal barriers to fish passage.

Mean weekly maximum and mean weekly minimum stream temperatures are typically used as metrics for habitat suitability and fish survival (Welsh et al.2001; McCullough 1999). Temperature measurements using DTS allow for an evaluation of mean weekly minimum and maximum temperatures at a 1 m spatial resolution (Figure 7). Thus, weekly metrics can be created with high spatial resolution and used to identify specific problem reaches or barriers to fish passage. One of the warmest sites in the study reach of the Shasta River is the mixing zone downstream of PCO inlet (Figure 6), which reached a daily maximum of 24.15°C during the study period. Although it has high daily maximum temperatures that may provide a thermal barrier during warm periods, this mixing zone cools sufficiently at night (average minimum of about 13°C) thus would probably not prevent fish passage during the observed season. With detailed temperature data over space and time, potential thermal barriers can be better defined and identified.

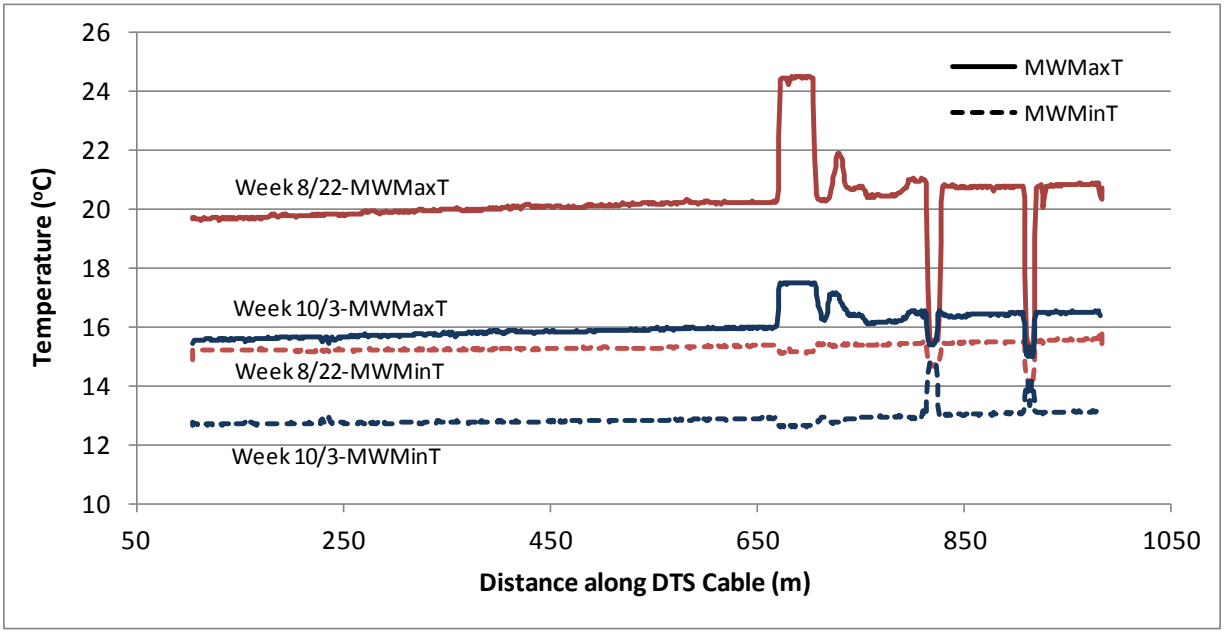

Figure 7. Mean weekly maximum and minimum stream temperatures at each location for the hottest and coolest week

Daily thermal variability

Stream temperatures are driven by both source temperatures and response to atmospheric conditions. Thus both modeled and measured daily maxima and minima were influenced by atmospheric conditions. However, modeled stream temperatures were less variable than measured DTS temperatures (Figure 8). The measurement period from mid-August to the first week in October had a combination of hot and milder days with maximum daily air temperature ranging from 15.4 to 36.9^{o}C (Figure 9). DTS daily maximum river temperatures were generally warmer than modeled peak temperatures. Likewise, DTS daily minima were cooler than modeled daily minimum temperature. Therefore, not quite enough heating occurs during the day and not quite enough cooling at night in the model for most locations. This leads to lower thermal variability of modeled compared to measured temperatures for all nodes upstream of PCO. Even so, the average difference between modeled and measured daily thermal variability for nodes 1 to 9 is between 0.10-0.63^{o}C for August 22 thru October 9.

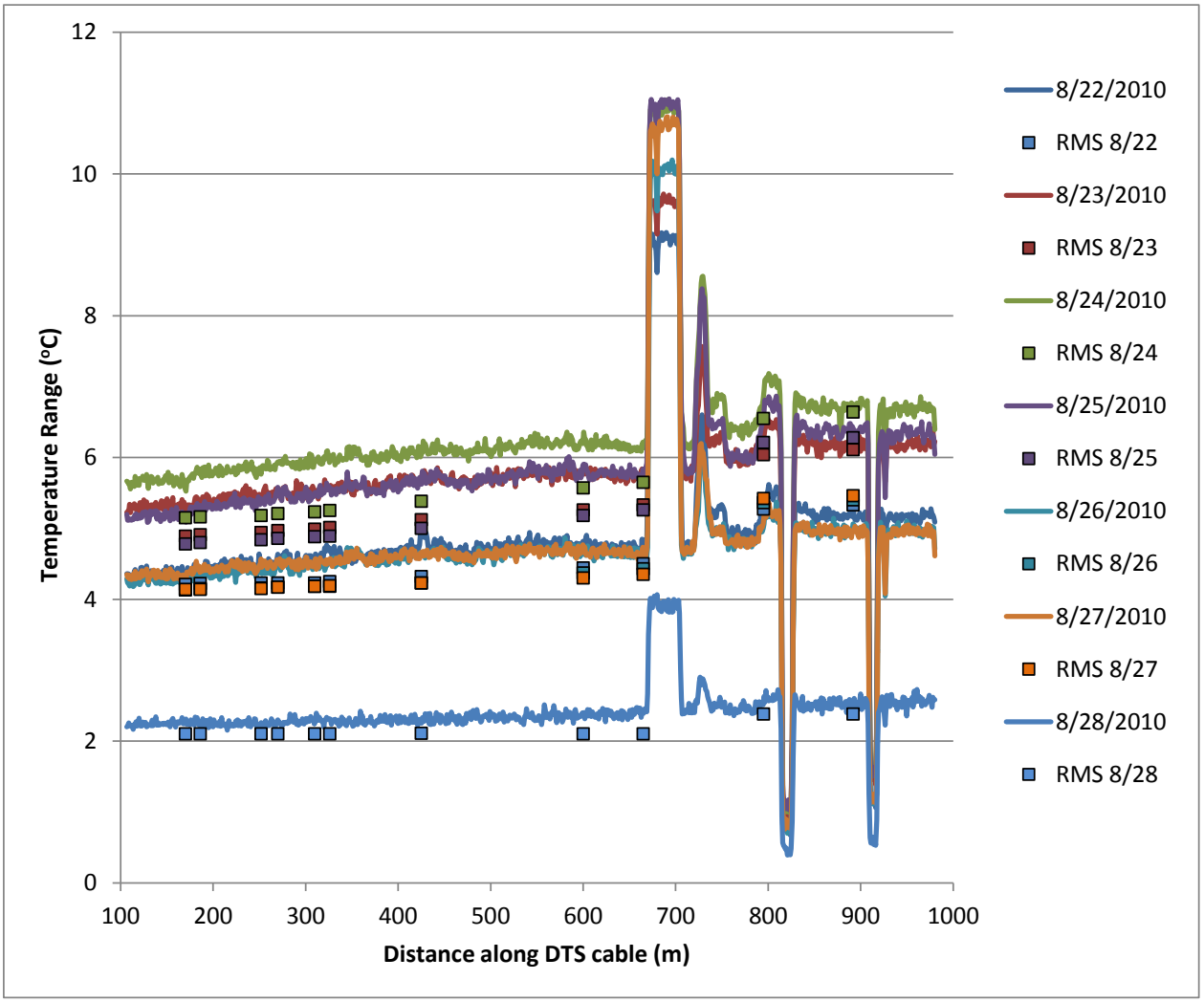

Figure 8. Daily thermal variability of stream temperature (daily max-min) from DTS measured and modeled results for the week of August 22

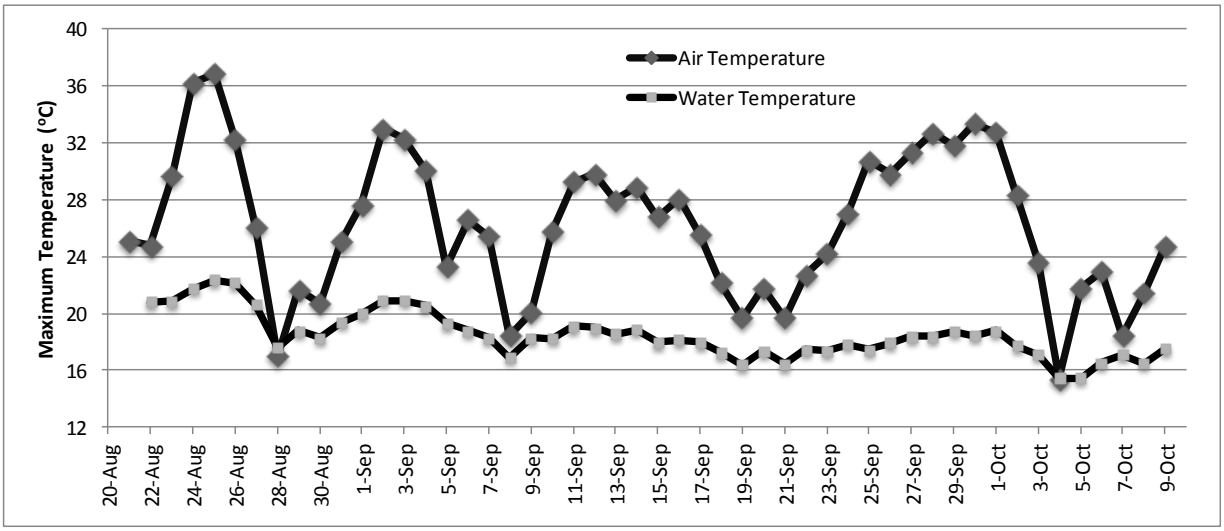

Figure 9. Measured maximum daily air and water temperature for model period

Stream temperatures at nodes 10 and 11 located downstream of PCO are influenced by this inflow and often modeled thermal variability is more extreme than what is measured (this occurs 41 out of 50 days). More accurate inflow data (rather than estimated constant flow value of 0.11 $m^3 s^{-1}$) would likely improve results. In reality, PCO inflow is not steady. It is probable that PCO inflow volume is too high on days that modeled thermal variability is more extreme than measured data. This illustrates why irrigation tail water (which is variable based on water rights, water availability, and watering schedules of multiple irrigators) can be challenging to model accurately. Furthermore the difference in volume between tail water return flow channels and the mainstem river mean that return flows or other smaller channels typically heat and cool at different rates and thus can contribute warmer or cooler water based on season, time of day, and water year (wet years versus dry years). The Shasta River is characterized by inflows of tail water returns and cool groundwater seeps and springs that are unquantified and often unmapped. This makes assessing habitat suitability difficult because modeled mainstem temperatures do not capture these local complexities. DTS technology allows measurement of thermal variability of these small micro-habitats. DTS data can be used to bracket the uncertainty and range of temperature that may occur in side channels, pools, and mixing zones of cool or warm inflows, or to gain more information on reaches that simulation modeling indicate may provide suitable habitat for coldwater species or are promising for restoration.

For example, the PCO mixing zone is influenced by inflow from the side channel and maximum and minimum temperatures significantly differ from mainstem temperatures just upstream (Figure 10). This thermally complex mixing zone is modeled with a single node (node 9). Maximum and minimum temperatures modeled at node 10 are compared to temperatures measured by DTS to explore the extent to which thermal variability differs due to the lateral inflow. Figure 10 shows maximum DTS temperatures can exceed modeled temperatures by as much as 5.6^{o}C. A difference of this magnitude could be significant in affecting the movement of coldwater species, like salmon and trout, though it is not captured by model results. Conversely, measured DTS daily minimum temperatures are less than modeled minimums by as much as 2.72^{o}C.

This demonstrates the utility of DTS data in providing insight on thermal variability of micro-habitats not simulated by modeling efforts. This could be important for analysis and application of modeling results used for evaluating habitat suitability. Analyzing the increased (or in cases of groundwater inflow, decreased) thermal variability resulting from local inflows can bracket the uncertainty of modeled temperatures.

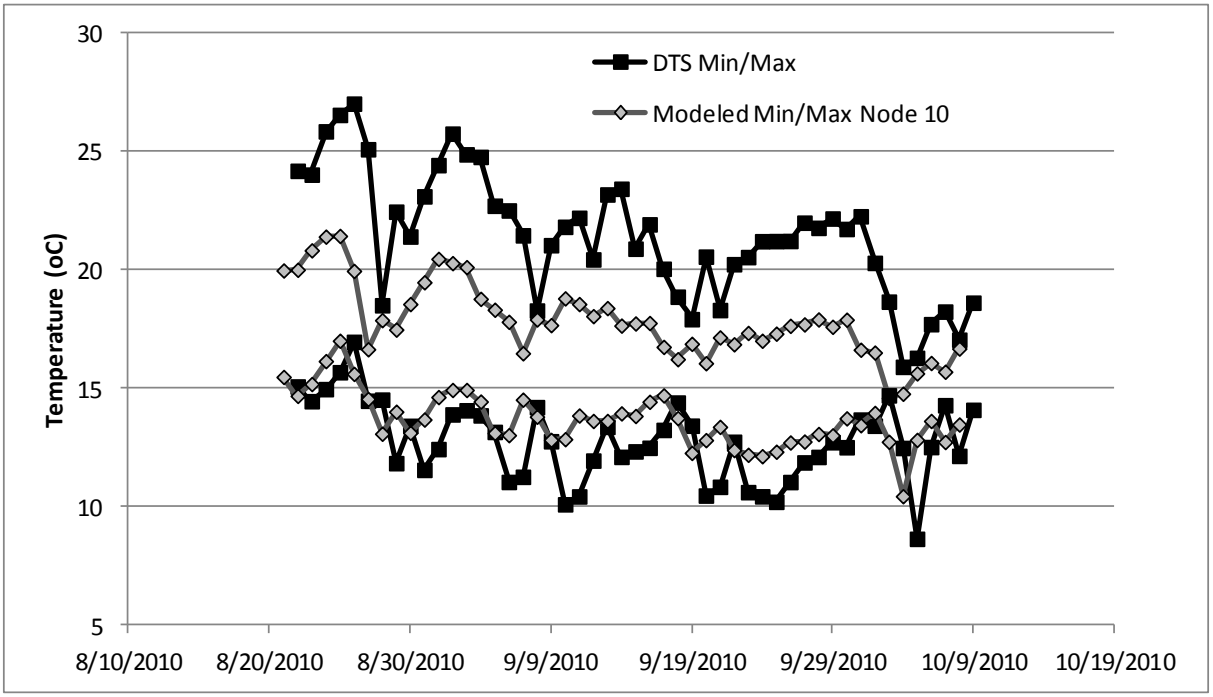

Figure 10. Maximum and minimum modeled and measured temperatures in mixing zone of Parks Creek Overflow and mainstem Shasta River

Longitudinal rate of heating

Generally, river temperatures warm in the downstream direction when the atmosphere is warmer than water temperatures (summer and early autumn). Examining longitudinal heating shows how stream temperatures change as water moves downstream, and is a function of source inflows and temperatures, travel time, and atmospheric conditions. This is important for managing temperature for aquatic species because it identifies where heating occurs most rapidly and can highlight those areas for restoration or other management efforts to preserve cooler, upstream temperatures. Longitudinal rate of heating is calculated for DTS as the average of measured temperatures near node 8 minus the average temperatures near node 1 normalized by the distance between them (386 m). The same is done for RMS results for node 1 and 8. This stretch of river does not have known inflows affecting mainstem temperatures.

We focus on the rate of longitudinal heating of water temperatures between nodes 1 and 8 on August 25-31; these six days span a period of higher to lower air (and corresponding water) temperatures and have a wide range in maximum daily solar radiation. Figure 11 shows the rate of longitudinal heating from DTS measured temperatures and RMS modeled temperatures with solar radiation (Figure 11A) and air temperature (Figure 11B). Modeled temperatures are driven primarily by solar radiation, following current understanding of solar radiation as a major factor influencing both air and water temperatures (Johnson 2003) and a major driver of heat energy flux (Caissie 2006). Measured peak heating rates lag peak solar radiation by four to five hours (especially on days with high maximum solar radiation), and appear to more closely coincide with the timing of peak air temperature. Measured daily maximum stream temperatures also lag peak solar radiation by approximately the same amount of time. This observation that air temperature correlates well with stream temperature reinforces similar findings of other investigators (Mackey and Berrie 1991; Mohseni and Stefan 1999; Sahoo et al. 2009), although improving understanding of causation or driving factors is outside the scope of this research. Regardless, our results show that the heat balance approach used by the numerical model may overemphasize the influence of solar radiation and fail to capture the full influence of air temperature on longitudinal rates of heating, particularly at night when modeled heating rates are significantly lower than measured heating.

These results suggest that stream temperature data measured at higher resolution, such as DTS datasets, are helpful for re-examining the assumptions of stream temperature drivers. Considerable research exists on air- and insolation-water temperature relationships (Caissie 2006; Danehy et al. 2005; Mohseni and Stefan 1999; Webb and Nobilis 2007). Continuing research is needed to improve understanding of the role of air temperature in physically-based models, particularly at differing scales (stream temperature modeling at fine-, landscape-, or meso-scale may be driven by different processes and conditions). DTS datasets that provide abundant temperature data in space and time could be useful for exploring and calibrating such efforts.

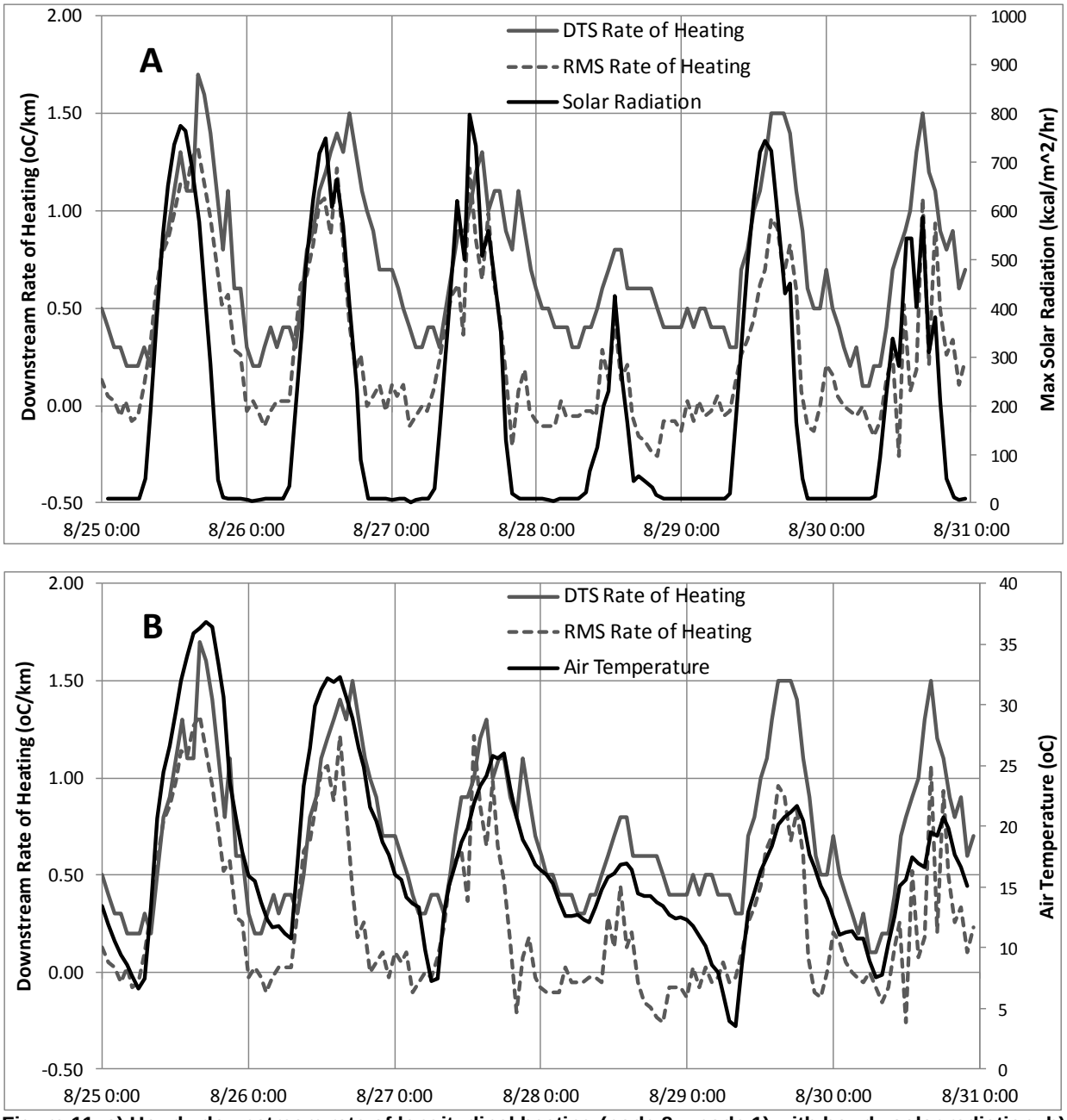

Figure 11. a) Hourly downstream rate of longitudinal heating (node 8 – node 1) with hourly solar radiation. b) Hourly downstream rate of longitudinal heating (node 8 – node1) with hourly air temperature

Limitations

Modeling provides the opportunity to explore hydrological processes as well as management alternatives, yet any modeling effort has limitations. Necessary simplification of physical processes and river geometry are inherent limitations to modeling river temperature. These have been described in greater detail for the Shasta River model elsewhere (Null 2008). For this study, an additional limitation is that upstream boundary condition data for the mainstem and Parks Creek Overflow (PCO) tributary were unavailable. Inability to develop a rating curve for mainstem flow due to excessive macrophyte growth and limited flow measurements introduced uncertainty in specifying the boundary condition for daily flow of the Shasta River. Although this affects the accuracy of the model to some degree, sensitivity analysis performed during model calibration show river temperatures are not very sensitive to this input. More importantly, DTS temperature data demonstrates that PCO inflow significantly affects downstream mainstem temperatures, therefore uncertainty in this inflow boundary condition reduces accuracy of modeled temperatures. This model could be further improved by measuring discharge for PCO and other small seeps that contribute flow to the mainstem and that may affect thermal variability.

Conclusions

River temperature datasets using DTS technology provide a rich opportunity to explore and compare measured and modeled river temperatures, and to improve model performance and development, post-process existing modeled temperature results, and refine our understanding of processes governing stream temperature heat budgets. Using DTS data for model input and to recalibrate the existing 2001 RMS stream temperature model for the Shasta River improved performance of modeled temperatures by reducing RMSE by almost 2.0°C. Increasing confidence in simulated temperatures can make models more useful and effective for evaluating temperature conditions and therefore management alternatives. DTS data helps improve model performance by providing high quality input and calibration data.

DTS datasets are also valuable for identifying and quantifying inflows from tail water, ungauged tributaries, side channels, and groundwater springs. DTS data helps identify mixing zones and in-stream thermal complexities to aid model node placement and frequency, thereby improving stream temperature model development. Side channels and groundwater seeps could be explicitly represented in future modeling studies if high resolution spatial data exits to define initial conditions, boundary conditions, and inform understanding of thermal dynamics.

Additionally, DTS data can be of value for better interpreting existing simulation results. Deterministic stream temperature models most often solve a one-dimensional problem simulating temperatures along the river's principal axis (Caissie 2006). This means areas of increased thermal variability and complexity are not well captured in modeled temperature results, as explored by this work. Measured DTS data can be used with existing simulation results to post-process a more realistic range of variability in stream temperature, especially when simulation results are used to assess habitat suitability or management alternatives. In these cases, the details regarding timing and measured temperature variations are important. This will help more realistically define potential thermal barriers to fish passage, thermal variability of micro-habitats, and more accurately capture the variety of temperature conditions present in rivers. Collecting DTS data after model development has utility and value for post-processing modeled temperature results and understanding local thermal variability in relation to the mainstem temperature.

Analysis of longitudinal heating of measured versus modeled temperatures revealed the overemphasis models such as RMS may place on solar radiation when estimating stream temperatures. This highlights the value of DTS data in revealing the strengths and weaknesses of heat budget representation in models. Although research generally indicates solar radiation is the most important factor driving heat flux (Johnson 2003), air temperature may still play a major role particularly with regards to the timing of longitudinal rates of heating. Future work should further explore representation of solar radiation and air temperature in physically-based temperature models to improve model performance, longitudinal heating rates, and more accurately model the timing and magnitude of daily maximum and minimum stream temperatures. DTS data can help refine our understanding of processes governing stream temperature heat budgets.

Acknowledgements
The fiber-optic distributed temperature sensing instrumentation and expertise were provided by the Center for Transformative Environmental Monitoring Programs (CTEMPs) at the Oregon State University and the University of Nevada, Reno. Data collected will be available through the CTEMPs Data Services Program. CTEMPs operates as an Affiliated Instrument Node of CUAHSI and is supported by the National Science Foundation's Division of Earth Sciences Instrumentation and Facilities Program (EAR/IF) under Cooperative Agreements EAR-0929638 and EAR-0930061.

References

Abbot, A. G. P. (2002). "The Effect of Riparian Vegetation on Stream Temperature in the Shasta River," U.C. Davis Dept. of Civil and Environmental Engineering, Master's thesis.

Arcement Jr., G. J., and Schneider, V. R. (1989). "Water-supply Paper 2339: Guide for Selecting Manning's Roughness Coefficients for Natural Channels and Flood Plains." United States Geological Survey.

Caissie, D. (2006). "The thermal regime of rivers: a review." *Freshwater Biology*, 51, 1389-1406.

Curtis, A., and Kyle, P. (2011). "Geothermal point sources identified in a fumarolic ice cave on Erebus volcano, Antarctica using fiber optic distributed temperature sensing." *Geophysical Research Letters*, 38, 7.

Danehy, R. J., Colson, C. G., Parrett, K. B., and Duke, S. D. (2005). "Patterns and sources of thermal heterogeneity in small mountain streams within a forested setting." *Forest Ecology and Management*, 208(287-302).

Fleckenstein, J. H., Krause, S., Hannah, D. M., and Boano, F. (2010). "Groundwater-surface water interactions: New methods and models to improve understanding of processes and dynamics." *Advances in Water Resources*, 33(11), 1291-1295.

GeoReports. (2011). "Temperature and Thermal Properties (Detailed)." Accessed Online, February 2011, British Geological Survey, http://shop.bgs.ac.uk/GeoReports/examples/modules/C011.pdf.

Hauser, G. E., and Schohl, G. A. (2002). "River Modeling System v4 - User Guide and Technical Reference." Report No. WR28-1-590-164; TVA River System Operations and Environment, Norris, Tennessee; May.

Hoes, O. A. C., Schilperoort, R. P. S., Luxemburg, W. M. J., Clemens, F., and de Giesen, N. C. V. (2009). "Locating illicit connections in storm water sewers using fiber-optic distributed temperature sensing." *Water Research*, 43(20), 5187-5197.

Jeffres, C., Dahlgren, R., Kiernan, J., King, A., Lusardi, R., Nichols, A., Null, S., Tanaka, S., and Willis, A. (2009). "Baseline Assessment of Physical and Biological Conditions Within Waterways on Big Springs Ranch, Siskiyou County, California." Report Prepared for: California State Water Resources Control Board.

Johnson, S. L. (2003). "Stream temperature: scaling of observations and issues for modelling." *Hydrological Processes*, 17, 497-499.

Keller, C., Huwald, H., Vollmer, M., Wenger, A., Hill, M., Parlange, M., and Reimann, S. (2011). "Fiber optic distributed temperature sensing for the determination of the nocturnal atmospheric boundary layer height." *Atmospheric Measurement Techniques*, 4(2).

Khan, A. A., Vrabie, V., Mars, J. I., Girard, A., and D'Urso, G. (2010). "Automatic Monitoring System for Singularity Detection in Dikes By DTS Data Measurement." *Instrumentation and Measurement, IEEE Transactions on*, 59(8), 2167-2175.

Lowry, C. S., Walker, J. F., Hunt, R. J., and Anderson, M. P. (2007). "Identifying spatial variability of groundwater discharge in a wetland stream using a distributed temperature sensor." *Water Resour. Res.*, 43(10), W10408.

Macfarlane, P. A., Forster, A., Merriam, D. F., Schrotter, J., and Healey, J. M. (2002). "Monitoring artificially stimulated fluid movement in the Cretaceous Dakota aquifer, western Kansas." *Hydrogeology Journal*, 10(6), 662-673.

Mackey, A. P., and Berrie, A. D. (1991). "The Prediction of Water Temperatures in Chalk Streams From Air Temperatures." *Hydrobiologia*, 210(3), 183-189.

Moffett, K. B., Tyler, S. W., Torgersen, T., Menon, M., Selker, J. S., and Gorelick, S. M. (2008). "Processes controlling the thermal regime of saltmarsh channel beds." *Environmental Science & Technology*, 42(3), 671-676.

Mohseni, O., and Stefan, H. G. (1999). "Stream temperature air temperature relationship: a physical interpretation." *Journal of Hydrology*, 218(3-4), 128-141.

Moyle, P. (2002). *Inland Fishes of California: Revised and Expanded*, University of California Press, Berkeley and Los Angeles.

Myrick, C. A., and Cech Jr., J. J. (2001). *Temperature effects on Chinook salmon and steelhead: a review focusing on California's Central Valley populations*, University of California Press, Davis, CA.

NMFS. (1997). "Proposed Rules: Designated Critical Habitat; Central California Coast and Southern Oregon/Northern California Coast Coho Salmon." N. M. F. S. N. O. a. A. Administration, ed.

NRC. (2004). "Endangered and Threatened Fishes in the Klamath River Basin Causes of Decline and Strategies for Recovery." N. R. Council, ed., National Academies Press, Washington DC.

Null, S. (2008). "Improving Managed Environmental Water Use: Shasta River Flow and Temperature Modeling," University of California, Davis.

Null, S. E., Deas, M. L., and Lund, J. R. (2010). "Flow and Water Temperature Simulation for Habitat Restoration in the Shasta River, California." *River Research and Applications*, 26(6), 663-681.

Roth, T. R., Westhoff, M. C., Huwald, H., Huff, J. A., Rubin, J. F., Barrenetxea, G., Vetterli, M., Parriaux, A., Selker, J. S., and Parlange, M. B. (2010). "Stream Temperature Response to Three Riparian Vegetation Scenarios by Use of a Distributed Temperature Validated Model." *Environmental Science & Technology*, 44(6), 2072-2078.

Sahoo, G. B., Schladow, S. G., and Reuter, J. E. (2009). "Forecasting stream water temperature using regression analysis, artificial neural network, and chaotic non-linear dynamic models." *Journal of Hydrology*, 378(3-4), 325-342.

Selker, J. S., Thevenaz, L., Huwald, H., Mallet, A., Luxemburg, W., van de Giesen, N., Stejskal, M., Zeman, J., Westhoff, M., and Parlange, M. B. (2006a). "Distributed fiber-optic temperature sensing for hydrologic systems." *Water Resources Research*, 42, W12202, doi:10.1029/2006WR005326.

Selker, J. S., van de Giesen, N., Westhoff, M., Luxemburg, W., and Parlange, M. B. (2006b). "Fiber optic opens window on stream dynamics." *Geophysical Research Letters*, 33(L24401).

Slater, L. D., Ntarlagiannis, D., Day-Lewis, F. D., Mwakanyamale, K., Versteeg, R. J., Ward, A., Strickland, C., Johnson, C. D., and Lane, J. W. (2010). "Use of electrical imaging and distributed temperature sensing methods to characterize surface water-groundwater exchange regulating uranium transport at the Hanford 300 Area, Washington." *Water Resources Research*, 46, 13.

Steele-Dunne, S. C., Rutten, M. M., Krzeminska, D. M., Hausner, M., Tyler, S. W., Selker, J., Bogaard, T. A., and de Giesen, N. C. V. (2010). "Feasibility of soil moisture estimation using passive distributed temperature sensing." *Water Resources Research*, 46, 12.

Tyler, S. W. (2009). "New User Facility for Environmental Sensing." EOS Vol. 90 No. 50.

Tyler, S. W., Burak, S. A., McNamara, J. P., Lamontagne, A., Selker, J. S., and Dozier, J. (2008). "Spatially distributed temperatures at the base of two mountain snowpacks measued with fiber-optic sensors." *Journal of Glaciology*, 54(187), 673-679.

Tyler, S. W., Selker, J. S., Hausner, M. B., Hatch, C. E., Torgersen, T., Thodal, C. E., and Schladow, S. G. (2009). "Environmental temperature sensing using Raman spectra DTS fiber-optic methods." *Water Resources Research*, 45, W00D23, doi:10.1029/2008WR007052.

Vercauteren, N., Huwald, H., Bou-Zeid, E., Selker, J. S., Lemmin, U., Parlange, M. B., and Lunati, I. (2011). "Evolution of superficial lake water temperature profile under diurnal radiative forcing." *Water Resources Research*, 47, 10.

Vogt, T., Schneider, P., Hahn-Woernle, L., and Cirpka, O. A. (2010). "Estimation of seepage rates in a losing stream by means of fiber-optic high-resolution vertical temperature profiling." *Journal of Hydrology*, 380(1-2), 154-164.

Ward, M., and Eaves, N. (2008). "Groundwater Data Needs Assessment." California Department of Water Resources.

Webb, B. W., and Nobilis, F. (2007). "Long-term changes in river temperature and the influence of climatic and hydrological factors." *Hydrological Sciences Journal*, 52(1), 74-85.

Westhoff, M. C., Bogaard, T. A., and Savenije, H. H. G. (2010). "Quantifying the effect of in-stream rock clasts on the retardation of heat along a stream." *Advances in Water Resources*, 33(11), 1417-1425.

Westhoff, M. C., Gooseff, M. N., Bogaard, T. A., and Savenije, H. H. G. (2011). "Quantifying hyporheic exchange at high spatial resolution using natural temperature variations along a first-order stream." *Water Resources Research*, 47, 13.

Westhoff, M. C., Savenije, H. H. G., Luxemburg, W. M. J., Stelling, G. S., van de Giesen, N. C., Selker, J. S., Pfister, L., and Uhlenbrook, S. (2007). "A distributed stream temperature model using high resolution temperature observations." *Hydrology and Earth System Sciences*, 11(4), 1469-1480.

Yamano, M., and Shusaku, G. (2005). "Long-term monitoring of the temperature profile in a deep borehole: Temperature variations associated with water injection experiments and natural groundwater discharge." *Physics of the Earth and Planetary Interiors*, 152, 326-334.

Chapter 3: Understanding Shasta Valley Groundwater through Numerical Simulation Modeling

Abstract

This chapter describes the development and calibration of a numerical groundwater model of the Pluto's Cave basalt aquifer and Parks Creek valley area in the eastern portion of Shasta Valley. This modeling effort produces an improved conceptual model of this fracture flow dominated aquifer. Model development provides insight on system dynamics, helps identify important and influential components of the system, and highlights additional data needs.

The objective of this model development is to reasonably represent regional groundwater flow, spring flow, and pumping and to explore the interaction between Mount Shasta recharge, pumping, and Big Springs flow. The model organizes and incorporates available data from a wide variety of sources and presents approaches to quantify the major flow paths and fluxes. Major water balance components are estimated for 2008-2011. Three calibrated steady state model scenarios using 2008 inputs explore the effects of varying amounts of groundwater flow across the model domain's northern and western boundaries, since this is a source of significant uncertainty. Sensitivity analysis assesses the degree to which uncertainty in boundary flow affects model results, particularly spring flow.

Background

Cascade hydrogeology

A significant body of work has explored the hydrogeology of the Cascade Range, mainly focused in Oregon (James and Manga 2000; Jefferson et al. 2006; Nathenson et al. 2003; Saar and Manga 1999; Tague et al. 2007; Tague and Grant 2004). Two geologic series describe the rocks of the Cascades and are present in the study area: the Western Cascades and the High Cascades (Figure 12). The Western Cascades are Tertiary in age and tend to have lower permeability than the younger basalt flows of the High Cascades. The High Cascades are Pleistocene to Holocene in age and are characterized by spring-fed rivers and young basalt aquifer systems with high transmissivities and large portions of precipitation recharging groundwater flow systems (Jefferson et al. 2006; Mack 1960). The Western Cascades tend to have shallow subsurface flow paths along steep gradients with high horizontal conductivities, whereas the behavior of the High Cascades reflects a deeper groundwater system (Tague and Grant 2004). The geology and geomorphology of these basins play a dominant role on flow patterns related to peak timing and magnitude of stream flow (Tague et al. 2007). The timing and shape of stream flow hydrographs and summer monthly stream flow volumes are related to the percentage of High Cascade geology in the contributing area (Tague and Grant 2004). Other work suggests recharge areas in the Cascades can extend beyond modern topographic boundaries (Jefferson et al. 2006). Well logs from the Oregon Cascades drilled in Quaternary lavas recorded static water levels higher than the elevation where water was first encountered during drilling suggesting the High Cascades aquifer system behaves as a confined aquifer, at least in some areas (Jefferson et al. 2006).

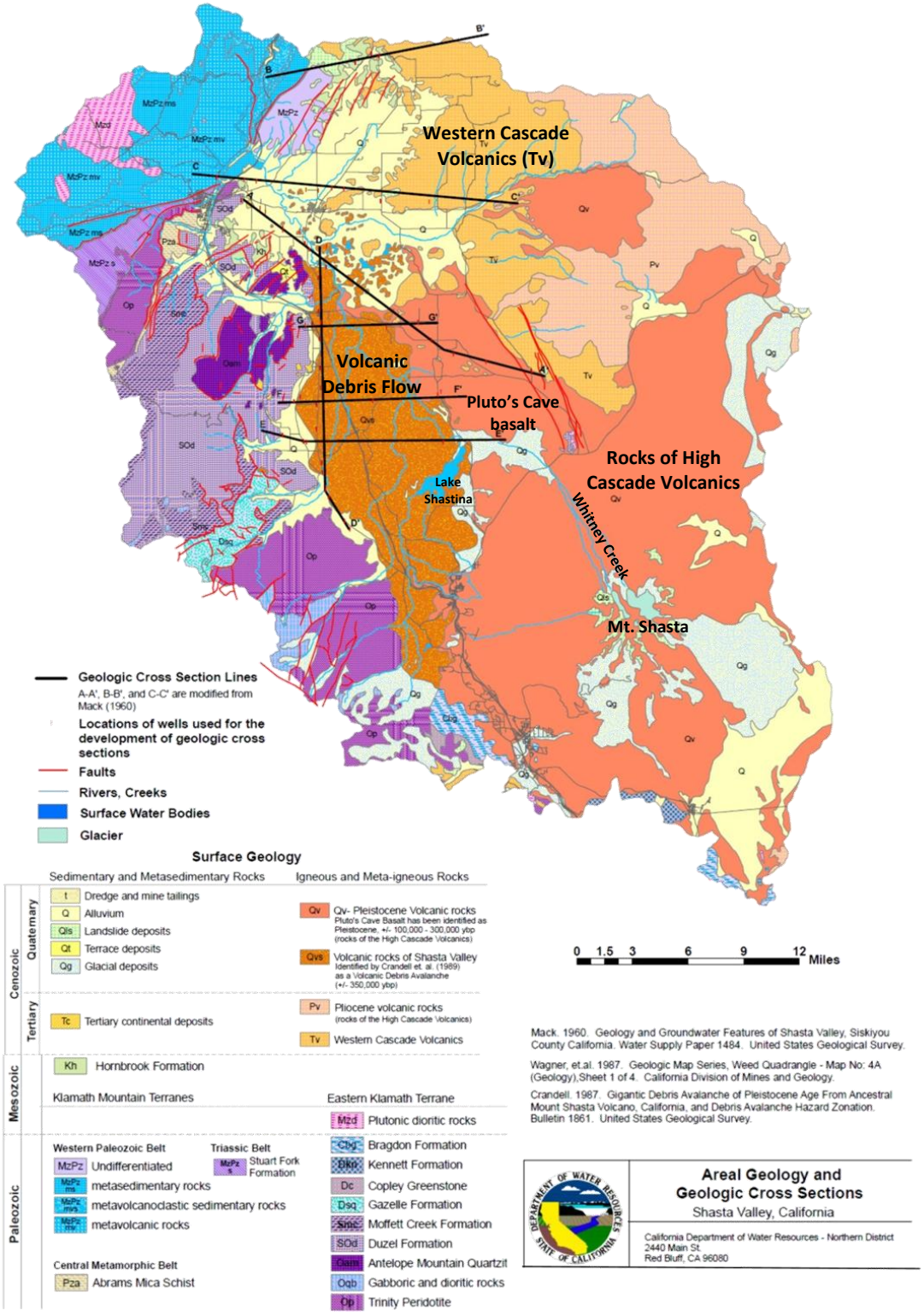

Figure 12. Areal geology of Shasta Valley area, Department of Water Resources (adapted from Ward and Eaves 2008)

A combination of approaches involving water quality, isotopic tracers, age dating, water balance estimations, stream flow time series analysis, water temperature of springs, and simple conceptual modeling is widely used in Cascade hydrogeology and groundwater research (James and Manga 2000; James et al. 2000; Jefferson et al. 2007; Jefferson et al. 2010; Jefferson et al. 2006; Manga 1996; Manga 1997; Manga 1999; Manga 2001; Manga and Kirchner 2004; Nathenson et al. 2003; Saar et al. 2005; Saar and Manga 1999; Tague and Grant 2004). The United States Geological Survey (USGS) has conducted a groundwater study of the Deschutes Basin (located in Central Oregon) involving development of a steady state numerical flow model (MODFLOW) and subsequently construction and calibration of a transient groundwater flow model (Gannett and Lite 2004). The Pluto's Cave aquifer in the Shasta Valley shares many of the characteristics described for other regions of the Cascade Range. This study uses available information specific to the Shasta Valley with general understanding of Cascade hydrogeology derived from other studies in the region.

Study area hydrogeology

The Shasta River watershed is a geologic mix of coastal range alluvial valley, volcanic debris flow, and basalt flows (Figure 12). The model domain is the Pluto's Cave basalt aquifer in the southeastern portion of Shasta Valley (Figure 13). Sources conflict on the origins of the Pluto's Cave basalt. According to a recent Department of Water Resources (DWR) groundwater assessment report (Ward and Eaves 2008), Deer Mountain and Whaleback Mountain provide the source of its volcanic flows (Figure 13). According to Mack (1960), the Pluto's Cave basalt flowed from fissures on the northeastern slopes of Mount Shasta and spread over the southeasterly quarter of the valley as a series of flow layers (Fairchild and McClurg 1964; Mack 1960). Blodgett et al (1988) indicate the basalt flows in the Juniper Flats area came from fissures near the northwestern base of Mount Shasta (Figure 13). The conceptual model for this effort assumes Mt. Shasta is the primary source of the basalt and main recharge area for the basalt aquifer.

Marine sedimentary rocks of the Hornbrook Formation and volcanic debris flow underlie the basalt (Ward and Eaves 2008) (Figure 14). The volcanic debris flow (older than basalt flows) resulted from a debris avalanche from Mount Shasta. It is composed of a block and matrix facies of volcanic rocks and fine sandy ash-rich material, respectively. Its chaotic deposition leads to a lack of internal structure and low

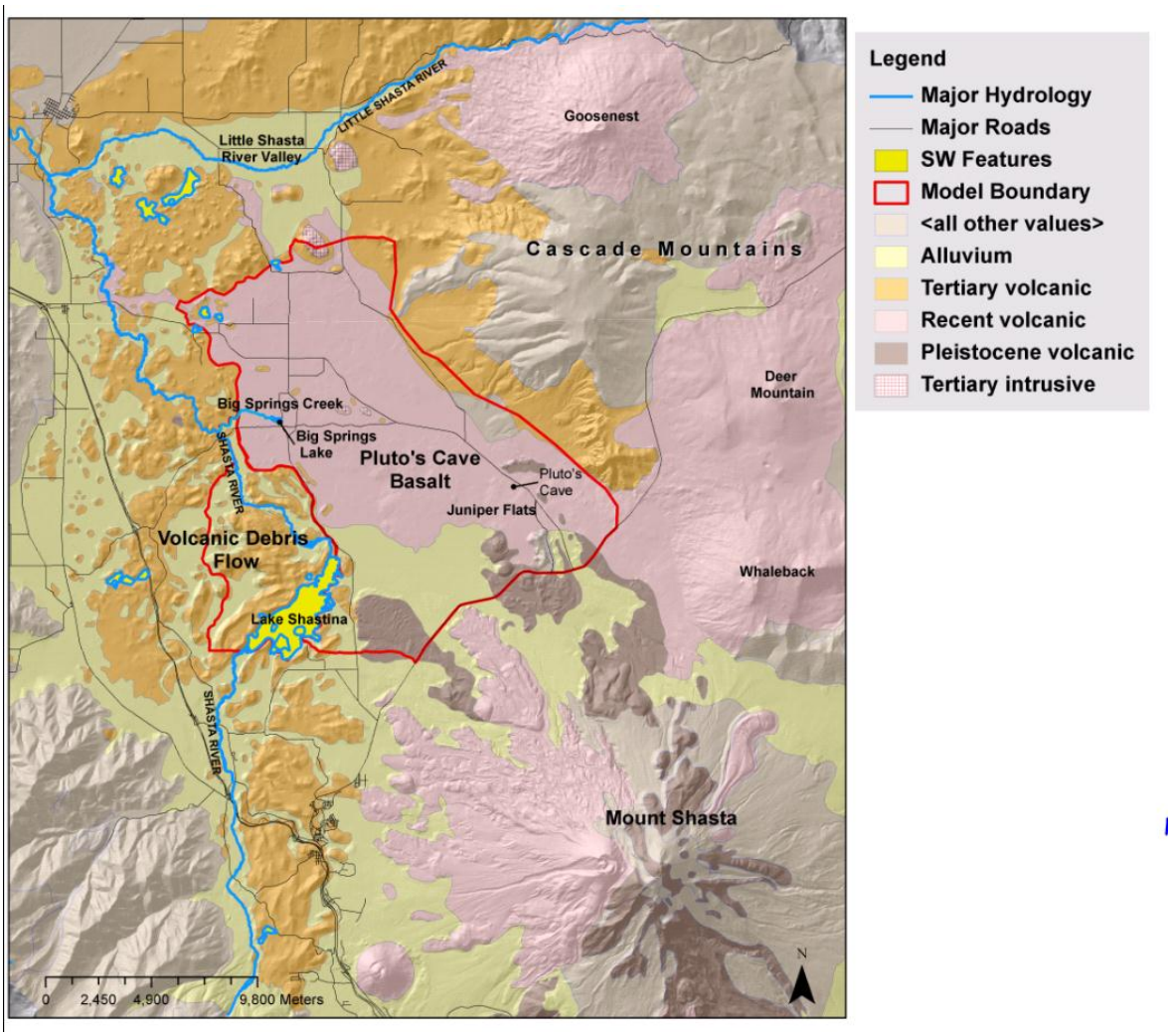

Figure 13. Shasta Valley geology and major features of interest

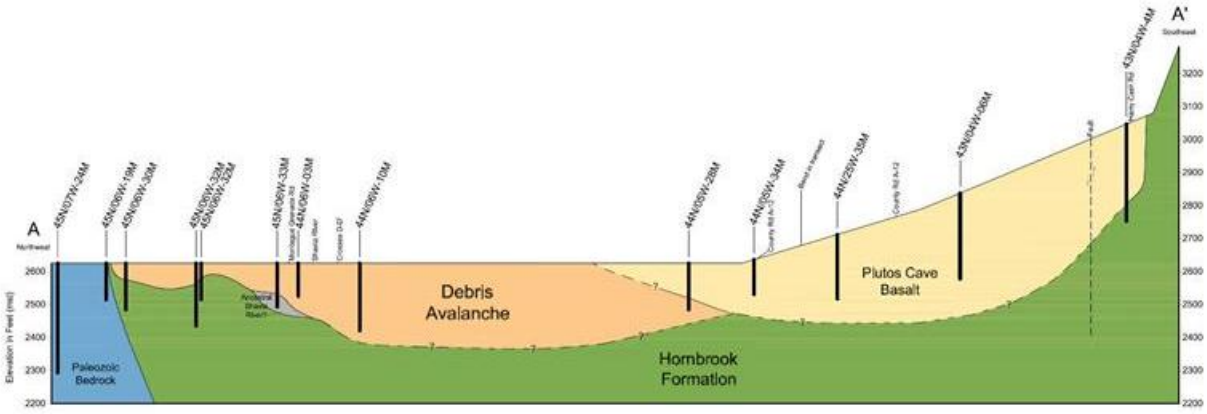

Figure 14. DWR Geology cross-section A' (adapted from Ward and Eaves 2008)

permeability and is reported by Ward and Eaves (2008) to serve as a boundary impeding groundwater flow from the basalt, thereby giving rise to numerous springs along the contact between the formations. Mack (1960) suggests the rocks of the Western Cascades (what is now known and understood to be the debris flow material) do not form barriers to groundwater movement in the valley, except perhaps locally. Its ability to convey water is most strongly evidenced by the high leakage rates through the western wall of Lake Shastina (Dwinnell Dam). However, compared to the high conductance potential of the Pluto's Cave basalt (part of the High Cascade series), the debris flow material appears to hinder groundwater flow, causing locations of significant spring flow (for example, Big Springs Lake and Alcove Springs in Big Springs Creek) (Figure 13). Previous work suggests this spring water is slightly thermal (higher temperature, indicating high recharge elevations, above 2500m) and likely interacts with marine sediments at depth giving it elevated levels of nitrate, phosphate, chloride and sulfate (McClain 2008; Nathenson et al. 2003). Water quality samples from data reported in Mack (1960) show the Pluto's Cave basalt contains the highest average concentration of silica, 63 ppm, of waters in the valley which may be partly from the pyroclastic debris and glacial outwash deposits of the recharge area on the north slopes of Mt. Shasta. In contrast, water draining the andesitic rocks of the debris flow material has an average of 45 ppm of silica.

The Pluto's Cave basalt ranges from 2-3 m thick to more than 240 m thick in some areas (Blodgett et al. 1988). Near Big Springs, it is reportedly about 30 m thick (Fairchild and McClurg 1964) and thins to the west. Though in this area especially, its thickness is variable. The lava flow contains many large lava tubes (including Pluto's Cave) and many drillers' logs report loss of circulation which may indicate voids or inter-basalt rubble zones (Blodgett et al. 1988). DWR Bulletin 87 (1964) describes groundwater in the basalt aquifer as "transmitted along the vesicular contacts between flow layers, through joints and fractures within the flow, and through open and collapsed lava tubes where these occur below the water table." High producing wells generally occur in the vicinity of Big Springs and at the northern terminus of the basalt near the Little Shasta River (Mack 1960). In contrast, wells in the Juniper Flat area have low yields and depth to water can be 210 m below ground surface (Blodgett et al. 1988). Mack (1960) describes the hydraulic gradient throughout the valley with the greatest slope between Mt. Shasta and Lake Shastina in the glacial material having a northwestward slope of 28 m/km due to the steep terrain or low permeability, or both. The next steepest gradient occurs sloping northwest immediately west of Lake Shastina (19 m/km) which likely reflects recharge to the volcanic rocks from the reservoir. Little Shasta Valley has a hydraulic gradient of 5.7 m/km and the Big Springs area in the Pluto's Cave basalt only 4.7 m/km (Mack 1960). A number of factors including flow, aquifer thickness, recharge, and hydraulic conductivity affect the gradient.

Surface water and groundwater sources

The Pluto's Cave basalt conducts large volumes of water presumably recharging from snowfall and spring and stream discharge from Mount Shasta (Ward and Eaves 2008). Whitney Creek is an ephemeral stream draining snow and glacial melt from the north side of Mt. Shasta and recharging the aquifer, as its flow never connects to another surface water feature (Figure 12). In the summer of 1981, measurements indicated Whitney Creek lost flow to groundwater at a rate of 0.005 $m^3s^{-1}km^{-1}$ (Blodgett et al. 1988).

The connection between surface and groundwater is explicit in this system where day-lighting groundwater creates a river at its source at Big Springs Creek. Surface water diversions and groundwater pumping provide water for irrigating pasture, alfalfa, and a variety of other crops in the valley. Well yields in the basalt range from 380-15,000 liters per minute (100-4000 gpm) with an average of 4,900 L/min (1300 gpm) (Fairchild and McClurg 1964). Therefore, spring flow and groundwater pumping are notable groundwater outflows from the basalt aquifer.

The extent to which pumping and spring flow are related is less clear. The most well-known and semi-documented connection between groundwater pumping and spring discharge occurs between Big Springs and Montague Water Conservation District's (MWCD) pumping wells and the Big Springs complex that largely sustains Shasta River flows during summer months. The upper portion of the Big Springs complex is dammed and forms a small lake (Big Springs Lake, Figure 21A) from which riparian users divert water for flood irrigation. A court ruling against MWCD in the 1980s requires them to stop pumping if lake levels drop such that water cannot be diverted into riparian users' canals. This has

occurred several times since then. A collection of springs that are part of the Big Springs complex but downstream of the small lake (Alcove springs) yield about 1.1 m^3s^{-1} and remain fairly constant through the irrigation season (Jeffres et al. 2009). These springs seem to be unaffected by current pumping. Other smaller springs along the river and distant springs contribute cold water but their effect on river temperatures and effects of pumping on them is less clear and not documented.

Additionally, Lake Shastina (Dwinnell Dam), upstream on the Shasta River, stores water for surface diversions and induces large amounts of recharge into the groundwater basin (Deas 2009, Pers. comm.; Dong et al. 1974; Vignola and Deas 2005). Irrigation canals conveying water throughout the valley also recharge significant volumes of water. The Parks Creek valley to the northwest of Lake Shastina has numerous springs and seeps connecting to Parks Creek and the Shasta River. Bridge Field springs, Black Meadow springs, and an unnamed spring mapped by Mack (referred herein as the Mack spring) are located along the western base of the ridge forming the western wall of Lake Shastina (Figure 21B). Springs in this area are said to have increased in flow rate after the construction of the reservoir (Mack 1960). Kettle Springs also sits at the base of a debris flow ridge and flows into Parks Creek, when not diverted for irrigation. Spring flow, as well as diversions from Parks Creek and the Shasta River, provide for irrigating pasture in the Parks Creek valley and along the Shasta River between the dam and confluence with Big Springs Creek.

Existing water budget

Mack (1960) estimates the annual volume of groundwater outflow from the valley for 1953. The major mechanisms of outflow include net pumpage for irrigation, evapotranspiration (ET) from sub-irrigated lands, discharge from Big Springs, and groundwater discharge to the Shasta River (Table 3). His water balance reveals the significant contribution of sub-irrigated lands and the relatively small amount of pumping in the 1950s.

Table 3. Mack estimate of groundwater discharge from Shasta Valley in Million Cubic Meters (MCM), 1953 water year (Mack 1960, p. 65)

Description	Volume (MCM)
Net Pumpage	5
ET from sub-irrigated lands	35
Discharge from Big Springs	37
GW discharge to Shasta River	86

Conceptual model

The hydrogeology and surface water features, as described, form the basis for the conceptual model. The primary water bearing unit is the Pluto's Cave basalt and therefore is the focus of the one-layer numerical model domain (Figure 13). This approach assumes no interaction or groundwater flow with or between underlying units. Near Mount Shasta, the general direction of groundwater flow is understood to be from the southeast to the northwest and then westward toward the Shasta River, with Mount Shasta serving as the primary recharge source of the aquifer. Smaller sources of recharge include leakage from Lake Shastina and from water districts' irrigation canals, and deep percolation of applied water during the irrigation season. In the rain shadow of Mount Shasta, the valley is a high desert environment with hot, dry summers and cool winters. Due to low precipitation on the valley floor (33 to 38 cm in the low elevation areas of the valley), little recharge from deep percolation from precipitation occurs. Spring flow is the primary groundwater outflow with agricultural pumping being a more minor outflow. Some groundwater flow between the basalt and the debris flow material is likely, although to what degree is unknown. Hence, this aspect is further explored with the numerical model.

Modeling approaches

Several approaches have been employed to represent aquifers with fractured rock and preferential flow paths in numerical modeling schemes. Modeling fractures or fracture dominated aquifers often use one of two main conceptual models: the discrete fracture model, or the equivalent continuum model (Blessent et al. 2009). In some cases these approaches are combined (Rubin et al. 2004; Van der Hoven et al. 2002). Discrete fracture modeling represents individual fractures explicitly and requires fracture

characteristics such as aperture, length, orientation, and distribution. In this way discrete fracture networks reflect the physical properties of the rocks (Graf and Therrien 2008). Numerous studies have used this approach both to explore the theory of fluid flow and transport (Blessent et al. 2009; Graf and Therrien 2009; Wang and Kulatilake 2008) and also for practical case study applications of contaminant transport and waste disposal (Graf and Therrien 2008; Grenier et al. 2009; Kristinof et al. ; Ophori 2004; Rubin et al. 2004). The disadvantage of discrete fracture modeling is the detail of required data. Many studies that model discrete fractures explore theoretical systems or have case studies where multiple efforts and decades of geophysical data have been collected. Alternatively, stochastic generation of fracture realizations are used to deal with uncertainty (Grenier et al. 2009; Hu et al. 2002; Wang and Kulatilake 2008).

The equivalent continuum model (also referred to as equivalent porous media model, distributed parameter model, single continuum approach, or heterogeneous continuum approach) is based on the groundwater flow equation (Shoemaker et al. 2008). The dual porosity nature of the aquifer, comprised of distinct flow paths or fractures in combination with less hydraulically conductive matrix material, is not explicitly represented. However, this approach has been successful in several studies (Gannett and Lite 2004; Scanlon et al. 2003). Modeling karstic processes (similar to basaltic aquifers with conduits and fractures) with equivalent porous media models has been shown to effectively simulate regional groundwater flow including spring discharge and hydraulic heads; however, they often fail to correctly predict aspects of transport like flow direction and velocity (Angelini and Dragoni 1997; Scanlon et al. 2003). Scanlon et al (2003) compare lumped parameter and distributed parameter models of the Barton Springs segment of the Edwards Aquifer in Texas and their ability to simulate regional groundwater flow. From a management perspective, they are concerned with maintaining spring flow during droughts and assessing current and future pumping effects on spring flow. Their lumped parameter model represents each of five creeks contributing recharge to the aquifer as a single cell with connections between them. It fairly accurately simulates variable spring flow over time, but as a lumped parameter model does not model the potentiometric surface in space. The distributed parameter model is a single layer steady state and transient model developed in MODFLOW-1995 calibrated by trial and error and use of inverse methods. Results show the ability of both the lumped and distributed parameter model to simulate regional groundwater flow, however they point out the necessity of the distributed parameter model for more local evaluation of pumping effects on spring flow (Scanlon et al. 2003).

In accordance with Scanlon et al. (2003) and with the fact that the fracture systems in the Pluto's Cave basalt formation are numerous and well connected on a regional scale, this modeling effort uses MODFLOW and an equivalent porous media modeling approach to organize water balance components and test our conceptual model of the Pluto's Cave basalt aquifer. The objective of this model development is to simulate regional groundwater flow including recharge, spring flow, and pumping. The modeling focuses on the Big Springs area and leakage from Lake Shastina. The process serves to organize and analyze existing groundwater data of Shasta Valley and helps identify what is unknown. It also captures our current understanding and conceptual model of the system with a mathematical model that can yield insights on system dynamics. The model is used to explore interactions between pumping, recharge, and spring flow.

Data sources

Most data input to the groundwater model are derived from publicly available data sources, many accessible online. The following websites are a few general sources providing useful data: California Spatial Information Library (CaSIL), Klamath Resource Information System (KRISWEB), California Data Exchange Center (CDEC), California Water Data Library (WDL), Parameter-elevation Regressions on Independent Slopes Model (PRISM), USGS GAP analysis program (GAP), and USGS Seamless Data Warehouse. Data and insights were also made available by a number of people through University of California Cooperative Extension (UCCE), Department of Water Resources (DWR), Shasta Valley Resource Conservation District (RCD), and UC Davis Center for Watershed Sciences (UCD CWS). They are in no way responsible however for this work or the results and interpretations herein.

Table 4. Data types and sources

Type	Source
Atmospheric - precipitation, snow course, ET, sublimation	CIMIS, CDEC, PRISM
Agricultural water use - ET, district boundaries, irrigation efficiency	CIMIS, CaSIL, UCCE
Land use - cropping patterns and water source per field	DWR land use survey
Land cover	GAP
Shasta River flow data	USGS gauges, UCD CWS
Lake Shastina - stage and storage	CDEC
Subsurface geology	DWR
Groundwater levels	DWR WDL
Spring flows	UCD CWS
Soils - properties and characteristics	SSURGO
DEM for the watershed	USGS seamless
Aerial Photos	CaSIL

Model description

Model development includes an unconfined steady state MODFLOW model for 2008 and data input for a four year transient model, 2008-2011 developed using Groundwater Vistas. The one-layer model grid is 200 x 210 elements with 100 meter square grid cells. A subset of the 42,000 cells are active cells with the rest designated as not active (no flow). Model units are meters and years.

The boundary conditions outline the active model domain in Figure 15. General head boundaries (GHB) define the northern and a portion of the western edge of the active model. A constant head boundary defines the Lake Shastina area and the River Package is used to represent the Shasta River below Dwinnell Dam and Parks Creek along the western boundary south of Big Springs Creek confluence with the Shasta River. A constant flux boundary defines the southeastern boundary comprised of 154 'wells' that distribute recharge originating from Mount Shasta precipitation. The eastern edge has a specified flux of zero making this a no flow boundary. Other wells within the model area represent irrigation (pumping) wells or irrigation canals that recharge groundwater to the aquifer (injection wells). The Drain Package represents eleven of the major springs in the model domain and Big Springs Creek. The modeled springs include: Big Springs Lake complex, Alcove springs complex, Little Springs, Hole in the Ground, Clear Spring, Hidden Valley Spring, Kettle Springs, Black Meadow Springs, Bridge Field Springs, Mack Spring, and spring-fed lakes in the northwestern corner of the model domain.

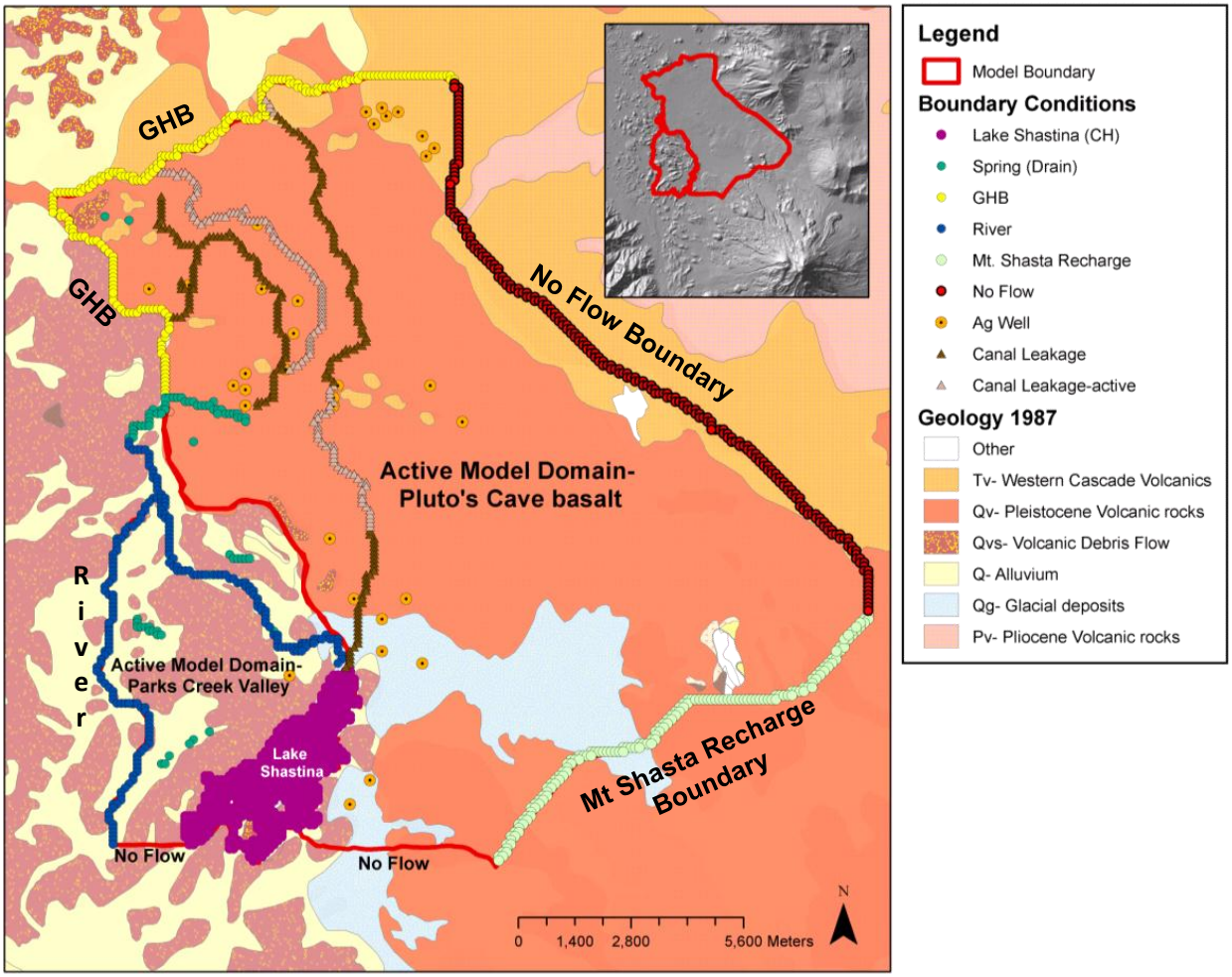

Figure 15. Study area geology and model boundary conditions

The model's top elevation is based on ground surface elevation as specified by a NED 1/3 arc second (10 meter) raster of elevation in ArcMap. The intersect point tool (from suite of Hawth's tools) is used to assign an elevation from the raster to each node of the model grid. Well logs were evaluated to estimate the thickness of the basalt at points based on township, range, and section of the wells throughout the model domain. These point estimations were interpolated to create a shapefile layer of bottom elevations which was imported into Groundwater Vistas. Some additional adjustments to the bottom elevation were made to increase the model thickness for numerical stability, specifically in the southeast area.

Locations with known or estimated groundwater head were used to interpolate static water levels throughout the model domain. Sampling the raster at each model node location assigned an initial head to each model element. In some cases, interpolated initial heads were above the ground surface elevation. These were adjusted to be 10 meters less than the ground surface elevation of the model node.

The following sections describe development of boundary conditions in detail.

Lake Shastina – constant head

Lake Shastina loses considerable amounts of water to groundwater, especially when the lake is full. Leakage is primarily through the lake's northwestern wall, comprised of debris flow material (Dong et al. 1974; Vignola and Deas 2005). The Parks Creek valley has numerous seeps and springs. The flow rate

of those along the base of the volcanic ridge forming the lake's northwestern wall increased after the construction of the reservoir (Mack 1960).

To simulate this hydrologic feature, a constant head boundary is assigned to all model elements overlying the geographic extent of the reservoir. The volume of leakage is calibrated by adjusting the hydraulic conductivity of the lake's northwestern ridge (zone 1, Figure 20). By using a constant head boundary with the defined topography, the simulated lake "leaks" to the northwest through the side of the reservoir rather than only leaking out the bottom as would be the case using MODFLOW's Lake or River Package. The average annual stage of the lake is specified as the constant head for each water year (Table 5). This is calculated by averaging reservoir elevation data obtained from CDEC for Dwinnell Reservoir near Edgewood (station DRE). This is a simplification since the lake level changes throughout the year (Figure 16) as it fills with snowmelt and winter runoff and is drained during the irrigation season primarily to supply the Montague Water Conservation District's (MWCD) canal. Future development could expand the numerical model to have quarterly or monthly time steps to better capture effects of lake level dynamics and lake interaction with the aquifer.

Table 5. Lake Shastina annual average lake elevation, 2008-2011

Water Year	Stage (m)
2008	847
2009	846
2010	848
2011	851

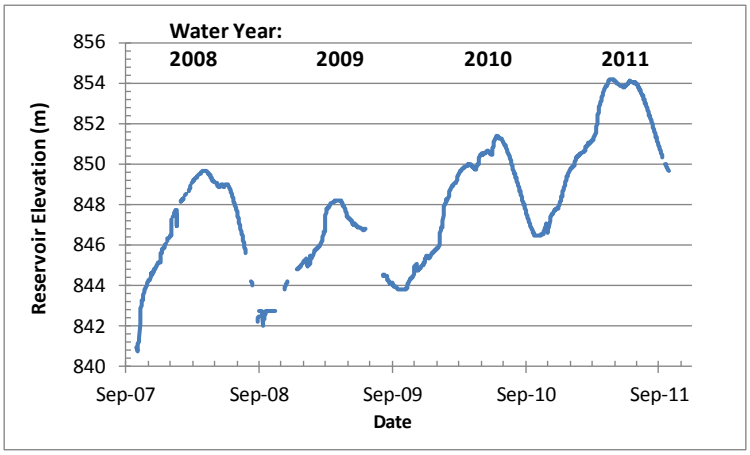

Figure 16. Average daily Lake Shastina elevation (meters). Breaks indicate missing or questionable data.

Parks Creek and Shasta River – river boundary

The River Package (RIV) is meant to simulate the effects of flow between surface water features and the groundwater system (Harbaugh 2005). Each river reach represents the stretch of river corresponding to a model cell. Thus aquifer seepage is simulated between the reach and the model cell that contains that reach. Flow between the river and the groundwater system is given by

$$QRIV_n = CRIV_n(HRIV_n - h_{i,j,k})$$

Where:
$QRIV_n$ is the flow between the river and the aquifer
$HRIV_n$ is the water level in the river
$CRIV_n$ is the hydraulic conductance of the river-aquifer interconnection
$h_{i,j,k}$ is the head at the node in the cell underlying the river reach (from Harbaugh (2005))

Using the River Package, Parks Creek and the Shasta River are represented by 205 adjacent model elements. River Package cells are located near the course of the river in the model cell with the lowest top elevation such that the river is properly located along the geographic lows in the model. The river stage is set to 1 meter below the top elevation in the model cell and the river bottom is 1 meter below the stage elevation. Additional elevation surveying and data on river width and depth would improve the representation of these rivers in the groundwater model. A simple representation is employed here (Table 6). Domenico and Schwartz (1997) gives a hydraulic conductivity range of 10^{-3} – 10^{1} m/d for course sand. Hydraulic conductivity of 10 m/d is assigned to reflect the presence of sand and some gravel composing the river bed. This is also a calibration parameter.

Table 6. River package inputs

River	K (m/d)	Width (m)	Thickness (m)
Shasta River	10	9	1.5
Parks Creek	10	4	1

Mount Shasta recharge – constant flux boundary

A specified flux boundary follows Highway 97 and distributes recharge from Mount Shasta precipitation over the length of this boundary (154 grid cells). This is considered to be the main recharge source for the Pluto's Cave aquifer. The north side of Mount Shasta does not have surface water drainage, so precipitation is either consumed by vegetation, sublimated, or recharges to groundwater. A recharge zone is defined in ArcMap based on DWR defined subareas and understanding of the basin (Figure 17). The general method to estimate total recharge from Mount Shasta is to calculate precipitation volume over the defined zone, estimate evapotranspiration (ET) from native vegetation, and estimate a sublimation rate as a percentage of total precipitation. Total recharge is then calculated by subtracting the volume of ET and sublimation from the total precipitation. This volume for each water year, 2008-2011, is divided by the number of grid cells along this boundary (154) to establish the injection rate of wells in MODFLOW (Table 9). The following describes the basis for estimating annual precipitation, ET, and sublimation volumes.

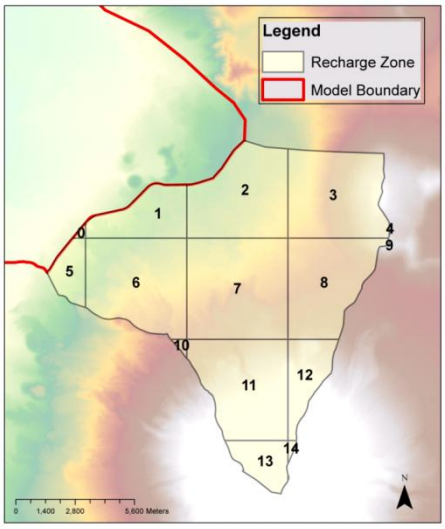

Figure 17. Mount Shasta recharge zone

Monthly precipitation data was downloaded from PRISM data available online for 2007-2011 (PRISM 2010). Using raster addition in ArcMap, a single raster of precipitation is created for each water year. This data set is converted to a polygon shapefile and clipped using the recharge zone layer (Figure 17). Total volume of precipitation for the recharge zone is calculated by multiplying precipitation rate by each sub-area and summing them.

Estimating ET of native vegetation within the defined recharge zone is done using the Ecosystem Water Program (ECOWAT), a model for estimating ecosystem evapotranspiration (Spano et al. 2009). The ecosystem is the northeast slope of Mount Shasta characterized by Juniper woodland, and mixed Conifer forest along with rock outcrops and glaciers near the mountain summit. ECOWAT requires inputs of climate data (monthly solar radiation, minimum and maximum air temperature, wind speed, dew point temperature, precipitation, number of rainy days, and daily ET and precipitation), soil water characteristics including available water holding capacity and effective rooting depth, and site characteristics (latitude, elevation, slope, orientation). Percentage of vegetative shading is also specified. Output includes daily ET.

ECOWAT first calculates E_o (reference ET) from monthly climate data which is then adjusted by a series of K factors (like crop coefficients, K_c). K_m adjusts E_o to E_m (reference ET of the microclimate) by using local microclimate data rather than regional climate data (like CDEC or CIMIS), $K_m=E_m/E_o$. To calibrate a

new ECOWAT model, weather data would ideally be available from a local weather station within the ecosystem and a regional weather station. Since a local weather station is not available for our study area, a calibrated ECOWAT model for Vaira Ranch near Ione, California served as the base model and was obtained from Dr. Richard Snyder. Inputs for this model were changed appropriately to represent the Mount Shasta ecosystem. Regional climate data was downloaded from CDEC Weed Airport station data for solar radiation, minimum and maximum temperature, and wind speed. This data is also used as the 'local' climate data so that a K_m would be calculated adjusting for the slope and orientation of the ecosystem. Dew point temperature is calculated from air temperature and relative humidity. Since data at the Weed Airport station is not collected over an irrigated grass surface, it's ET_o is higher than ET_o collected from the Tulelake CIMIS station. No CIMIS station is within the Shasta Valley so Tulelake is a reasonable alternative (Orloff 2011, Pers comm.). Tulelake CIMIS station is judged to be more similar to the microclimate of the recharge zone than the Weed station, so this served as the source for daily ET_o for ECOWAT. The Weed Airport station provided the daily precipitation data. A representative elevation of 1876 meters above mean sea level and a slope of 7.3^o were estimated from Google Earth.

The other K factors that are considered in calculating daily ET for the ecosystem (ET_p) are:

- **K_v**- vegetation factor
- **K_d**- adjusts for canopy density
- **K_s**- accounts for plant water stress
- **K_e**- bare soil evaporation factor which is the lower limit for ET (Spano et al. 2009)

Water holding capacity is set to 0.09 based on analysis of available water capacity as reported in the physical soil properties report from SSURGO data for soils in the defined Mount Shasta recharge zone. The effective rooting depth is set to 0.5 meters since the bulk of the feeder roots are in the top couple feet of the soil (Nakamura 2011, Pers comm.). Conifers growing north of Mount Shasta like ponderosa pine, white fir, Douglas-fir, incense-cedar, and western juniper have tap roots but they are not known to extend very deeply. A good estimate of tap root depth for these trees is about two meters (Powers 2011, Pers comm.).

Percentage of shading is varied between 10-80% in ECOWAT. This provides an ET volume for each water year for each level of shading. This is used to estimate ET for different vegetation land covers in the recharge zone.

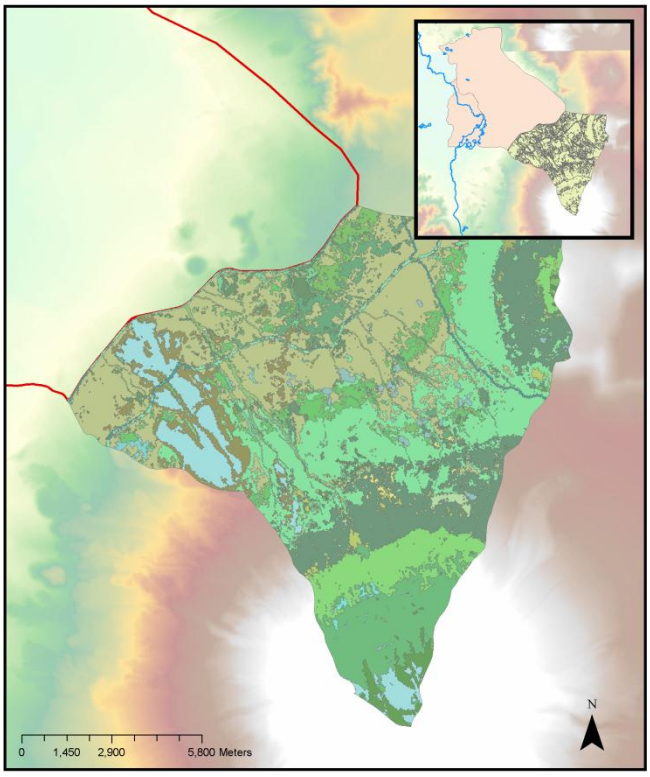

Figure 18. GAP land cover ecosystems in recharge zone

The USGS Gap Analysis Program provides spatial land cover data describing ecological systems in the United States. This data describes the geographical coverage, plant species, soil characteristics and sometimes percent of plant cover characteristic of each ecosystem. The recharge zone falls in zone 7. A shapefile of GAP land cover dataset was downloaded from their website (http://gapanalysis.usgs.gov/). Total area of each unique ecological system within the recharge zone is calculated (Table 7). Using GAP descriptions combined with observation from aerial photographs, level of percent shading is estimated for each ecosystem/land cover type. The ECOWAT calculated ET_p corresponding to the level of shading is then multiplied by the corresponding area to estimate a total volume of annual ET for each water year.

Table 7. GAP ecological systems with vegetation within the recharge zone

Ecological System- land cover	Area (m^2)	% Shading
Rocky Mountain Aspen Forest and Woodland	64,755	0.2
Columbia Plateau Western Juniper Woodland and Savanna	1,087,748	0.2
Klamath-Siskiyou Upper Montane Serpentine Mixed Conifer Woodland	18,937	0.6
Mediterranean California Dry-Mesic Mixed Conifer Forest and Woodland	5,848,402	0.3
Mediterranean California Mesic Mixed Conifer Forest and Woodland	28,352,205	0.6
Mediterranean California Lower Montane Black Oak-Conifer Forest and Woodland	486,672	0.6
California Montane Jeffrey Pine Woodland	34,690,930	0.4
Mediterranean California Red Fir Forest	19,058,330	0.5
Mediterranean California Subalpine Woodland	7,876,250	0.4
Northern California Mesic Subalpine Woodland	901,085	0.1
Sierra Nevada Subalpine Lodgepole Pine Forest and Woodland	444,910	0.4
Sierran-Intermontane Desert Western White Pine-White Fir Woodland	20,686	0.5
Inter-Mountain Basins Aspen-Mixed Conifer Forest and Woodland	463,041	0.6
Inter-Mountain Basins Mountain Mahogany Woodland and Shrubland	2,601,106	0.1
North Pacific Wooded Volcanic Flowage	6,136,714	0.5
Mediterranean California Alpine Fell-Field	304,375	0
Inter-Mountain Basins Big Sagebrush Shrubland	3,562,569	0.2
California Montane Woodland and Chaparral	453,289	0.8
Klamath-Siskiyou Xeromorphic Serpentine Savanna and Chaparral	365,147	0.2
Columbia Plateau Steppe and Grassland	1,426,825	0.2
North Pacific Montane Grassland	2,698	0.2
Introduced Upland Vegetation - Annual Grassland	8,094	0.2
Recently burned forest	141,231	0.5
Harvested forest-tree regeneration	929,175	0.5
North Pacific Lowland Riparian Forest and Shrubland	162,785	0.3
North Pacific Montane Riparian Woodland and Shrubland	1,822,928	0.4
Columbia Basin Foothill Riparian Woodland and Shrubland	50,330	0.2
Mediterranean California Foothill and Lower Montane Riparian Woodland	1,050,468	0.5

Sublimation is a significant part of the water balance for snow dominated environments (MacDonald et al. 2010) and so should be included in estimating volume of recharge from Mount Shasta. This is a topic of extensive research. Reviews of the literature contained within four papers provided an abundance of information for estimating a percent of annual precipitation lost to sublimation (Table 8) (MacDonald et al. 2010; Molotch et al. 2007; Pomeroy et al. 1998a; Pomeroy et al. 1998b). The literature describes three distinct types of sublimation: sublimation by interception, blowing snow sublimation, and sublimation of snowpack (Pomeroy et al. 1998b). Sublimation by interception (snow intercepted by the canopy) can cause loss of 10% to over 30% of seasonal snowfall (Pomeroy et al. 1998b). Blowing snow sublimation can account for a loss of 3% to as much as over 70% of annual snowfall in locations such as on summits, crests or ridges. Sublimation from the snowpack itself is reportedly 1-15% of cumulative snowfall (MacDonald et al. 2010). Independently or together, these different types of sublimation can contribute to significant loss of snowfall that otherwise becomes runoff or in the case of Mount Shasta, recharges to

groundwater. Based on these studies and those they reference, a 30% loss of precipitation falling on the slopes of Mount Shasta is used to represent sublimation.

Table 8. Sublimation rates in the literature

Citation	Sublimation by Interception	Blowing Snow Sublimation	Sublimation of Snowpack	Environment	Total Sublimation
From Pomeroy et al., 1998: An evaluation of snow accumulation and ablation processes for land surface modeling					
Pomeroy and Gray, 1995	30±40% annual loss of snow cover			Coniferous forest	
Pomeroy et al., 1997b		28% of annual snowfall		Tundra in the western Canadian Arctic	
Benson, 1982		32% of annual snowfall		Alaska north slope	
From Pomeroy et al., 1998: Coupled modeling of forest snow interception and sublimation					
Pomeroy and Gray, 1995	25±45% of the annual snowfall				
Pomeroy et al., 1998b	30 to 32%			Pine	
Pomeroy et al., 1998b	38±45% of seasonal snowfall			Black spruce	
Pomeroy et al., 1998b	10±15% of seasonal snowfall			Mixed-wood	
From Molotch et al., 2007: Estimating sublimation of intercepted and sub-canopy snow using eddy covariance systems					
Montesi et al., 2004	exceed 30%			Coniferous forest	
Molotch et al., 2007	0.70 mm/d		0.41 mm/d	Spruce, pine forest	
Pomeroy and Essery, 1999			1.2–1.8 mm d^{-1}	Canadian Prairies	
Fassnacht, 2004			0.75 mm d_1	Open mountainous locations	
Schmidt et al., 1998			0.36 mm d_1	Fraser Experimental Forest	
Parviainen and Pomeroy, 2000	0.5 mm d_1			Boreal forest	
From MacDonald et al, 2010: On the importance of sublimation to an alpine snow mass balance in the Canadian Rocky Mountains					
Strasser et al., 2008		Over 70% of annual snowfall (in some locations, summit crest and ridges)		Mountainous region, southeast Germany	24%
Pomeroy and Gray, 1995		15 to 41% of annual snowfall		Canadian Prairies	
Pomeroy et al., 1997		28% of annual snowfall		Canadian Arctic tundra	

Liston and Sturm, 2002		18–25% of winter precipitation		Alaskan arctic	
Bintanja, 1998		up to 20% of the annual precipitation		Alaskan ice sheet	
Mann et al., 2000		3.7% of snowfall		Halley Station in Antarctica	
Montesi et al., 2004	20–30% of snowfall			Sub-alpine forest, USA	
Satterlund and Haupt, 1970	4.5– 5.2% of snowfall			Northern Idaho	
Bengtsson, 1980			0.36mm/d	Continental Sweden	
Golding, 1978			1–2mm/d	Eastern Canadian Rockies	
Hood et al., 1999			15% of snowfall	Alpine site in Colorado Front Range	
MacDonald et al., 2010		17– 19% of cum snowfall	1–15% of cumulative snowfall	Front Ranges of Canadian Rockies	20-32% of cumulative snowfall

Thus, total annual recharge of Mount Shasta is calculated:

$$Precipitation\ (m^3) - ET_p * Area\ (m^3) - Sublimation\ (m^3)$$

where

Sublimation= 0.30*Precipitation
And $ET_p = f$(% shaded ground cover)

Groundwater inflow into the southern model domain is arrived at by dividing the average recharge volume up-gradient of the recharge boundary for the water year by the number of elements along the southeastern recharge boundary (154 elements). These results show the wet and dry nature of these four years and demonstrate the high variability of precipitation (Table 9).

Table 9. Mount Shasta recharge zone precipitation, estimated ET, sublimation, total upper and lower bound recharge volume and groundwater flow rates (modeled as injection pumping rate, MCM) per model cell on the southeastern constant flux boundary

	Water Year			
Units: MCM	**2008**	**2009**	**2010**	**2011**
Precipitation	98.6	110.8	128.7	151.1
ET- lower bound	32.4	31.7	35.5	37.3
ET- upper bound	36.4	37.0	40.4	40.9
Sublimation	29.6	33.2	38.6	45.3
LB recharge	32.6	40.5	49.7	64.8
UB recharge	36.6	45.8	54.6	68.5
Ave. recharge	34.6	43.2	52.1	66.6
Recharge rate per element	0.23	0.28	0.34	0.43

No flow boundaries

The southern no flow boundary east of Lake Shastina (Figure 15) traces the sub-region boundary between the Pluto's Cave sub-region and the Weed sub-region, as specified in the DWR Assessment

report (Ward and Eaves 2008). Water chemistry data from the two sub-regions indicate different sources and paths of recharge and suggest little connection between these areas (Ward 2011a; Ward and Eaves 2008).

The east-side boundary following the ridgeline is also represented as a no flow boundary. Though the material is said to be porous, numerous springs daylight along the contact in the north and ephemeral streams flow toward Little Shasta Valley. Faults along the east side also exist and are mapped, although their role in blocking groundwater flow is unclear. Considering this boundary as no flow is a reasonable assumption, but future work could estimate potential recharge from precipitation in this region (see Appendix A).

General head boundaries

A general head boundary (GHB) along the northern border is based on historical water level data from sparse wells north of the boundary (Mack 1960) and approximated elevations of the Shasta River and Little Shasta River estimated in ArcMap. Representing this border as a general head boundary allows the model to calculate a flux across the boundary. This may be important since outcrops of Pluto's Cave basalt occur to the north of the boundary and are known to be productive (Davids Engineering 2010; Ward 2011b). Groundwater from the Pluto's Cave basalt is also believed to discharge to the Shasta River. A combination of data from well logs and reported water levels for wells in the Mack report provide head at estimated distances from this boundary. Estimated 1954 groundwater elevation contours from Mack (1960) (scanned and included in Figure 19) suggests groundwater flow may occur through the model's northwestern corner entering from the north and continuing through the western border toward the Shasta River (Figure 19). Otherwise, the contours practically perpendicular to the northern model boundary suggest little to no groundwater flow is likely across the model boundary in that area, though the dashed lines in Figure 19 indicate uncertainty.

The northern GHB is divided into reaches based on the geology along this border (Figure 15). This includes sections of Pluto's Cave basalt, alluvial material, and debris flow. The initially assigned hydraulic conductivity (K) is related to the associated geologic material between the model boundary and the head data. A single, representative distance to the location of known water level is assigned to each reach. Limited data makes the specified heads for the northern GHB very rough estimates and this presents a significant data gap and limitation to the model. These heads are generally not based on 2008-2011 data. One exception is a reach using water level reported in a hydrogeology study done on the Hart Ranch by Davids Engineering (Davids Engineering 2010). Otherwise, data from the Mack report providing known water level locations are from the 1960s. Water level data from other DWR monitored wells in the valley indicate little long term change in water level so this map is likely still representative of current conditions.

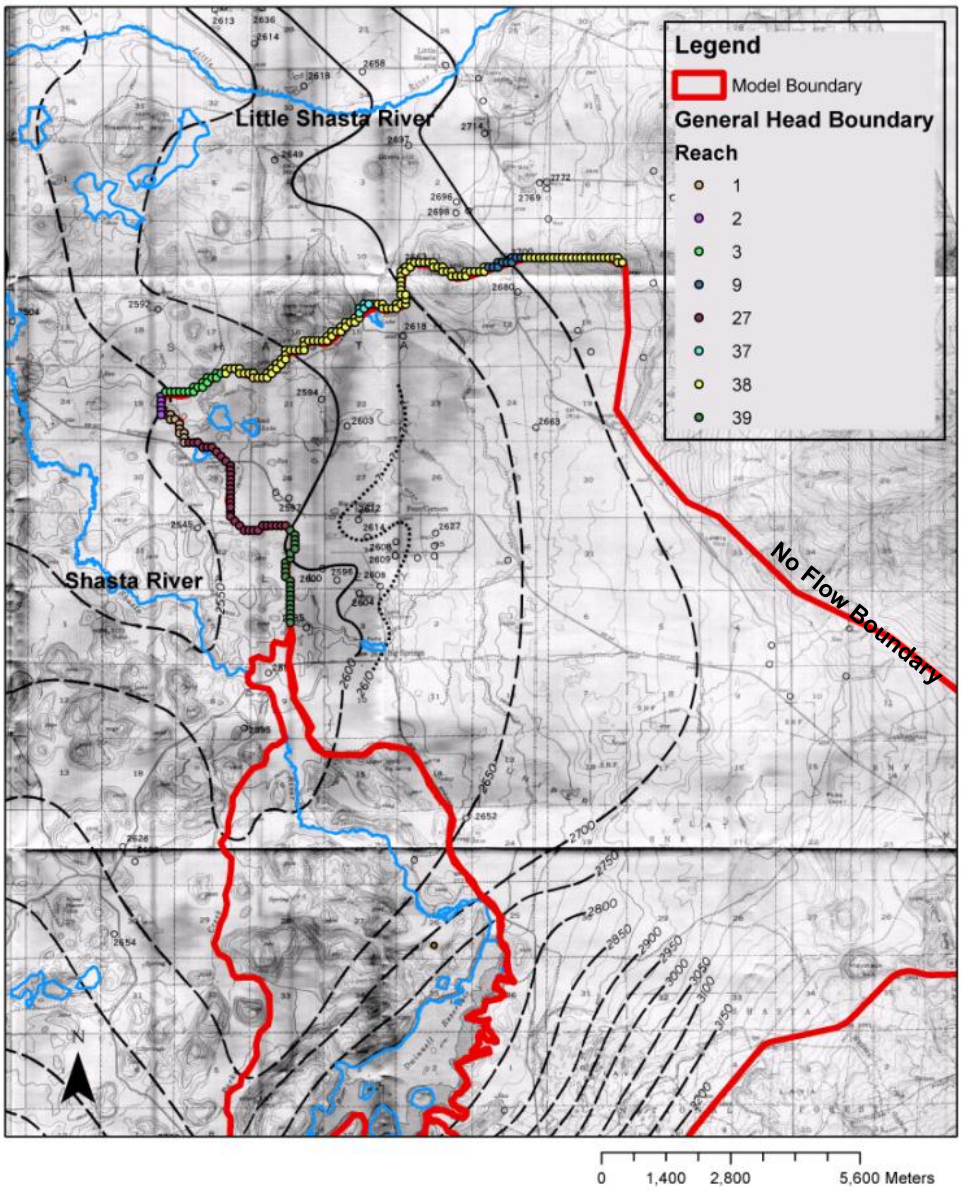

Figure 19. General head boundary with 1954 water level elevation contours from Mack (1960)

The western boundary traces the sub-region boundary between the debris flow sub-region and the Pluto's Cave sub-region as specified in the DWR Assessment report (Ward and Eaves 2008). The Shasta River provides the specified head beyond the model boundary for the GHB. Tools in ArcMap calculate the distance from the river to model elements along the border. Model elements are grouped into reaches based on geologic material. A single elevation point at the river is estimated in ArcMap for each reach. Element width is 100 m and saturated thickness is 40 m for all elements in the western GHB. An effective hydraulic conductivity (K) is assigned to each reach roughly based on the geology between the head boundary and the model boundary associated with the reach. Reaches associated with debris flow material have an initial K of 10^{-3} m/d. Reaches corresponding mainly to alluvial material are assigned an initial K of 10 m/d. Hydraulic conductivity value for alluvial material is assigned based on the range given in Domenico and Schwartz (1997) for unconsolidated alluvium. Reaches associated primarily with the debris flow material is given a small K since this material is less conducive to groundwater flow due to its unsorted and chaotic nature.

Model properties and components

The groundwater model generally represents the subsurface as homogeneous, isotropic media with zones having different hydraulic conductivity (K) values. The zones are first based on geology (Figure 15), and secondly roughly based on changes in aquifer thickness as represented in the model estimated from available well logs. This is highly simplified since in reality the system is extremely complex characterized by fractured porous media and potentially even lava tubes. Regional hydraulic conductivity values attempt to capture the complexity with a representative hydraulic property. The range given in Domenico and Schwartz (1997) for permeable basalt, 10^{-3} – 10^{2} m/d, guided the initial choice of 86 m/d for zones 2, 4, 5, 6 and 7. This is within the range bracketed by Jefferson et al (2006) of about 26-863 m/d. The effectiveness of this equivalent porous media approach is evaluated during model calibration as are values for each K zone.

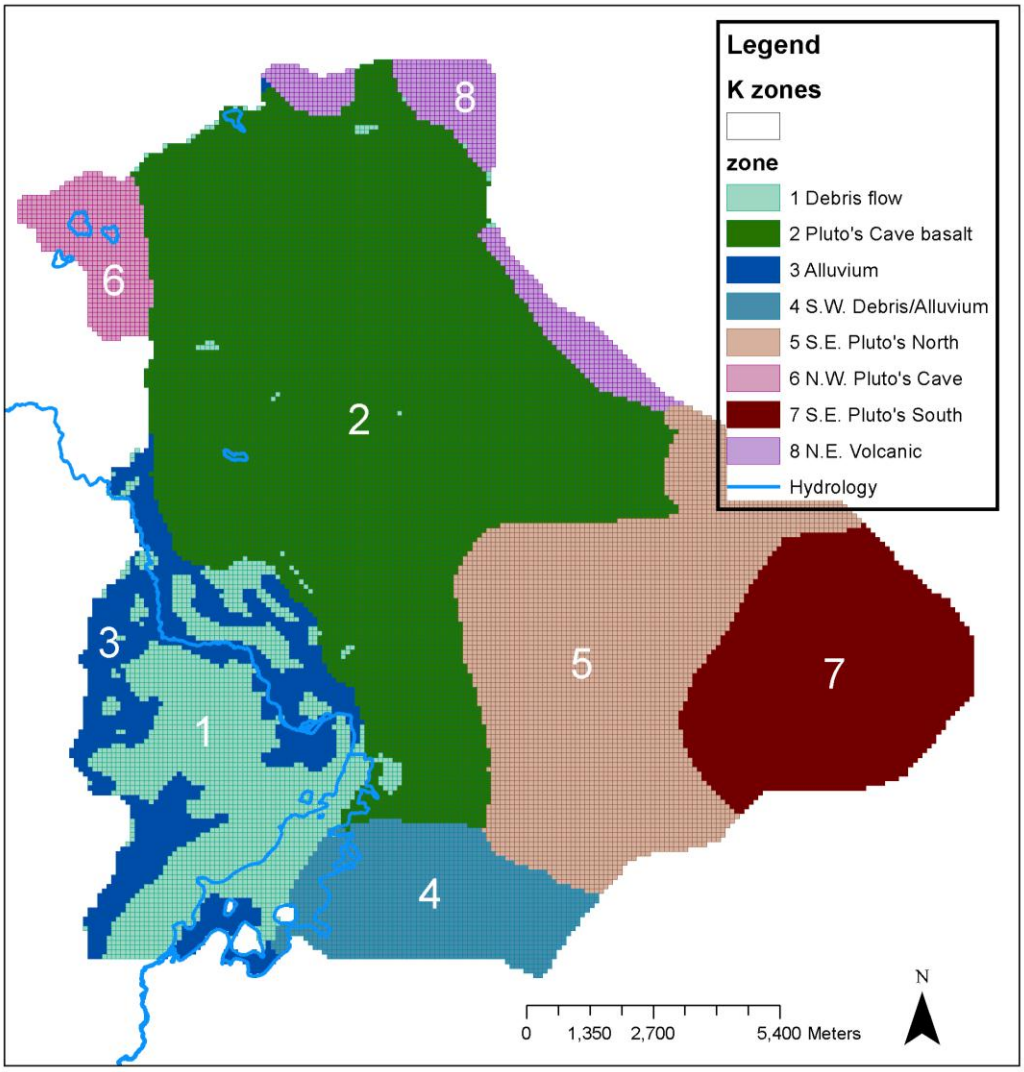

Figure 20. Hydraulic conductivity (K) zones

Spring flow representation- drain package

Springs can be simulated with MODFLOW's Drain package (DRN) by assigning the elevation of the land surface where the spring daylights as the drain elevation (Batelaan and De Smedt 2004; Scanlon et al. 2003). As long as the aquifer head is higher than the drain head, the "drain" flows. An arbitrarily high conductance can be set to simulate spring flow.

$$Q_{out} = CD(h_{i,j,k} - HD)$$

when $h_{i,j,k}$ > HD, where

Q_{out} is the flow from the aquifer into the drain
CD is the drain conductance
HD is the drain elevation
$h_{i,j,k}$ is the head in the cell containing the drain (from Harbaugh (2005))

The Drain Package is used to represent several major springs within the model domain. These include Big Springs complex in Big Springs Lake (Figure 21), Big Springs Creek (including Alcove springs area), Little Springs, Hole in the Ground, Clear Springs, Hidden Valley Spring, Kettle Springs, Black Meadow Springs, Bridge Field Springs (north and south), Mack spring, and the northwestern spring-fed lakes. Drains were placed in model elements overlying the geographic extent of Big Springs Lake reflecting the presence of numerous springs near the lake outlet and on the eastern end of the lake (McClain 2008). Since Big Springs Creek largely flows over bedrock and flows originate from its major spring complexes (Big Springs Lake and Alcove Springs) and smaller seeps along its course, the Drain Package was used to represent this entire hydrologic feature rather than the MODFLOW River Package. This allows any groundwater intercepting the drain elevation (which is set at 1 meter below the estimated elevation of the stream course) to escape from the aquifer as 'spring flow'. This simplification reflects the model's equivalent porous media model approach and as such, spring flow cannot be successfully concentrated at more discrete locations as is the case in reality where flow through fractures and possibly lava tubes or volcanic rubble create distinct flow paths. The model is calibrated so spring flow from Big Springs Creek and Big Springs Lake has a reasonable magnitude, estimated to be about 58 MCM per year and 37 MCM per year, respectively, by Mack (1960). More recent data suggests an estimated 73 MCM from the entire Big Springs complex based on data reported in Jeffres et al (2009). Parameters required for each drain are stage, width, length, thickness of drain bed, and hydraulic conductivity (K). Along with heads at observation wells, spring flow (i.e. drain flow) will be used to calibrate and assess the reasonableness of the model.

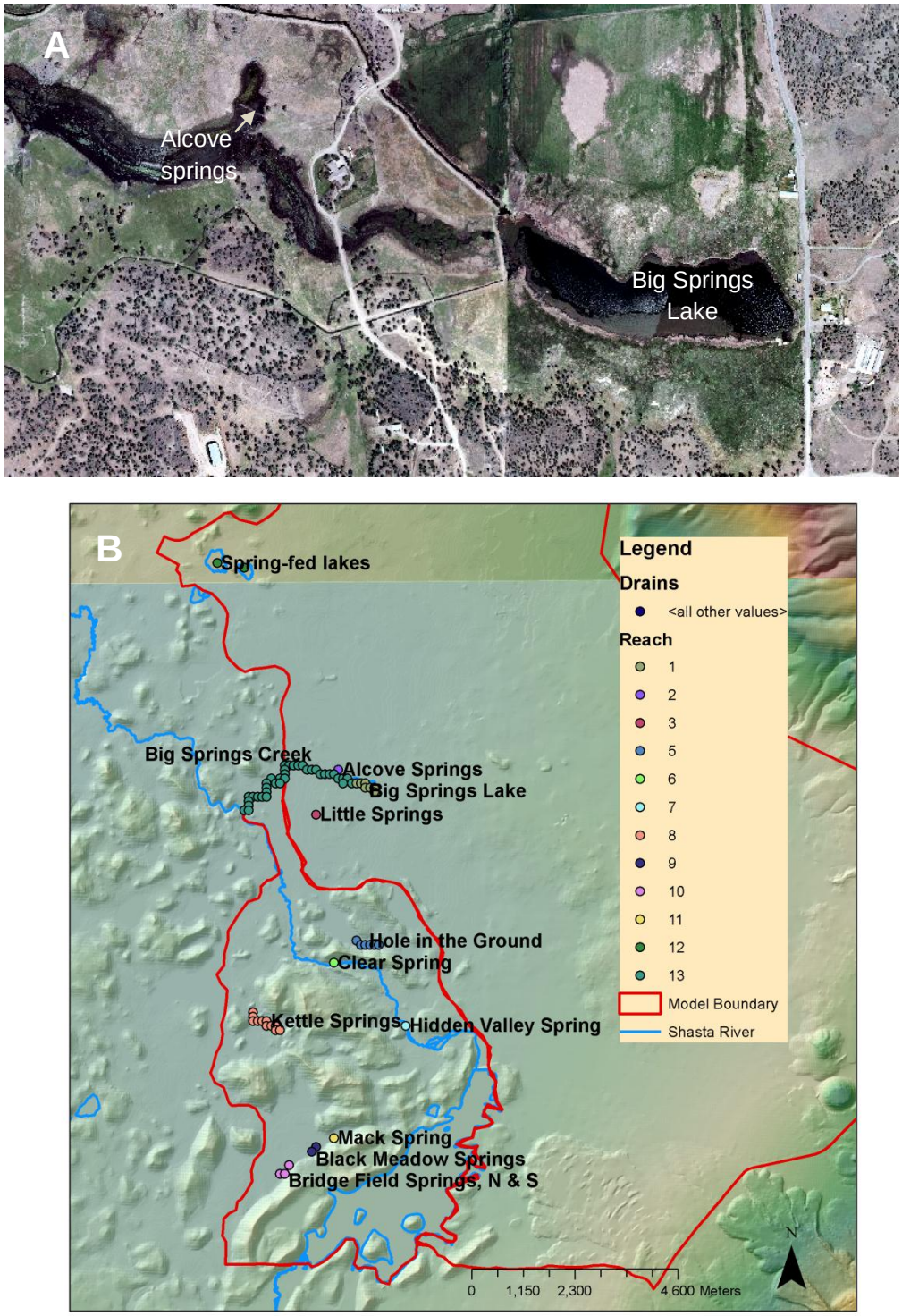

Figure 21. a) Big Springs complex: Big Springs Lake and alcove springs in Big Springs Creek b) Springs modeled as drains

Groundwater pumping

In addition to spring flow, an important source of groundwater outflow is pumping from irrigation wells. Since groundwater pumping records are not available, pumping is calculated based on estimated crop demand. Well logs from the Department of Water Resources, Northern District were used to approximate the distribution of irrigation wells. The Pluto's Cave area has seven main areas of agriculture irrigated by groundwater, according to the 2001 DWR land use survey (Figure 22). These defined agricultural zones are identified based on their geographical location and assigned a number of wells that generally reflects the estimated distribution of wells in that area:

1. Northeast corner – 8 wells
2. Big Springs Irrigation District (BSID) – 1 well
3. Big Springs Area (non BSID) – 10 wells
4. East-central – 2 wells
5. North of Shastina – 5 wells
6. Lake Shastina Municipal Water Company (golf courses) – 2 wells
7. West-central – 1 well
8. Surface Irrigated Agriculture – no wells
9. Non-irrigated Ag Land – no wells
10. Shasta Springs Ranch – 1 well

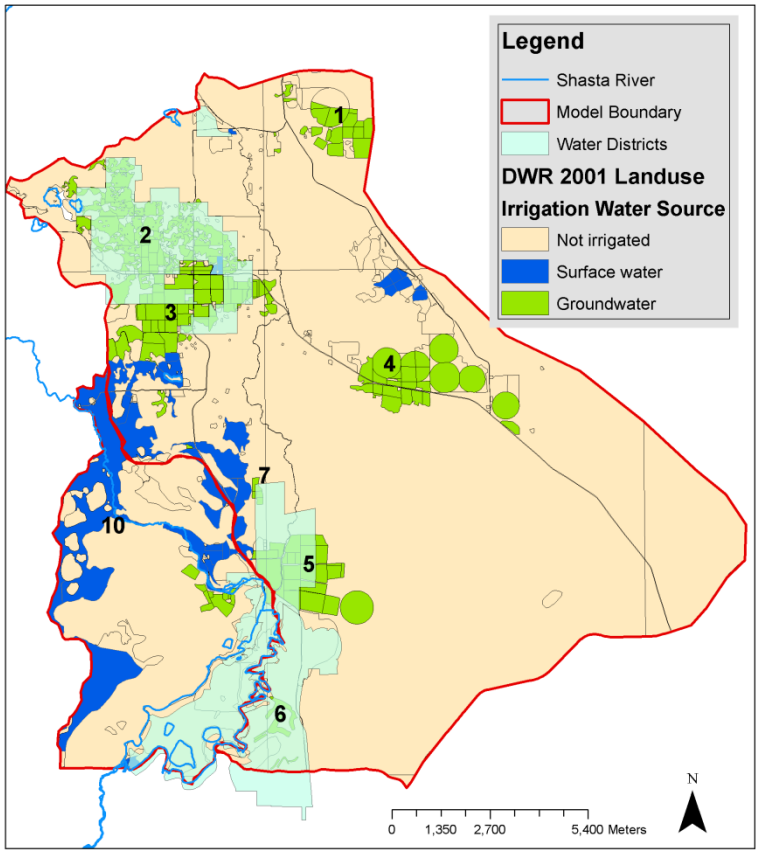

Figure 22. Landuse map within model domain. Green polygons are groundwater irrigated agricultural lands with irrigation district boundaries overlain

The 2001 land use survey includes information on water source, land use class, acreage, and irrigation method for fields throughout the Shasta Valley. This is used to assign each model element a land use type. Percent ground cover is assigned to non-cropped land use (i.e. native vegetation, idle, barren) using estimates from aerial photos (Table 10). This is important for estimating ET of native vegetation using ECOWAT. Model elements associated with cropland are assigned an agricultural zone.

Table 10. Land use codes assigned to model elements (cropland and non-cropland) and associated % ground cover and area

Land Use Code	Description	% Ground Cover	Hectares
B *	Bare	10%	0
G *	Grain and Hay crops	NA	74
G T	Grain, tilled	NA	10
G2*	Wheat	NA	0
G6*	Misc/mixed grain and hay	NA	67

G6X	Misc/mixed grain and hay, partially irrigated	NA	8
I *, I0*, I3*, I4*	Idle	10%	17
I1*	Idle, recently cropped	10%	167
I1T	Idle, tilled	10%	0
NBB*	Barren	10%	6
NR *, NR0*	Native Riparian	80%	9
NR2*	Nat Rip, high water	80%	469
NR2X	Nat Rip, high water, partially irrigated	80%	277
NV *, NV0*, NV0X, NV4*	Native Vegetation	30%	15414
NV2*, NV2X	Native Veg- scattered, light	10%	310
NV44*	Nat Veg >70% cover	70%	1483
NVb*, NVbX, NB *	Native Veg- bare	10%	1882
NVbg*	Native veg- bare, grass	10%	42
NVbw*	Native Veg- bare, wash	10%	31
NW *, NW0*, NW2*, NW2X, NWb*	Water	NA	324
P *, P0*	Pasture	NA	4
P F	Pasture, fallowed	NA	0
P1*	Alfalfa	NA	44
P3*	Mixed Pasture	NA	63
P4*	Native Pasture	NA	252
P4X	Native Pasture- partially irrigated	NA	0
P5*	High water table, native pasture	NA	4
S *, S0*, S1*	Farmsteads	NA	20
T18*	Truck- Misc	NA	30
T18X	Truck- Misc, partially irrigated	NA	8
T20*	Truck-strawberries	NA	33
UC *	Commercial	NA	10
UC6*	School	NA	2
UC7*	Municipal building	NA	1
UI *	Industrial	NA	4
UI13*	Sewage Treatment	NA	3
UI2*	Rock Quarry	10%	16
UI3*	Industrial- storage and distribution	NA	9
UL1*	Lawn area	NA	4

UL2*	Golf Course	NA	56
UR *, UR0*	Residential	10%	12
UR1*	Urban- single family	10%	577
UR44*	Urban w/ ET of NV44	70%	436
UV4*	Paved Area	NA	57

In the modeled area, most cropland is grain and hay, alfalfa, and pasture with smaller acreages of strawberries, onion/garlic, lawn area, and golf course. Some fields are categorized as idle meaning they were not cropped during the current or previous season but have been cropped within the past three years. This acreage is significant (15% of agricultural land). The 2001 land use data is used to estimate pumping for each water year, 2008-2011, thus this assumes the 2001 survey generally represents the common crop mix and amount of irrigated acreage. At the time of analysis, the 2010 land use survey for this area had not yet been released by DWR. Future work could update pumping estimates based on new land use data. The 2001 land use survey is used to estimate annual applied water volumes. Since pumping records widely do not exist nor are they available if they do exist, groundwater pumping is estimated by calculating ET of applied water (ETAW) and then dividing by irrigation efficiency to yield a total pumping volume used to meet crop demand.

The Basic Irrigation Scheduling (BIS) program by Snyder et al (2007) is used to calculate annual crop water demand per acre for each crop type in the model area. Mean daily ET_o from Tulelake CIMIS station data as well as the number of rainy days per month from CDEC Weed Airport station are input to the program. Start and end dates for each crop were also specified and a few of the K_c values were adjusted based on information from the local Farm Advisor (Orloff 2011, Pers comm.). The BIS program creates a time series of daily ET_c for each crop type. The sum of this time series provides an annual ET_c value for each crop (Table 11). An average of the grain ET_c rate is used.

Significant precipitation occurring during the irrigation season is assumed to help meet crop demand (Table 11). Thus crop demand for a particular field is ET_c minus precipitation that occurs April through September.

Table 11. Inputs to BIS program

Crop	Start Date	End Date	Changes	ETc/acre (meters)			
				2008	2009	2010	2011
Alfalfa	1-Mar	1-Oct	K_cC,K_cD=.94	0.84	0.84	0.86	0.88
Pasture	15-Feb	15-Oct	K_cB-K_cE=.90	0.91	0.91	0.92	0.94
Grain/Hay	15-Mar	1-Aug		0.50	0.50	0.52	0.52
Grain (winter)	1-Nov	15-Jul		0.06	0.04	0.06	0.06
Onion/garlic	15-Oct	1-Jul		0.08	0.07	0.07	0.08
Strawberries	15-Apr	1-Oct	K_cC-K_cE=.87	0.59	0.57	0.61	0.61
Turf-grass	1-Jan	31-Dec	K_cB-K_cE=.70	0.83	0.83	0.84	0.86
Truck Crops (Vegetables)	1-Apr	30-Sep		0.75	0.75	0.75	0.77
Irrigation Season Precipitation	1-Apr	30-Sep		0.04	0.04	0.05	0.05

Of the total groundwater irrigated acreage, 29% of the area is irrigated by wild flooding followed by side-roll sprinklers (27%), as assigned by the DWR land use survey. Irrigation efficiency fractions for the Shasta Valley were estimated based on information from UCCE Farm Advisor for Siskiyou County (Orloff 2011, Pers comm.). For each field, crop demand (ET_c minus irrigation season precipitation) is multiplied

by the acreage then divided by the irrigation efficiency fraction associated with the irrigation method used on that field. This yields an estimate of the volume of applied water for each field. Total applied water is summed for each agricultural zone. This volume is divided by the number of wells in each zone, thus distributing the pumping across the agricultural zone. This approach is taken since the exact location of wells is unknown as are the fields that are associated with each well. Representative pumping wells in each agricultural zone are placed based on evaluation of well logs indicating the general distribution and number of irrigation wells in the model area. The wells in the model do not represent particular irrigation wells.

Table 12. Irrigation method and efficiency

Irrigation Method	% Area	Efficiency Range (%)	Efficiency Used (%)
Border	1%	65-75	70
Center Pivot	16%	85-90	87
Hand move sprinkler	2%	70-80	75
Side Roll Sprinkler	27%	70-75	72
Surface Drip	1%	85-90	87
Wild Flooding	29%	60-65	65
Unknown: likely GC-sprinklers	18%		75
Sub-irrigation	5%		75

Volume of pumping from the Montague Water Conservation District well is estimated based on it producing at a rate of 11,700 Liters/min (3,100 gpm) for an irrigation season which may require an estimated 81 days of pumping (Hoss 2010, Email). At this rate over this time, it amounts to 1,384 TCM for an irrigation season. Without more specific information, this is the volume used for 2008 thru 2010. It is believed the pumps were not operational during the 2011 irrigation season and thus no pumping is assigned for that water year.

The model includes one well in the Parks Creek valley area, Seldom Seen well, on the Shasta Springs ranch. This well pumps 12 hours on, 12 hours off throughout the irrigation season to irrigate nearby fields. For the 2010 irrigation season, this amounted to 613 TCM (Davids Engineering 2011c). This volume is used for the 2008 steady state model.

Canal leakage

Drainage studies on irrigation ditches in the valley indicate that significant losses to groundwater occur during conveyance. The two primary irrigation canals are those owned and operated by Montague Water Conservation District (MWCD) and Big Springs Irrigation District (BSID). MWCD canal conveys water diverted from Lake Shastina as well as groundwater pumped into the ditch by high producing groundwater wells. In 1953, MWCD diverted about 17.2 MCM into the main canal from the reservoir (Mack 1960). This water is conveyed across the model area for use mostly on irrigated lands north of the model domain. The BSID canal conveys groundwater pumped from their production wells into an upper and lower ditch that provides deliveries throughout their district. Representation of recharge from these ditches is incorporated into MODFLOW as a series of injection wells in the model elements overlying the path of the canals. Therefore, a recharge rate for each “well” is needed.

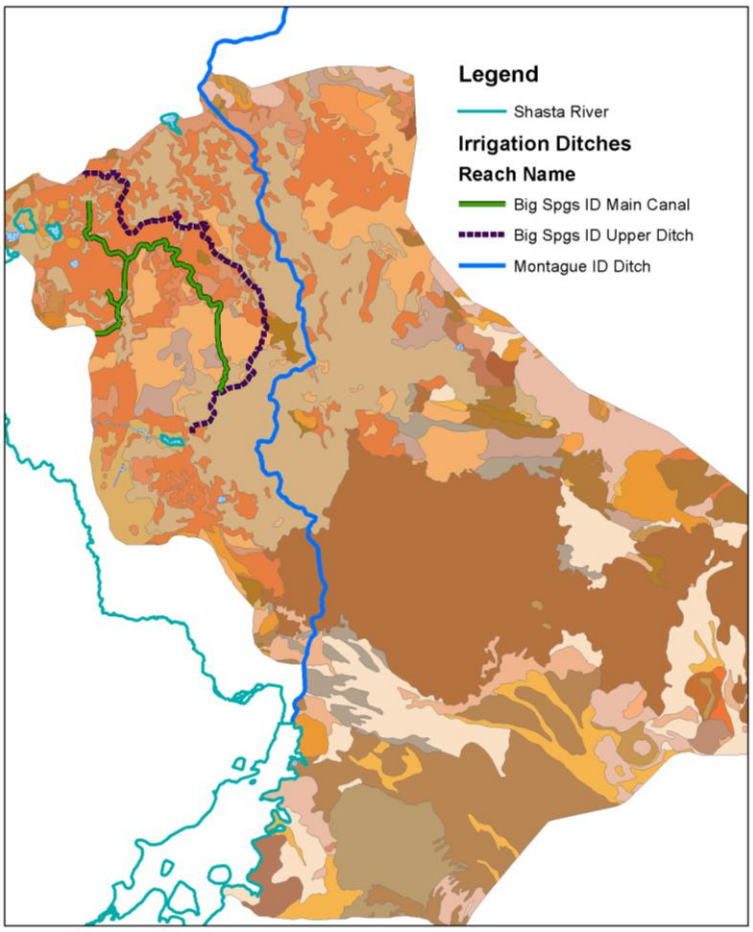

Figure 23. District irrigation canals in model area overlying soils layer

The Shasta Valley Resource Conservation District (RCD) authorized a report assessing water use efficiencies for BSID. Assessing overall district water use efficiency indicates a conveyance loss of 32% of groundwater pumped from the district well (based on measurements in 2004) (Forsgren Associates 2006). This estimate is used to quantify conveyance leakage in the groundwater model. The Upper Ditch overlies mainly Louie Stony Loam and Rock Outcrop- Louie Complex as mapped by the USDA soil survey. The Main Canal passes through areas mainly with soil types of Louie Loam and Louie Stony Loam. Top layers of these soils have permeability classified as moderately slow (water movement of 1.5 to 3.0 centimeters per hour) while below a 7.6 cm thick hardpan is a stratified sand, gravel, cobble, and stone layer with rapid permeability (15 to 50 cm per hour) (Forsgren Associates 2006). This allows for significant downward movement of water from these canals. The Upper Ditch conveys more of the water (about 0.5 m^3s^{-1}, in 2004) and the Main Canal system distributes approximately 0.2 m^3s^{-1} (Forsgren Associates 2006). Flow measurements indicated significant loss of flow over the length of the Upper Lift Ditch. The Main Canal maintains flow along its length but also receives significant amounts of unquantified tail water as inflow from fields served by the Upper Ditch. The report concludes that Main Canal losses are approximately equal to its inflows (Forsgren Associates 2006). Given the uncertainty of losses in the Main Canal, conveyance loss is completely assigned to the Upper Ditch in the groundwater model. The leakage rate per model element is calculated as:

$$Q_{injection} = f_{rch} * Q_{Ag\ zone\ 2}/n$$

where
f_{rch} is the fraction of recharge from total pumped groundwater = 0.32 (Forsgren Associates 2006)
$Q_{injection}$ is the injection rate (m^3/yr) of the conveyance leakage "well"

$Q_{Ag\ zone\ 2}$ is the pumping rate (m^3/yr) of the well for ag zone 2 which is BSID
n is the number of model elements representing the Upper Ditch

This distributes the recharge from the canal over the length of the Upper Ditch.

A study assessing efficiency of the MWCD Main Canal was also recently completed in 2010. This work highlights reaches where losses are the greatest. In the model area, this includes a 4.8 km reach with a loss rate of about 0.3 m^3s^{-1} and a shorter section (0.5 km) near the model's northern boundary with a loss rate of approximately 0.03 m^3s^{-1} (Willis and Deas 2010). The number of days the canal carries water is estimated to convert this loss rate into a total annual volume per model element with canal leakage. Since the primary source of water in the canal is releases from Lake Shastina, decreasing water elevation of the lake using CDEC stage data is used as an indicator to estimate the number of days the canal could carry water during the irrigation season. For 2008-2011, the estimate ranged from 143 to 165 days, usually beginning in mid-April (with the exception of 2011, which started in May due to a wet spring) with lake stage falling through mid-August to late September. A total annual volume is calculated for each losing reach and then divided by the number of model elements in that reach. The MWCD canal runs approximately 16.9 km across the model area. Other than these two losing reaches, the other model elements associated with the canal's location are assigned a leakage rate of zero. This approach is an extremely rough estimation of recharge from conveyance losses from the MWCD canal and may overestimate its value if the ditch does not convey significant water for that length of time. However, without better information for the canal's operation, this rough estimate provides an idea of the magnitude of conveyance loss (Table 13).

Table 13. Conveyance recharge (MCM)

	Conveyance Recharge (MCM)			
Canal Reach	**2008**	**2009**	**2010**	**2011**
BSID Upper Ditch	3.3	3.2	3.2	3.2
MWCD- km 3.9-8.7	3.8	4.4	4.3	3.8
MWCD- km 17.5-18.0	0.38	0.44	0.43	0.38

Local recharge: applied water and precipitation on the valley floor

The sum of recharge from precipitation and applied water comprises the volume of total recharge within the model domain. A recharge rate (meters/year) is applied to each model element for each period (water year) of the model.

To estimate groundwater recharge from precipitation (PPT), a tipping bucket model of the soil root zone is developed (e.g., (Ruud et al. 2004). The model, implemented in a spreadsheet, tracks root zone soil water content on daily time-steps as a function of significant precipitation and ET of native vegetation:

$$\theta_t = \theta_{t-1} + Sppt_t - ETp_t$$

where

t is the time step in days
Θ is soil water content (mm)
S_{ppt} is significant precipitation (mm)
ET_p is native vegetation evapotranspiration (from ECOWAT results) (mm)

Significant precipitation is defined as any daily precipitation that is twice the reference ET for that day. CDEC Weed Airport weather data provides daily precipitation and the Tulelake CIMIS station is used for daily reference ET.

Daily groundwater recharge (DP_t) is the amount of water in excess of the field capacity (FC) of the root zone, after accounting for precipitation and ET, according to the following equation:

$$If\ \theta_t > FC\ then\ DP_t = \theta_t - FC$$

The field capacity is calculated as the available water holding capacity (WHC) of the soil multiplied by the rooting depth. A representative water holding capacity of the soil is set to 0.11 m/m based on analysis of available water capacity reported by SSURGO for soils underlying native vegetation in the model area. The rooting depth is one meter since widely spaced conifers like pine and juniper are common in the Pluto's Cave basalt area and have fine root systems that fully occupy the upper soil horizons pulling water from a meter depth (Powers 2011, Pers comm.). This leads to a field capacity of 110 mm (WHC*Rooting depth). Daily DP is summed by water year to yield an annual groundwater recharge rate (m/yr) from precipitation for the model domain.

It was assumed that no runoff occurs due to the highly permeable landscape and the lack of surface water drainage features in the majority of the model area. It was also assumed that recharge to groundwater occurs instantaneously (no delay through the deep vadose zone). This latter assumption has negligible impact on model results, as the groundwater model only considers an annual average recharge and groundwater recharge through the deep vadose zone occurs within less than one year, as indicated by high saturated hydraulic conductivity values of soils in the model domain (SSURGO physical soil properties data).

The spreadsheet model is applied separately to native vegetation land use categories that correspond to four different levels of percent of ground cover (10, 30, 70, and 80%). ET of native vegetation (ET_p) is estimated for these various percents of ground cover using an ECOWAT model for the Shasta Valley floor in the model domain. Inputs include climate data from CDEC and daily ET_o from CIMIS (as with the ECOWAT model for the Mount Shasta recharge zone), WHC and rooting depth as described above, as well as latitude, elevation, orientation and slope (Table 14). The latter are estimated using Google Earth tools.

Table 14. Shasta Valley ECOWAT inputs

Latitude	41.6
Elevation	900 m
Orientation	Northwest (-135^o)
Slope	1.6^o
WHC	0.11 m/m
Rooting Depth	1 m

The tipping bucket spreadsheet model and ECOWAT assumes precipitation measured at the Weed Airport falls across the valley equally. This is not the case since rainfall in the Shasta Valley can vary significantly spatially. However, PRISM data, which provides spatially varying precipitation for the valley, seems unreasonably high compared to weather station data and knowledge of the area's climate and average rainfall. Therefore, this simplification seems necessary and is a limitation in the calculation. This approach also assumes all agricultural land in the model domain recharges precipitation equally without regard to soil type, slope, etc.

The tipping bucket model for recharge estimation begins on October 1, 2007 with zero mm water content in the soil profile. The initial condition was determined by changing initial water content to various values and noting the water content on October 1, of 2008. Regardless of the initial water content in 2007, Oct 1, 2008 always showed zero mm water content. Hence, zero mm is used as the initial value for Oct. 1, 2007. The soil water content increases when significant rainfall exceeds ecosystem water demand (ET_p)

and recharge occurs if the water content exceeds its field capacity, 110 mm. Annual recharge from precipitation for native vegetation (NV) is the sum of the calculated daily recharge for each of the water years, 2008-2011 (Table 15). This is done for a range of percent of ground cover as assigned to model elements based on their native vegetation land use codes (Table 10).

Table 15. Annual recharge from precipitation for different amounts of native vegetation (NV) ground cover

	Recharge (mm/WY)			
% NV Ground Cover	**2008**	**2009**	**2010**	**2011**
80%	21.0	0.0	17.4	42.6
70%	27.0	0.0	19.6	47.5
30%	55.6	0.0	71.1	107.4
10%	99.4	6.9	127.9	173.3

Four categories of percent ground cover describe non-cropped land. Ground cover is estimated from aerial photos for each model element corresponding to areas designated by native vegetation in the 2001 DWR land use survey (Table 10). Idle land is treated as native vegetation with 10% ground cover since in some cases the fields are tilled but not planted, thus having little vegetation and mostly bare soil. Residential and urban-single family land use types are also assigned recharge based on 10% ground cover of native vegetation, also estimated from aerial photos (Table 10). An annual recharge rate (m/year) is assigned to each model element not in an agricultural zone according to its assigned land use category and corresponding percent ground cover.

Recharge on agricultural land

Total recharge for agricultural land includes recharge of applied water as well as recharge from precipitation. A recharge rate with this dual component is assigned to all model elements that correspond to an agricultural zone (indicating cropped land), defined by geographical areas in the model domain (Figure 22). Total volume of recharge is calculated for each agricultural zone but different approaches are used for the non-irrigation season versus the irrigation season. During the non-irrigation season (October through March) when most of the precipitation occurs, cropland is assumed to evapotranspire equivalent to native vegetation with 70% ground cover for ET_p, representing the presence of mostly native grasses. Hence, recharge computed for the 70% native vegetation class is also applied to cropland, during the non-irrigation season. The recharge rate of precipitation for 70% NV ground cover is multiplied by the total acreage of each agricultural zone to yield the volume of recharge from precipitation associated with each zone:

$$PPT\ Recharge_{Ag\ zone}(m^3) = PPT\ Recharge_{Ag\ zone}(m) * Area_{Ag\ zone}(m^2)$$

For the irrigation season (April through September), recharge of applied water is calculated for each field as follows:

$$AW\ Recharge_{field}(m\text{^}3) = \left(1 - Eff_{field}\right) * AW_{field}\ (m\text{^}3) \quad \text{Equation 3.1}$$

where *Eff* is irrigation efficiency and *AW* is applied water.

This assumes all applied water not consumed by the crop (ET) is recharged to groundwater. This is a reasonable assumption for groundwater irrigated fields, however surface water irrigated croplands can have significant tail water that returns, in some cases, to a stream channel. Most of the surface water irrigated land within the model area is not directly adjacent to a channel and thus, though this assumption may overestimate recharge, is a reasonable simplification for agricultural zones 1-8. Future work could refine this approach by identifying fields having surface runoff and then adjusting the rate of recharge for those fields. If we made the opposite assumption for surface water irrigated lands, that non-consumed applied water all runs off the field and none recharges to groundwater, there would be on the order of 1.8 MCM less recharge per year to the aquifer (Table 16).

A similar approach is used for ag zone 10. However, these fields are mostly surface water irrigated and significant volumes of tail water return to Parks Creek and the Shasta River. Therefore, assigning a recharge rate using the above approach overestimates recharge volume from these fields although this water likely ends up as outflow to Parks Creek or the Shasta River, which is the same end result. The Shasta Springs Ranch (ag zone 10) is mostly wild flooded pasture with a reported irrigation efficiency of 0.65 and ET rate of 2.4 acre-feet/acre in 2008 (Davids Engineering 2011b; Davids Engineering 2011c). These values were used to estimate applied water and therefore the rate of recharge in this area.

Table 16. Total recharge summary (from applied water (AW) and precipitation) for cropland, agricultural zones 1-8 (MCM)

	2008	2009	2010	2011
Total AW recharge	6.72	6.69	6.58	6.64
AW recharge (SW irrig land)	1.81	1.81	1.77	1.78
Precip recharge	0.64	0.00	0.46	1.12
Total recharge	7.35	6.69	7.05	7.76

Equation 3.1 calculates a recharge volume for each field. Each field is in an agricultural zone, so recharge of applied water is summed for each zone. Total recharge volume (sum of recharge from AW during the irrigation season and from PPT during the non-irrigation season) for each agricultural zone is converted to cubic meters and divided by the number of model elements in each zone. Thus, the annual volume of recharge for each zone is distributed equally to its model elements. Recharge is input to MODFLOW as a rate (in this case, meters/year), so the recharge volume is converted to a rate by dividing by model element area (10,000 m^2). As a result, each agricultural zone has an associated recharge rate.

In this way, each model element is appropriately assigned recharge from precipitation and/or recharge from applied water depending on whether it is designated as cropland or native vegetation.

Model calibration

Calibrating a model is the "process of matching historical data, and is usually the prerequisite for making predictions with the model" (ASTM 2008). The calibration process tests the conceptual model, data quality and data completeness of model inputs, and helps provide confidence in the model's predictive capabilities. Therefore, calibration requires the identification of calibration targets which are historical head or flux data compared to model outputs. The difference between the target (observed value) and modeled value is the residual. Acceptable residuals and residual statistics need to be established as well as calibration parameters identified. Calibration parameters are hydraulic properties or boundary conditions with uncertain values such as transmissivity or boundary conductance (ASTM 2008). The following section describes the calibration process for the Pluto's Cave basalt and Parks Creek valley steady-state 2008 groundwater model.

Targets: observed water levels

Available head data from wells in the model area are imported into Groundwater Vistas as targets. The Department of Water Resources (DWR) monitors a grid of about 30 wells in the Shasta Valley twice a year taking a fall and spring measurement. This data is available online from the Water Data Library. Five of these wells are currently monitored and located within the model area. The water surface elevation from the October measurement for these five wells is incorporated as targets. The spring level is used when a fall measurement is not available. With the DWR wells alone, the model lacks targets in the eastern and southeastern areas of the domain (Figure 24). In an effort to provide some information about water levels in those areas, well logs obtained from DWR are analyzed to yield additional water surface elevation data points. Well logs sometimes record depth to first water or the static water level after well development. Well logs with drill dates between 2008 and 2010 located within the domain that record static water level are selected. Since the exact location of the wells is unknown, the targets are located at the centroid of the Township Range and Section (TRS) of the well. Ground surface elevation (GSE) is identified at that location. Using the GSE and reported static water level, an estimated water

surface elevation is calculated. This introduces significant uncertainty since ground surface elevation can vary considerably within a TRS. However, this additional information, even if uncertain, is useful for model evaluation, sensitivity analysis, and calibration.

The head at Big Springs Lake and a few other spring locations are also specified as targets. They are set to 1-2 meters below the top elevation of the model node representing the elevation of the spring at that location. This allows a quick assessment of which springs are active and flowing or not.

These targets (Table 17) are used by Groundwater Vistas to calculate calibration statistics. Modeled heads are compared to observed heads at these locations to evaluate model performance.

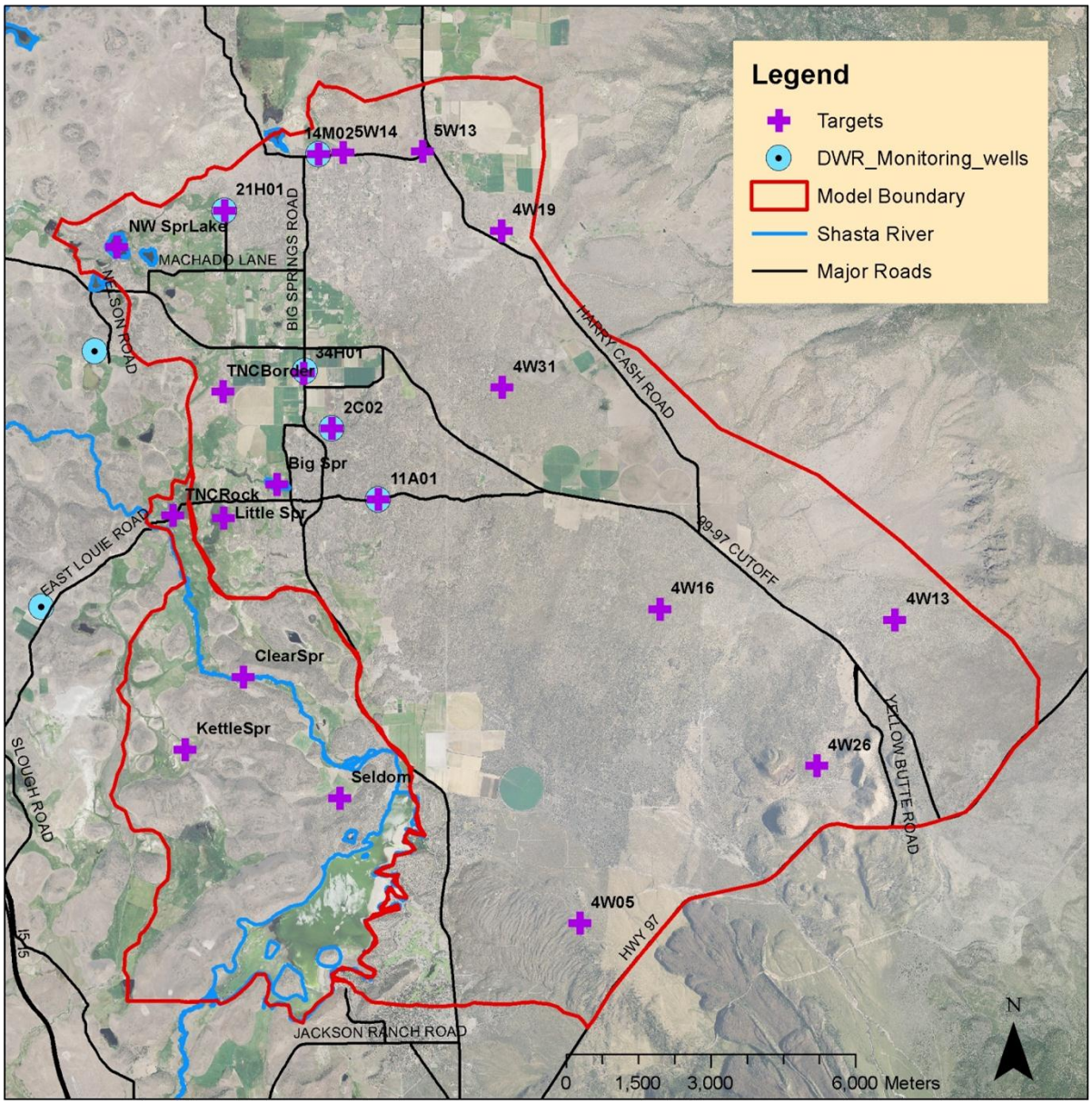

Figure 24. Groundwater head targets for 2008

Table 17. Target groundwater surface elevation (m)

Target Name	Elevation (m)
44N05W21H001M	789
Big Springs Lake	794
M43N04W26	991
M43N04W16	845
M43N04W13	1015
43N05W11A001M	795
43N05W02C002M	797
44N05W34H001M	795
44N05W14M002M	803
M42N04W05	862
M44N04W19	819
M44N04W31	807
M44N05W14	814
M44N05W13	820
Seldom Seen Well	818
Kettle Spring	792
Clear Spring	799
NW springfed lake	786
TNC Border Field M	768
TNC Rock House	762
Little Springs	794

Targets: spring flow

Groundwater flux can also be a useful target. In this case, spring flow data is not directly measured, but stream gauging in 2008 and 2009 at a few locations along Big Springs Creek provide an estimate of spring flow for the Big Springs complex (Big Springs Lake and Alcove springs combined) and Little Springs (Jeffres et al. 2009). Spring flow rates translated to volumes estimate 32 MCM from Big Springs Lake, 41 MCM from the Alcove springs complex, and 6.2 MCM from Little Springs. This amounts to approximately 73 MCM for the Big Springs complex and a total of 79 MCM from these three springs represented in the model. Mack (Mack 1960) reports 37 MCM from Big Springs Lake and an estimated 58 MCM from Big Springs Creek in the 1950s. Obtaining modeled spring flow overall for the Big Springs complex (Big Springs Lake, Alcove springs, and Big Springs Creek) in this range is the calibration target. Flows from Hole in the Ground spring are estimated at 4.9 MCM annually based on UC Davis data from 2009 (Jeffres et al. 2009; Nichols 2012, Personal Comm.).

Estimates of springs in the Parks Creek valley are tabulated in the Shasta Springs Ranch Hydrogeologic Assessment and used in this modeling effort as targets for these springs (Davids Engineering 2011c; Davids 2012, Personal Comm.). Annual 2010 flow volume for each spring is reported in Table 18.

Table 18. Parks Creek valley spring flow targets (MCM)

Spring Name	Annual Volume (MCM)
Clear Spring	1.9
Hidden Valley Spring	1.1
Kettle Springs	6.2
Black Meadow Springs	0.7
Bridge Field Springs	2.8

Another flux of interest is leakage from Lake Shastina. A water balance on the lake requires estimating inflows (complex and limited data), rainfall on its surface, evaporation, releases (data not accessible) and change in storage. Given these terms, groundwater leakage can be arrived at by difference. Such a balance was conducted for the 1972 period and it estimated groundwater seepage losses as 37.1 MCM (Dong et al. 1974; Vignola and Deas 2005). DWR reservoir storage and stage data only go back until 2005. However, based on precipitation at Montague inferred from Yreka data, 1972 was an average year with about 30.7 cm of rain (Davids Engineering 2011a). The 2008 water year was a dry year with less than 22 cm of precipitation. Presuming a drier year means lower lake levels, leakage in 2008 could be less than in 1972 (not accounting for other potentially influential factors). However, 37.1 MCM is used as a general estimate for lake leakage.

Little is currently known about the magnitude of groundwater flux to the west or north of the Pluto's Cave basalt flows. An unknown number of seeps and springs are present along the Shasta River upstream of its confluence with Big Springs Creek. They may be fed by groundwater flow from the Pluto's Cave aquifer suggesting some flow across the western model boundary. This is plausible since the contact between the Pluto's Cave basalt and the debris flow material does not directly follow the delineated model boundary and numerous springs occur along the contact of these formations (Mack 1960; Ward and Eaves 2008).

Calibration parameters

A number of model inputs are unknown or uncertain and so become candidates for calibration. Inputs with some level of uncertainty include GHB conductance, GHB head, river conductance, drain conductance, and hydraulic conductivity of aquifer material. The conductance term is a function of hydraulic conductivity (K), cross-sectional area (Area), and distance to specified head, as follows:

$$Conductance = \frac{K * Area}{distance}$$

This term has the same components for drain (springs), GHB, and river conductance but they have slightly different physical representations. The most influential unknowns in this term are the hydraulic conductivity (K) and saturated thickness. These can vary considerably (by orders of magnitude, especially for K).

The K value for GHB reaches, K zones, and the Shasta River and Parks Creek were adjusted to calibrate the 2008 steady state model. Reasonable ranges for the calibration parameters are established based on quality of the data or a reasonable range from the literature (Table 19).

Table 19. Parameter ranges for hydraulic conductivity (m/d) for calibration

Parameter	Reach #	Parameter	Material	Range Min	Range Max	Notes
GHB K & K zones	3,27,39	K(m/d)	Debris	10^{-5}	10^{3}	Max: upper end for gravel; Min: lower end for silt, not conductive
	1	K(m/d)	Alluvial	10^{-1}	10^{3}	Max: upper end for gravel; Min: low end of sand
	2,9,37	K(m/d)	Pluto's Cave	10^{-2}	10^{3}	K range for permeable basalt
River Conductance	all	K(m/d)	Alluvial/basalt	10^{-4}	10^{2}	Max: upper end for course sand; Min: low end for silt
Spring Conductance	all	K (m/d)	Fractured basalt/Debris flow	10^{-2}	10^{3}	K range for permeable basalt

(Domenico and Schwartz 1997)

Using Groundwater Vistas' automatic sensitivity analysis during model development identified General Head Boundary (GHB) conductance and head, river elevation, spring elevations, and aquifer hydraulic conductivity as sensitive parameters. The river and drain elevations were set based on model topography to be 1-1.25 meters below the model's top elevation in each model element corresponding to a river or spring location. GHB conductance and aquifer hydraulic conductivity as well as river conductance became the primary calibration parameters.

Model scenarios

Initial calibration efforts suggested the magnitude of groundwater flow across the northern and western boundaries has a significant effect on spring flow from the Big Springs complex. These boundaries are also a main source of uncertainty in the conceptual model. Therefore, instead of calibrating the model to reflect a single conceptual model with respect to these GHBs, three model scenarios were developed and calibrated.

The lack of groundwater head data available near and along the northern boundary introduces uncertainty in the GHB representation. The geology in the area is complex as well since the alluvial valley of the Little Shasta River meets debris flow material and tongues of the Pluto's Cave basalt (Figure 15). Given the contours in Mack (1960) (Figure 19), it is possible this border could effectively be a no flow boundary if set perpendicular to the water level contours. Additional and more recent points of measured water level along the boundary would serve to refine the water level contours and improve the representation of the GHB. This could be important given the high productivity of wells just north of the model domain on the Hart Ranch (pumped 1.85 MCM during the 2009 season) (Davids Engineering 2010). The western GHB is also important as it affects modeled spring flow and groundwater levels in the model domain. However, the amount of groundwater flow from the modeled area regionally into the debris flow material to the west or escaping from seeps and springs along the Shasta River further downstream is also uncertain.

To explore the role of these boundary flows in light of their uncertainty, three different model scenarios were calibrated by adjusting K values of the river, GHB conductance and K zones (Figure 20). The goal of the three scenarios was to achieve target spring flow for the major springs, lake leakage and stream-groundwater interaction of Parks Creek and Shasta River (Table 23) by calibrating different magnitudes of flow across the western and northern model boundaries. One conceptual model assumes relatively large flows across the northern and western boundaries calibrated with high K values for these GHB reaches (hereafter referred to as HIGH) while meeting target flows for the key springs and lake leakage. None of

the GHB reaches are no flow boundaries in this scenario. The second scenario takes the middle ground and assumes moderate inflows across the northern boundary with outflow only across the northern stretch of the western GHB (MODERATE). For this scenario, GHB reaches 1 and 39 were set as no flow boundaries and the remaining GHB Ks were adjusted by trial and error to achieve target spring flows (Figure 19). The third scenario assumes both the northern and western boundaries are no flow boundaries (the opposite extreme from the first scenario), with the exception of a short reach in the upper northwest corner of the model domain (Reach 2). This reach represents a tongue of the Pluto's Cave basalt extending toward the Shasta River (LOW). Together, these three conceptual models explore the relationship between these boundaries and spring flow by adjusting River, K zone, and GHB K values. The models are calibrated such that spring flow results from the three models are similar (Table 23). They aim to have similar model performance with regards to modeled groundwater head and spring flow.

Results

Modeled groundwater in the Pluto's Cave basalt aquifer flows northwestward and then west toward the Shasta River (Figure 25). Groundwater flow direction is perpendicular to water level contours. Closely spaced contours indicate higher hydraulic gradients. To maintain higher heads in the southeast area of the model where modeled aquifer thickness is greater, lower K values were assigned to the K zones in those areas (zones 4, 5, and 7). Differences in contours in the northern portion of the model domain reflect the differences in flow occurring across the northern and western boundaries in the different model scenarios. The HIGH model scenario shows significant groundwater flow across the northern border, through the model domain, and out the western border north of Big Springs Creek. In contrast, the LOW model maintains groundwater flow in a northwest direction with the only outflow occurring through the northwestern tip of the model domain (Figure 25).

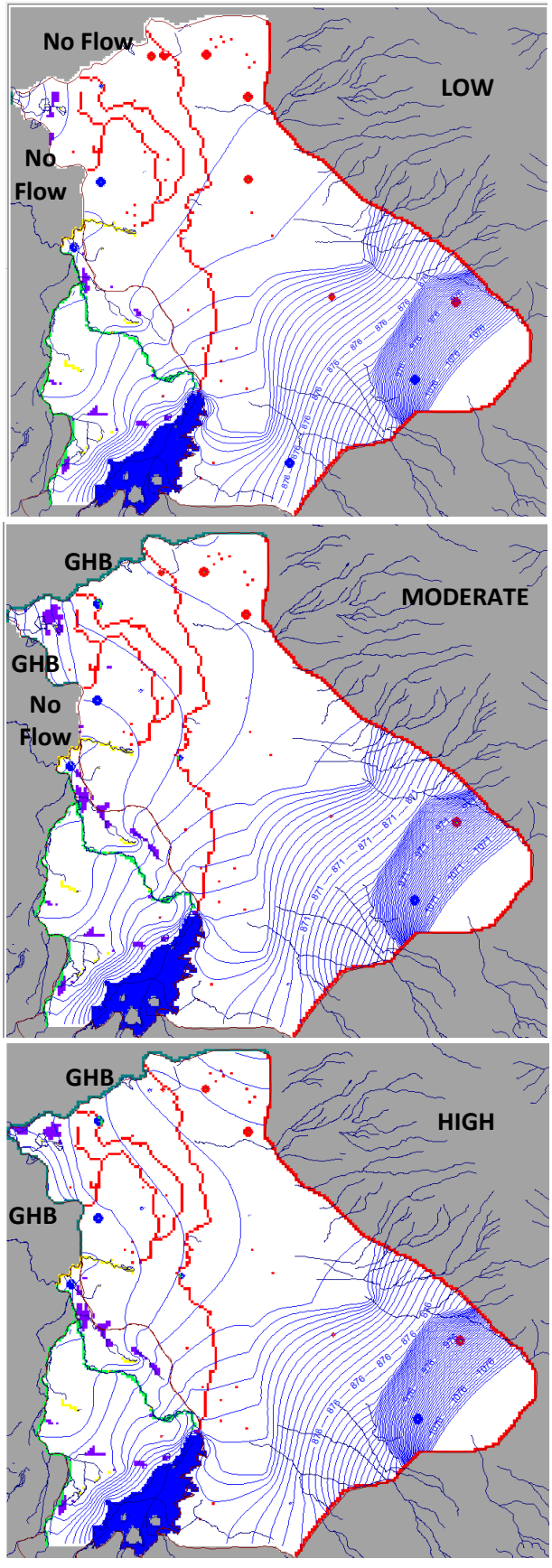

Figure 25. Groundwater level contours (blue) for three model scenarios: HIGH, MODERATE, and LOW. Red cells are 'wells' (injection wells for canals and Mt. Shasta recharge boundary; extraction wells for pumping), Blue is Lake Shastina, Green cells are Parks Creek and Shasta River, Purple cells are where ground surface is below water surface elevation, gray area is no flow (outside active model domain)

Measured v. modeled heads and fluxes

A single hydraulic conductivity (K) homogeneous model was not adequate for modeling heads reasonably close to their target values. Therefore, additional K zones were added to reflect changing transmissivity due to varying modeled aquifer thickness and different geological materials (Figure 20).

Calibrated K values were initially set and adjusted by trial and error based on their effect on modeled heads compared to target heads. Then K values were further adjusted based on resulting dynamic groundwater fluxes (spring flow, lake leakage, stream-groundwater interaction). Generally, areas with greater modeled thickness were assigned smaller K values. This was especially important in the southeastern portion of the model domain where groundwater levels are furthest from the ground surface but the aquifer is thickest. A range of K values for each K zone, river reach and GHB reach were explored with some reaches having a large range (on the order of 275 m/d) to others having a tighter range of K that yielded reasonable results (on the order of 0.3 m/d). Table 20 shows the minimum and maximum K values for each reach and the range experimented with during the calibration process. Some reaches were more sensitive to changes in K than others. For example, the debris flow and S.E. Pluto's South (K zone reaches 1 and 7) directly affected lake leakage from Lake Shastina. Only a narrow K range resulted in reasonable spring flows from the Parks Creek valley springs. Other reaches such as the Pluto's Cave basalt (K zone reach 2) could vary considerably depending on the values of other K zones and the GHB K values. Final parameter values are shown in Table 21.

Table 20. Minimum, Maximum and Range of K (m/d) considered for each reach during calibration (See Figure 19 and Figure 20 for reach locations)

		K values (m/d)		
Reach #	**Name**	**Minimum**	**Maximum**	**Range**
Rivers				
20	Shasta River	2.2	10	7.8
21	Parks Creek	10	10	0.0
K zones				
1	Debris flow	1.4	1.9	0.5
2	Pluto's Cave basalt	96	411	315
3	Alluvium	27	82	55
4	S.W. Debris/Alluvium	6.8	16	9.0
5	S.E. Pluto's North	2.2	4.1	1.9
6	N.W. Pluto's Cave	2.7	178	175
7	S.E. Pluto's South	0.41	0.82	0.41
8	N.E. Volcanic	68	205	137
GHBs				
1	Alluvium	68	274	205
2	Pluto's Cave basalt	205	274	68
3	Debris/Alluvium	0.27	137	137
9	Pluto's Cave basalt	14	274	260
27	Debris/Alluvium	2.7	137	134
37	Pluto's Cave basalt	68	274	205
38	Volcanic	0.27	55	55
39	Debris/Alluvium	14	137	123

Table 21. Calibrated K values for river conductance, GHB conductance, and aquifer K zones. NA indicates reaches that are set as no flow boundaries to define the three different scenarios with remaining K values calibrated. (See Figure 19 and Figure 20 for reach locations)

		K values (m/d)		
Reach #	**Name**	**HIGH**	**MODERATE**	**LOW**
Rivers				
20	Shasta River	4.1	4.1	2.7
21	Parks Creek	10	10	10
K zones				
1	Debris flow	1.6	1.6	1.4
2	Pluto's Cave basalt	205	178	288
3	Alluvium	49	49	41
4	S.W. Debris/Alluvium	15	16	6.8
5	S.E. Pluto's North	4.1	4.1	4.1
6	N.W. Pluto's Cave	14	8.2	14
7	S.E. Pluto's South	0.41	0.41	0.41
8	N.E. Volcanic	205	205	205
GHBs				
1	Alluvium	274	NA*	NA
2	Pluto's Cave basalt	274	205	274
3	Debris/Alluvium	137	0.27	NA
9	Pluto's Cave basalt	137	205	NA
27	Debris/Alluvium	137	14	NA
37	Pluto's Cave basalt	137	205	NA
38	Volcanic	55	1.1	NA
39	Debris/Alluvium	14	NA	NA

* NA indicates reach set as no flow boundary conditions, other Ks calibrated

Modeled groundwater levels compared to targets guided K value calibration. Table 22 shows the difference between the modeled and target heads at each of the target locations for the three scenarios. The largest residuals occur at two wells in the southeastern area of the model, M43N04W26 and M43N04W13 (Figure 24). From well logs, static groundwater in this area can vary by more than 60 meters within a Section (1-mile square). A residual of +/- 30 meters was therefore considered acceptable. The other high residual occurs for the TNC Border Field Middle and TNC Rock House targets. The negative value indicates that the modeled water level is too high relative to the target groundwater elevation. These two residuals indicate the complexity of the geology that is not captured by this regional model. The water surface elevation in these wells is relatively low considering their proximity to Big Springs Creek and spring flow conditions. If these groundwater heads were matched, no spring flow from the Big Springs complex would occur in the model.

Table 22. Calibration statistics and residuals (measured minus modeled water level) (Figure 24)

Target	Residual (m)		
	HIGH	MODERATE	LOW
44N05W21H001M	-11	-13	-5
Big Springs Lake	0	0	1
M43N04W26	-32	-32	-32
M43N04W16	4	4	8
M43N04W13	27	27	28
43N05W11A001M	-6	-6	-1
43N05W02C002M	-1	-1	3
44N05W34H001M	-4	-4	2
44N05W14M002M	-4	-3	9
M42N04W05	-2	-2	-11
M44N04W19	10	13	24
M44N04W31	1	1	9
M44N05W14	5	7	20
M44N05W13	9	13	26
Seldom Seen Well	0	0	1
NW springfed lake	1	0	0
TNC Border Field M	-27	-28	-24
TNC Rock House	-26	-26	-26
Little Springs	1	1	2
Calibration Statistics (m)			
Residual Mean	-3	-2	2
Res. Std. Dev.	13	13	16
Sum of Squares	3564	3874	5122
Abs. Res. Mean	8	9	11
Min. Residual	-32	-32	-32
Max. Residual	27	27	28
Range	253	253	253

Note: Negative value indicates modeled water elevation is higher than target elevation.

Residuals between the three models are very similar and generally fall near the one-to-one line (Figure 26).

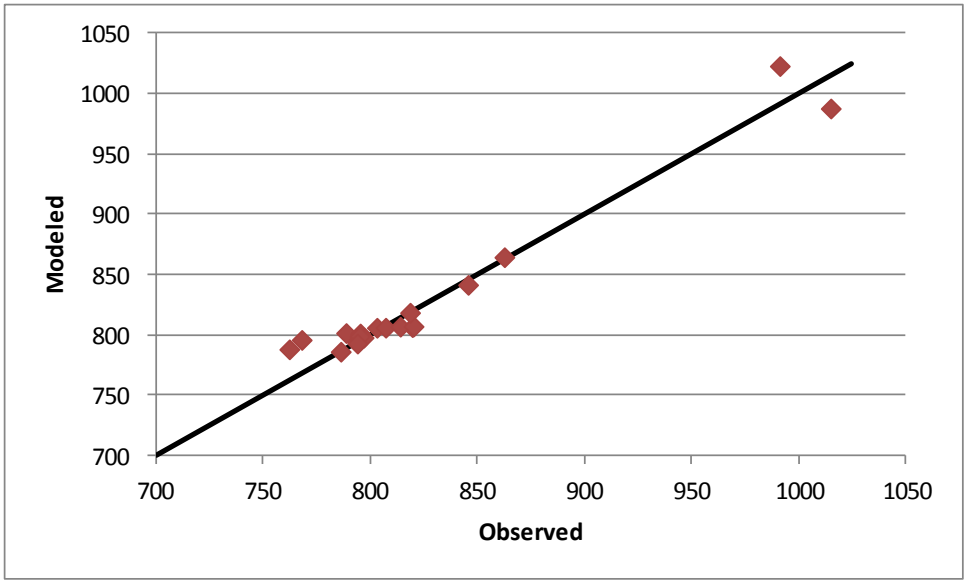

Figure 26. Observed vs. modeled groundwater surface elevation (meters) at targets compared with one-to-one line

Simulated annual spring flow volume for each modeled spring compared to its estimated target is shown in Table 23 and includes flow results for surface water features and GHB reaches. The springs with modeled flows closest to their target annual flow include Big Springs Creek, Hole in the Ground, Clear Spring, Black Meadow Spring, and Bridge Field Spring. The most problematic springs are Hidden Valley Spring, Little Springs, and Kettle Springs. All but Hidden Valley Spring have smaller modeled flows than their target flow. Uncertainty in Hidden Valley Spring's exact geographical location (and its associated specified elevation) may contribute to its high flow. If the modeled elevation is too low, this would cause higher than observed spring flow. In general, these springs' more complicated responses to changes in K zone K values, stream-groundwater interaction dynamics, and to a lesser degree, GHB flows make them more difficult to calibrate. Little Springs has zero flow in all three model scenarios because groundwater head is always a meter or two below the modeled spring (model drain elevation) at that location (Figure 21). Adjusting the representation of the Big Springs complex (Big Springs Lake and Big Springs Creek) may be beneficial for modeled flow from Little Springs since the Big Springs Lake and Creek modeled springs highly influence groundwater heads in the area (Figure 21). However, it is already difficult to simulate high enough flows from the Big Springs complex due to Big Springs Lake's lower modeled flows than estimated actual flow. It was difficult to get much higher flows from this modeled spring. In reality, the physical system is not a homogenous aquifer but fractures and possibly even lava tubes or collapsed lava tubes play a significant role in providing high conductivity flow paths and a source of water to the Big Springs complex. This complexity is not represented by this regional model. Additional K zones that provide greater heterogeneity and represent localized high flow zones or reduced K downstream of the spring may improve model results. Results, however, suggest modeled spring flow from Big Springs Lake at least partially depends on flow from the northern GHB (Table 23). Modeled spring flow from Big Springs Lake is greatest when high flows enter the northern model boundary (HIGH scenario) and is maintained with reduced but MODERATE boundary inflows. In contrast, no spring flow occurs from Big Springs Lake when the northern and most of the western boundary are no flow boundaries (Table 23). Groundwater inflow from the north seems necessary to maintain heads that support spring flow from the Big Springs complex.

Table 23. Detailed modeled flow results (MCM) for surface water features, general head boundaries (GHB) and spring flows. Note: Positive value is flow into groundwater, Negative value is flow out of groundwater.

	WY 2008 Flow Volume (MCM)			
Feature/Reach #	**Target**	**HIGH**	**MODERATE**	**LOW**
Surface Water				
Lake Shastina	37.1	38.3	35.4	36.4
Shasta River		-0.4	-0.7	3.9
Parks Creek		-4.7	-4.7	-4.3
Northern GHB				
GHB 3		16.1	0.1	0
GHB 9		9.2	30.4	0
GHB 37		3.1	3.7	0
GHB 38		62.8	15.5	0
Total		91.1	49.7	0
Western GHB				
GHB 1		6.1	0	0
GHB 2		-17.5	-5.0	-8.2
GHB 27		-43.9	-12.0	0.0
GHB 39		-8.9	0	0
Total		-64.2	-17.0	-8.2
Springs				
Big Springs Lake	-37.0	-18.2	-17.9	0
Big Springs Creek	-58.0	-62.5	-63.6	-53.6
Little Springs	-6.2	0	0	0
Hole in the Ground	-4.9	-3.8	-3.9	-2.5
Clear Spring	-1.9	-0.7	-0.7	-0.3
Hidden Valley Spring	-1.1	-4.6	-4.8	-2.9
Kettle Springs	-6.2	-3.5	-3.5	-2.9
Black Meadow Spring	-0.7	-0.9	-0.9	-0.8
Bridge Field Spring	-2.8	-3.1	-3.1	-2.5
NW Springfed Lake	< 1.2	-0.5	-2.1	-0.5
Mack Spring	0.0	-2.6	-2.6	-2.2
Total	-117.5	-100.5	-103.1	-68.2

Note: Big Springs Lake and Big Springs Creek make up the Big Springs complex.

Model water budget

Model mass balance results for groundwater inflows and outflows show the relative contributions of different flow paths (Table 24). These vary between the three scenarios, as shown with pie charts (Figure 27). Inflows in the LOW model are composed only of Mount Shasta recharge, local recharge (deep percolation of applied water/precipitation and canal leakage), and Lake Shastina leakage. The fraction of lake leakage increases in the LOW model partially compensating for the loss of inflow from the northern boundary. The portion of outflows attributed to net western GHB flow decreases from the HIGH to MODERATE to LOW model scenarios. Total spring flow increases as a total portion of outflows most significantly from the HIGH to MODERATE model even though the volume of spring flow for the two

models is virtually the same (about 100.5 and 103.1 MCM, respectively). This is because the total volume of outflows is so much greater in the HIGH model.

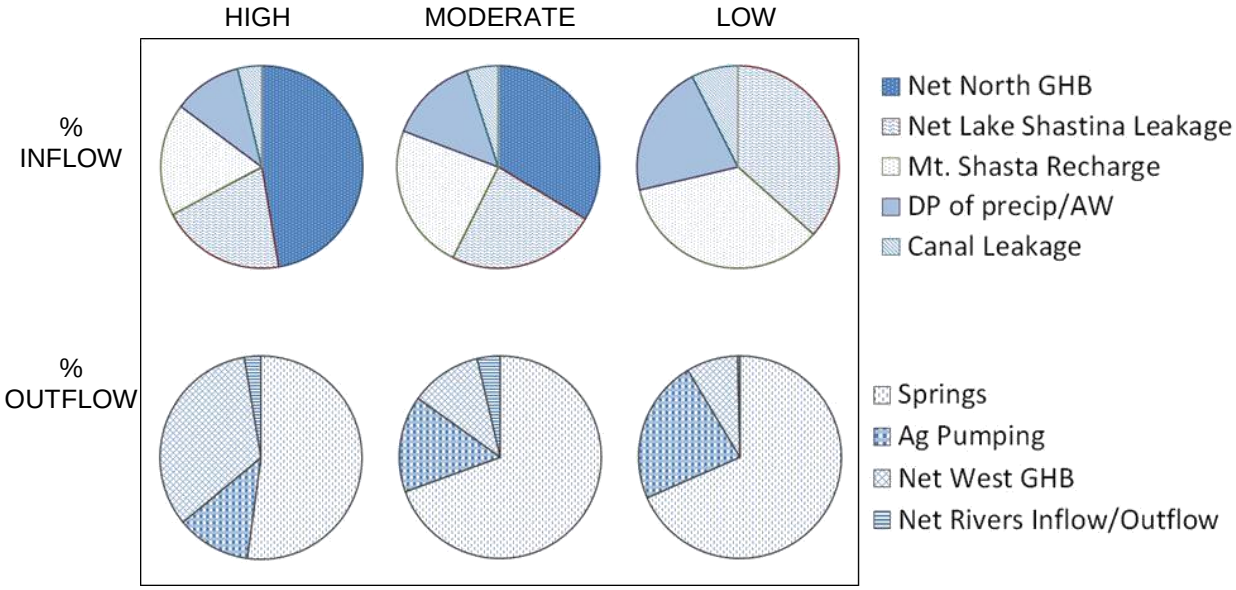

Figure 27. Percentage of inflow and outflow for major flow paths for each realization.

Table 24. Mass balance of model inflows and outflows (MCM/year) for the three model scenarios: HIGH, MODERATE, and LOW.

Flow Path (MCM/yr)	HIGH real.				MODERATE real.				LOW real.			
	IN	OUT	% IN	% OUT	IN	OUT	% IN	% OUT	IN	OUT	% IN	% OUT
Net North GHB	91.1		47%	0%	49.7		34%	0%			0%	0%
Net Lake Shastina Leakage	38.3		20%	0%	35.4		24%	0%	36.4		37%	0%
Mt. Shasta Recharge	34.6		18%	0%	34.6		23%	0%	34.6		35%	0%
DP of precip/AW	21.1		11%	0%	21.1		14%	0%	21.1		21%	0%
Canal Leakage	7.4		4%	0%	7.4		5%	0%	7.4		7%	0%
Springs		100.5	0%	52%	0.0	103.1	0%	69%	0.0	68.2	0%	68%
Ag Pumping		22.8	0%	12%	0.0	22.8	0%	15%	0.0	22.8	0%	23%
Net West GHB		64.2	0%	33%	0.0	17.0	0%	11%	0.0	8.2	0%	8%
Net Rivers Inflow/Outflow		5.1	0%	3%	0.0	5.5	0%	4%	0.0	0.4	0%	0%
Total	192.6	192.7	0%	0%	148.2	148.3	0%	0%	99.5	99.6	0%	0%
Model Mass Balance Error (%)	-0.037				-0.060				-0.088			

Sensitivity analysis

Due to uncertainties in model inputs, we explore model sensitivity to changes in Mount Shasta recharge, agricultural groundwater pumping, and local recharge (deep percolation of precipitation and applied water and canal leakage). For the sensitivity analysis, these model inputs are increased and decreased by 10-30% and the effect on major groundwater fluxes is evaluated separately for each of the three boundary flow scenarios. This further quantifies the significance or insignificance of model boundary fluxes under various groundwater flow conditions across the northern and western boundaries.

Sensitivity analysis for the three model scenarios involved 84 model runs in which model inputs for Mount Shasta recharge, pumping, and local recharge were increased and decreased by 10% and 30%. Resulting effects on groundwater fluxes were equal and opposite for increased vs. decreased inputs. Since the effect on fluxes was minor even at the 30% adjustment, the following presents results only for a 30% increase in each input.

Big Springs complex flow and Lake Shastina leakage are most sensitive to changes in Mount Shasta Recharge. The effect on the Big Springs complex flow of increased recharge from Mount Shasta of 30% is an increased spring flow of 4, 5 and 11 percent, respectively (Table 25). The Big Springs complex is most sensitive with the LOW model. This is also true for the Shasta River Springs (Hidden Valley Spring and Clear Spring) and Hole in the Ground spring (Table 25). Lake leakage decreases with a 30% increase in recharge from Mount Shasta by 9, 10, and 7 percent for the HIGH, MODERATE, and LOW models, respectively. The three scenarios respond similarly to lake leakage.

Table 25. Percent change in flow with a 30% increase in Mount Shasta recharge rate

Major Flow Path	HIGH	MODERATE	LOW
Big Springs Complex	4%	5%	11%
Parks Creek Valley Springs	0%	0%	0%
Shasta River Springs	2%	2%	4%
Hole in the Ground	3%	3%	6%
Northern GHB	-2%	-2%	NA
Western GHB	0%	1%	1%
Shastina Leakage	-9%	-10%	-7%

Adjusted pumping in different agricultural zones independently has a similar effect on spring flows, general head boundary flow, or lake leakage (within 3%) with the three model scenarios (Table 26). The greatest sensitivity to increased/decreased pumping in the ag zones on the Big Springs complex spring flow is pumping in ag zones 2 and 3. Even with this, the three models respond similarly to perturbed pumping. With a 30% increase in pumping in this area, the Big Springs complex flow decreases 3, 4, and 6 percent for the HIGH, MODERATE, and LOW models, respectively. Perturbed pumping in any other ag zones, at most, leads to a 1 or 2 percent response in spring flow, general head boundary flow, or lake leakage. When pumping in all wells in the model domain are increased by 30%, the Big Springs complex is most affected with a 5, 5, and 10 percent decrease in flow for the HIGH, MODERATE, and LOW models, respectively. The effect of pumping on spring flow is greatest in the LOW realization, but is only 5% different than for the other two scenarios. The HIGH and MODERATE model results are very similar for changes in pumping.

Table 26. Percent change in flow with a 30% increase in agricultural pumping rate

Major Flow Path	Ag zone 1			Ag zone 2 & 3			Ag zone 4			Ag zone 5, 6 & 7			All wells		
	HIGH	MODERATE	LOW	HIGH	MODERATE	LOW	HIGH	MODERATE	LOW	HIGH	MODERATE	LOW	HIGH	MODERATE	LOW
Big Springs Complex	0%	0%	-1%	-3%	-4%	-6%	-1%	-1%	-1%	0%	0%	-1%	-5%	-5%	-10%
Parks Creek Valley Springs	0%	0%	0%	0%	0%	0%	0%	0%	0%	0%	0%	0%	0%	0%	0%
Shasta River Springs	0%	0%	0%	0%	0%	-1%	0%	0%	0%	0%	0%	0%	-1%	-1%	-2%
Hole in the Ground	0%	0%	0%	-1%	-1%	-2%	0%	0%	-1%	0%	0%	0%	-1%	-1%	-3%
Northern GHB	0%	1%	NA	1%	1%	NA	0%	0%	NA	0%	0%	NA	2%	3%	NA
Western GHB	0%	0%	0%	0%	-1%	-1%	0%	0%	0%	0%	0%	0%	0%	-1%	-1%
Shastina Leakage	0%	0%	0%	0%	0%	0%	0%	0%	0%	1%	1%	1%	1%	1%	1%

All major flow paths are slightly sensitive to changes in local recharge (deep percolation of applied water and precipitation and canal leakage from Big Springs Irrigation District and Montague Water Conservation District canals). Local recharge refers to recharge that occurs within the active model domain. The most sensitive flux again is the Big Springs complex, on the order of a 4, 5, and 10 percent increase for the HIGH, MODERATE, and LOW models, respectively, with a 30% increase in local recharge. The Parks Creek Valley springs and Shasta River springs (Hidden Valley and Clear spring) increase 2 to 3 percent for the three model scenarios. Hole in the Ground increases the most, 5%, for the LOW model and 2 and 3 percent for the HIGH and MODERATE models, respectively. Increased groundwater levels in the model domain from increased local recharge lead to decreased flow across the northern boundary. However, the flow out of the model across the western boundary increases 1 to 2 percent. Lake Shastina

leakage decreases 2 percent in all three model scenarios. Overall, model performance and response to changed local recharge is very similar between the three models.

Table 27. Percent change in flow with 30% increased local recharge (deep percolation of applied water and precipitation and canal leakage rates)

Major Flow Path	HIGH	MODERATE	LOW
Big Springs Complex	4%	5%	10%
Parks Creek Valley Springs	2%	2%	3%
Shasta River Springs	2%	2%	3%
Hole in the Ground	2%	3%	5%
Northern GHB	-3%	-3%	NA
Western GHB	1%	1%	2%
Shastina Leakage	-2%	-2%	-2%

Discussion

Developing the mass balance of a system, with its major inflows and outflows estimated, is a useful way to assess our understanding of a system and get an idea of the relative importance of flow paths. Figure 28 shows the MODERATE scenario mass balance of inflows (+) and outflows (-) within the context of the area's topography and model domain. This makes it easy to see that the dominant outflow is spring flow, whereas the inflow is more divided between several sources: lake leakage and boundary flows (from Mount Shasta and from the north).

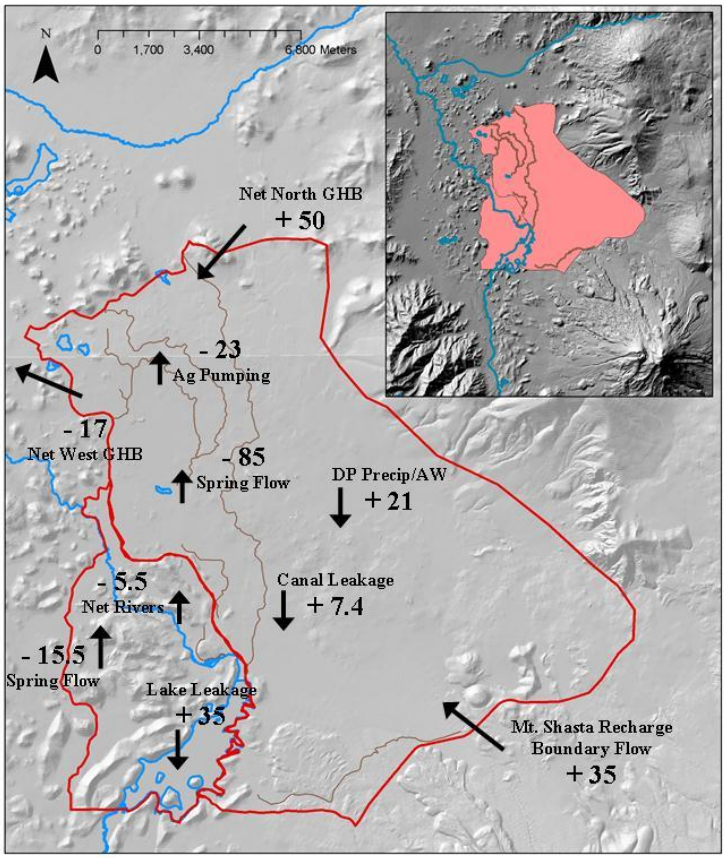

Figure 28. Mass Balance for MODERATE scenario with approximate flows in million cubic meters (MCM)

Using estimates of inflows and outflows developed for model input and calibration, a mass balance approach can be used to estimate the uncertain net boundary flows and stream-groundwater interaction as a single closure term (Table 28). This suggests a net inflow of about 40.8 MCM into the model domain.

Table 28. Mass balance summary based on estimates for model inputs. Closure term represents net boundary flows and stream-groundwater interaction.

	Annual Volume (MCM)	
	Inflow	**Outflow**
Mt. Shasta recharge	34.6	
Canal leakage	7.4	
Lake leakage	37.1[a]	
DP precip/AW	21.0	
Spring flow		118[b]
Ag pumping		22.8
Closure term	40.8	
Total	141.0	141.0

[a] *from 1972 water balance of Lake Shastina*
[b] *from sum of target spring flows in Table 23*

Going beyond mass balance analysis and developing a groundwater model however has added value and eliminates the need for a closure term. Flow paths such as boundary flows and stream-groundwater interaction can be difficult to explicitly estimate but can be simulated using head data and general head boundary conditions with a numerical groundwater model. Assumptions related to these closure term flows can be tested and explored within the framework the model. Developing the groundwater model of the Pluto's Cave and Parks Creek valley aquifer in the Shasta Valley is largely a mass balance exercise while also providing a tool that allows for sensitivity analysis and exploration of how inflows and outflows relate and may affect each other. It also provides a framework for assessing our uncertainty about the conceptual model and a way to evaluate the significance of data gaps or lesser quality data. The following discusses the sensitivity analysis and resulting flow dynamics that lead to conclusions not possible through mass balance analysis alone. The discussion includes analysis of Lake Shastina leakage, Parks Creek valley and its relation to the rest of the model domain, the Big Springs complex, and boundary flows.

Lake Shastina leakage responds similarly in all three model scenarios to the sensitivity analysis. Lake leakage is most sensitive to the K value of the debris flow on its northwest side (zone 1), K zone 4 on the southeast side, and Pluto's Cave basalt K (zone 2). During calibration, the debris flow K was calibrated to produce reasonable spring flows in the Parks Creek valley. Lake leakage into the basalt and through its southeast side is necessary to maintain a total leakage in the 37 MCM range while also hitting target head at the Seldom Seen well and reasonable spring flows. Therefore, K values for K zones 2 and 4 were in part calibrated to lake leakage and head at the M42N04W05 target. Results suggest Lake Shastina recharges the Pluto's Cave basalt aquifer and Parks Creek valley area.

The Parks Creek valley springs include Kettle Springs, Black Meadow Springs, Bridge Field Springs, and the Mack spring. These springs are generally isolated from the rest of the model and insensitive to changes in boundary conductance and most K zones including K of the Pluto's Cave basalt. Spring flow at Black Meadow Springs, Bridge Field Springs, and the Mack spring were calibrated primarily with the K value of the debris flow, as mentioned above. In addition to K zone 1, Kettle Springs is most sensitive to the K value of the Alluvium (K zone 3) and to some degree Parks Creek and Shasta River's conductance. Improved representation of Parks Creek's water surface elevation (head) may improve calibration for head in the Parks Creek valley and flow from Kettle Springs.

The Big Springs complex responds similarly to changes in pumping, Mount Shasta recharge, and local recharge. A 30% increase in pumping in agricultural zones 1-7 amounts to an additional 3.88 MCM extracted from the basin. A 30% increase in Mount Shasta recharge amounts to an additional 10.4 MCM inflow to the basin and a 30% increase in local recharge is an additional 6.33 MCM of inflow. Yet with these varying changes to inputs, the response of the Big Springs complex was consistently 4-5%, 5%, and 10-11% for the HIGH, MODERATE, and LOW models, respectively, for each of the changed inputs. This suggests Big Springs complex is almost equally sensitive to all three of these inputs regardless of the model scenario.

The three model scenarios explore changing flow dynamics with changes in the conceptual model regarding northern and western boundary conditions. The Big Springs complex is very sensitive to flow across the northern GHB. Hydraulic conductivity values for reaches along the northern GHB were important calibration parameters for Big Springs complex flow in addition to K zone 2, the Pluto's Cave basalt. Hole in the Ground spring flow was also sensitive to the volume of flow from the north, although to a lesser degree. From spring flow and head results for the three scenarios, some flow from the north seems necessary to contribute to spring flow as well as increase water levels in the northeast corner of the model domain. The magnitude seems to be less important than that some occurs. For example, the LOW model (with zero flow across the northern boundary) was unable to produce Big Springs complex flows much above 53 MCM without inflow from the north. However, the HIGH model resulted in 91.1 MCM across the northern border and 64.2 MCM outflow across the western GHB. This equates to 2.04 m^3s^{-1} over the course of the year across the western border which is unreasonably high if it were to contribute to Shasta River flows downstream. The Shasta River accretes some flow from minor seeps and springs (probably 0.03-0.14 m^3s^{-1}). The only spring flow of this higher magnitude contributing to Shasta River flow is the Big Springs complex. The MODERATE model results are more reasonable with regards to the western GHB outflow; its 17.0 MCM of outflow amounts to about 0.54 m^3s^{-1}. This is more on par with possible outflow to the Shasta River. Further analysis of groundwater accretions to the Shasta River downstream of the Big Springs Creek confluence would help to better calibrate outflow from the western GHB. The high flows across the northern boundary in the HIGH model are largely compensated for by high flow across the western GHB. So the HIGH and MODERATE models perform and respond similarly to changes in inputs, as shown by the sensitivity analysis. Improved groundwater head data in the north and additional hydrogeologic information in that area would improve the representation of the northern GHB and provide greater confidence in the calibration of its conductance values. However, for the exploration of regional aquifer dynamics, the magnitude of flow across the northern and western boundaries does not significantly affect model results given at least some flow occurs across both boundaries. A portion of the inflow to the model domain across the northern GHB flows out of the model domain across the western boundary.

Calibrated K values ranged from 0.3 m/d to 275 m/d for the three model scenarios for the eight K zones. The range for the MODERATE scenario was 0.3 to 205 m/d. This is well within the range estimated in other studies for areas with similar hydrogeologic systems. Calculated hydraulic conductivities in Jefferson et al (2006) range from about 25 to 860 m/d for volcanic aquifers in Oregon's High Cascades. To the east of their study area in the Deschutes River basin, Gannett and Lite (2004) calibrate a MODFLOW model for the basin with a similar range of K values, 10^{-3} to 300 m/d. Basalt flows on Kilauea, Hawaii, also have similar hydraulic conductivities (Jefferson et al. 2006).

In its current state, this steady state groundwater model allows for testing variations of our conceptual model and observing more specifically how changing flow magnitudes affect each other (see Appendix A for an adjusted conceptual model and initial results). Additional development would add to its value and utility. This includes expanding the model in time to span a series of years, or to make it a multi-year model with seasonal or monthly time steps. This would better capture hydrologic variability within and between water years, which is significant and important for understanding timing of system dynamics (Huntington and Niswonger 2012; Tague and Grant 2009). This would be useful in further exploring the variability and relationships between spring flow and Mount Shasta recharge and pumping as well as Lake Shastina leakage. With further development and calibration of the Parks Creek valley area, the model could be used to explore management of local water diversions, pumping, and reservoir releases in the Upper Shasta River and Parks Creek system. As is, the results and current model are not

sufficiently developed to make management conclusions for this system and resulting policy decisions. It is currently useful for exploring our regional scale understanding/misunderstanding of the system and evaluating what additional data would be most valuable.

Assessment of data needs

The process of groundwater modeling requires a thorough evaluation of a system's major components and flow paths in its water balance and allows for exploration of aquifer dynamics. This illuminates influential data gaps that limit model performance and understanding of the physical system.

Areas of limited data include measured annual spring flows. Work by researchers at the UC Davis Center for Watershed Sciences have collected data since 2004 that provide general magnitudes useful as a starting point for many of the major springs associated with the basalt aquifer (Jeffres et al. 2009). Recent studies on the Emmerson Ranch conducted in cooperation with the California Department of Fish and Game have also provided some valuable baseline data for spring flow in that part of the valley (Davids Engineering 2011b; Davids Engineering 2011c). However, for long term assessment of spring flow, recharge, and pumping interaction, major springs should continue to be measured. Better and more accurate spring flow measurements would also increase confidence in model calibration.

Additional chemistry and isotope analysis of springs and seeps along the Shasta River above Big Springs Creek and below Dwinnell Dam could further elucidate their source, whether it is primarily recharged from Lake Shastina or flow from the Pluto's Cave basalt to the east. This would help better qualitatively and perhaps quantitatively describe the degree to which flows from the Pluto's Cave basalt outflow to the Shasta River or flow into the debris flow material.

Due to the important influence of local hydrogeologic features on specific well conditions and the resulting highly variable well production, the value of pumping tests in this area to improve model parameters and representation may be low. The parameters in the model reflect regional effective hydraulic conductivities in contrast to localized parameters that are estimated from pumping tests. Instead, better characterizing the aquifer's extent (geologic formation boundaries) and depth would improve model representation and calibration results. Cores to determine the extent and depth of the Pluto's Cave aquifer in the southern area near Juniper Flats, along the east side, and in the north would help refine the modeled aquifer thickness which influences the calibrated hydraulic conductivities. Existing well logs could also be used to more thoroughly map hydrogeologic features and aquifer depth and refine K zones.

Lake Shastina is important hydrologically in influencing spring flow and water elevations in the Parks Creek valley (Davids Engineering 2011c). The only comprehensive available water balance for the reservoir is from 1972 data (Dong et al. 1974). Conducting a water balance on the reservoir would require additional measurements of smaller surface water inflows (such as Garrick Creek), accurate inflow data for the Shasta River, and cooperation with MWCD to obtain releases to their canal. Doing this for a variety of year types in conjunction with spring flow (of Kettle Springs, Clear Springs, Bridge Field Springs and Black Meadow Springs), Shasta River gauging, and water level measurements would help characterize the leakage and the lake's interaction with the groundwater system. This could be used to further calibrate the groundwater model and refine the K zones in this area.

Additional water level monitoring with better geographic coverage would further strengthen modeling efforts by providing additional head targets on which to calibrate. Many of the currently used targets are from well logs and as a result their ground surface elevation is not surveyed and unknown. Therefore, the water surface elevation of these targets is estimated based on the ground surface elevation at the centroid of their township, range, and section. Specifically, additional water level data near the northern, western and eastern model boundaries would help better define flow directions across these boundaries or clarify if there is likely no flow across them. More specific geologic mapping along formation boundaries and corresponding water level data in these areas would also be valuable in better understanding groundwater flow across and between geologic formations.

This modeling effort assigns a no flow boundary to the eastern border of the model domain. The appropriateness of this assumption could be further explored (see Appendix A). Future work could estimate the potential recharge from the east to gain a sense of its magnitude and whether or not it may

be a significant contributor. A thorough assessment would require a survey and evaluation of springs and runoff features draining that area. Future work should further refine the definition of the recharge areas by identifying elevation bands corresponding to the average recharge elevation indicated by available isotope data available for the Big Springs complex. Furthermore, model calibration could be refined by using age data from Big Springs compared to calculated travel times from the groundwater model results to help calibrate K.

Limitations

Modeling efforts inherently have limitations as simplifications, imperfect data, and assumptions are unavoidable. The greatest simplification is the use of an equivalent porous media model to represent a very complex fracture flow system. This is necessary due to the lack of data and specific understanding of the aquifer's subsurface. However, it requires a caveat on applications of this modeling work. The assumption that the fracture system can be represented as an equivalent homogeneous porous media has validity if the scale of investigation far exceeds the scale of individual fracture systems. Internal boundary fluxes (recharge, pumping, spring flow) and external boundary fluxes (via boundary conditions) represent effective flow rates in the general vicinity of the specific location of these boundary fluxes. The model is not intended to be used to assess pumping effects of a specific well on spring flow or even groundwater flow direction at a specific location, as these are highly dependent on local hydrogeologic features. The presence of preferential flow paths (possibly lava tubes or contacts between basalt flow events) plays a huge role in the magnitude of local fluxes within this aquifer, at a scale less than a few hundred meters. This is evidenced by highly variable well production and groundwater elevations. This model represents general flow magnitudes and regional dynamics but should not be used to assess specific conditions at a particular well or location. A few other limitations warrant specific mention.

Limitations on data accessibility necessitated broad assumptions in some cases. This is true of the estimated volume of pumped groundwater from Montague Water Conservation District (MWCD) wells. Pumping from Big Springs Irrigation District wells and other private pumping can be estimated based on water demand estimates and irrigation efficiency of crops since direct pumping data is not available. However, pumping estimates for MWCD wells is complicated by their access to surface water resources. Simplifying assumptions were also necessary to estimate the volume of canal recharge since the exact volume of water released to the MWCD canal was unknown. In addition, the use of the Weed station precipitation data to represent precipitation input throughout the model domain limits the accuracy of the estimated deep percolation from precipitation. This approach should be refined in future work.

The steady state model is limited and not able to explore the timing and effects of seasonal and inter-annual fluctuations in groundwater boundary fluxes, particularly pumping and recharge. In addition, Lake Shastina head varies considerably over the course of a year and this appears to play a role in the timing of spring flows (Davids Engineering 2011c). This annual steady state model is not able to simulate the timing and effects of these varying fluxes. Transient simulation is necessary for exploring the timing of peak groundwater discharge and its relationship to pumping and recharge. This is needed to better understand the dynamics of the system and for future analysis of potential climate change impacts or changed management activities on groundwater resources (Huntington and Niswonger 2012).

The assumption of the one-layer model with no leakage or interaction with the underlying formation is a potentially limiting representation of the system and should be further explored. Better characterization of the formation contact between the Pluto's Cave basalt and underlying Hornbrook formation would help inform the validity of this assumption. Additional water chemistry analysis from wells and springs could also indicate what areas or to what extent flow paths include interaction with the underlying formation at depth.

Conclusions

This work identifies, describes, and quantifies the major flow paths and fluxes in the Pluto's Cave basalt aquifer system and a portion of the debris flow in the Parks Creek valley. Initial model development did not include the Shasta River or Parks Creek area, but due to sources suggesting the large loss of leakage through the northwestern wall of Lake Shastina, the region was incorporated and additional springs represented. The model provides a framework to organize and include data and ideas presented in

previous work describing the aquifer system and its hypothesized dynamics, providing more detail and insights than strictly aquifer mass balance analysis.

The model currently reflects the general conceptual model: major recharge sources are from Mount Shasta and leakage from Lake Shastina as well as canal leakage and deep percolation of applied water. Major components of groundwater outflow are spring flow, subsurface boundary outflow, and pumping. Estimates of major fluxes in the system's mass balance, either calculated as model inputs or resulting from the MODERATE scenario model simulation, include the following inflows: 35 MCM Mount Shasta recharge; 7.4 MCM canal leakage; 21 MCM deep percolation of precipitation and applied water; 35 MCM of Lake Shastina leakage; and 50 MCM net northern GHB. Outflows include: 85 MCM Big Springs complex and Little Springs; 15.5 MCM Parks Creek valley spring flow; 5.5 MCM net stream-groundwater interaction; 23 MCM agricultural pumping; and 17 MCM net western GHB. The net northern GHB flow from the MODERATE scenario is likely too high and instead a more likely magnitude is on the order of 16 MCM (see Appendix A). The Mount Shasta recharge estimate seems low and is likely in the range of 45-65 MCM. Based on recent flow data and Mack (1960), the Big Springs complex likely flow range is 73-95 MCM. The inter-annual variation of the other major fluxes is also uncertain but not bracketed at this time.

Steady state model calibration indicates the regional K value for the Pluto's Cave aquifer (K zone 2) is on the order of 178 m/d with a likely range of 96 to 288 m/d. The fluxes significantly affected by this parameter include Lake Shastina leakage, Shasta River stream-groundwater interaction, GHB flux, and the Big Springs complex. K values for the alluvium were on the order of 49 m/d with a likely range of 27 to 82 m/d. Fluxes most sensitive to this parameter include stream-groundwater interaction of Shasta River and Parks Creek, Big Springs Lake flux, Hole in the Ground spring flow and spring flow from the Parks Creek valley springs. A K value on the order of 1.6 m/d represents the debris flow material with a likely range of 1.5 to 2 m/d. This was more tightly calibrated due to Lake Shastina leakage and Parks Creek valley spring flows that are highly sensitive to this parameter.

A significant source of uncertainty is the degree of groundwater flow across the northern boundary and to the west toward the Shasta River through the debris flow material (western GHB). This was explored by calibrating three model scenarios with varying degrees of flow across these boundaries. With limited to zero flow across the north and western boundaries, the Big Springs complex does not yield more than about 53 MCM. This is less than its approximate target of 73 MCM. This and groundwater heads in the north suggest the northern (or perhaps the eastern) boundary indeed contributes some flow to the model domain and is an important component of groundwater dynamics in the model area. However, calibrated models with high and moderate flows across the north and western boundaries responded similarly to changes in model inputs (Mount Shasta recharge, pumping, and local recharge). This suggests the details and degree of the boundary flow is less important than the fact that some occurs. Improved and updated input data for the northern general head boundary and better estimates of groundwater accretion to the Shasta River downstream of the Big Springs Creek confluence would improve confidence in results and guide recalibration. Alternatively, some of this flow may instead come from the east side (see Appendix A for preliminary investigation).

Aside from boundary conditions, spring flows and specifically the Big Springs complex, are most sensitive to Mount Shasta recharge and agricultural pumping. Although the equivalent porous media model approach excludes the ability to evaluate impacts of specific pumping on specific springs, collectively, groundwater pumping from the system affects spring flow magnitudes. Modeling suggests the Big Springs complex is most sensitive to pumping in agricultural zones two and three, which are nearest these springs. The hydrogeologic interconnectedness of this volcanic system is complex, yet the basic connectivity between the groundwater system and surface water system is made explicit by spring flow. Collectively, changes to the groundwater system will affect spring flow magnitudes if the regional magnitude of the change is great enough. A 30% adjustment to pumping was large enough to see only minor changes to individual springs. Hence, modeling suggests on a regional scale the system probably has significant buffering capacity.

Lake Shastina is a significant hydrologic feature in this portion of Shasta Valley both as a water management resource but also as a source of groundwater recharge and enhanced spring flow. Model results suggest Lake Shastina is a source of recharge to the Pluto's Cave basalt aquifer as well as to

spring flow in the Parks Creek valley. Leakage through its northwestern side alone does not amount to the magnitude of leakage estimated by a 1972 water balance of the lake (Dong et al. 1974). Modeled groundwater contours suggest some flow occurs out its southeast side as well. Conducting a water balance for Lake Shastina under varying water year types while measuring spring flows would help better characterize and calibrate this part of the system. The area south of Parks Creek confluence with Shasta River including the Parks Creek valley is largely isolated from the rest of the model domain in its response to changes in K values for K zones and boundaries. Additional access to or collection of surface water data for this area along with groundwater level measurements could improve model representation of spring flow and stream-groundwater interaction. This would be of value for exploring management alternatives related to spring flow, pumping, and reservoir releases (as in Chapter 4).

Future model development should transition this steady state model to a transient simulation. This is needed to better understand the timing and dynamics of the system. The eastern boundary as a recharge source should be further explored and evaluated (see Appendix A for initial analysis). Estimates of Mount Shasta recharge should also be refined by identifying elevation bands corresponding to the average recharge elevation indicated by available isotope data for the Big Spring complex. Additionally, MODPATH could be used to explore groundwater flow directions in the model to better understand what inflow sources (Mount Shasta recharge, lake leakage, other boundary flows) sustain groundwater heads necessary to maintain spring flow in various locations throughout the model domain.

Key next steps include continued and additional data collection of spring flow (Big springs complex, Little Springs, Hole in the Ground, and the Shasta River and Parks Creek valley springs). Other useful data for model improvement includes water balance data for Lake Shastina, ideally over the course of multiple water years. Additional chemistry and isotope analysis of springs and seeps along the Shasta River could further clarify their source, whether primarily derived from Lake Shastina leakage or the Pluto's Cave basalt to the east, shedding light on the connectedness of the Shasta River upstream of Big Springs Creek to the Pluto's Cave basalt aquifer system. Geologic cores and a thorough evaluation and mapping of information from well logs would help better define the extent and depth of the aquifer. Finally, additional water level monitoring with greater geographic coverage would be valuable for model improvement and calibration.

Though more data is often useful, the model's role in this study is to test our conceptual model of the system, capturing major processes and components, and therefore does not need to perfectly simulate reality to be useful. Model results provide insights on what components of the system are significant and how they interact with others.

References

Angelini, P., and Dragoni, W. (1997). "The problem of modeling limestone springs: The case of Bagnara (north Apennines, Italy)." *Ground Water*, 35(4), 612-618.

ASTM. (2008). "Standard Guide for Calibrating a Ground-Water Flow Model Application, D 5981 - 96." ASTM International.

Batelaan, O., and De Smedt, F. (2004). "SEEPAGE, a New MODFLOW DRAIN Package." *Ground Water*, 42(4), 576-588.

Blessent, D., Therrien, R., and MacQuarrie, K. (2009). "Coupling geological and numerical models to simulate groundwater flow and contaminant transport in fractured media." *Computers & Geosciences*, 35(9), 1897-1906.

Blodgett, J. C., Poeschel, K. R., and Thornton, J. L. (1988). "A Water-Resources Appraisal of the Mount Shasta Area in Northern California, 1985." U.S. Geological Survey, Sacramento.

Davids Engineering, I. (2010). "Hydrogeologic Assessment of the Cowley and Hart Ranches, Little Shasta Valley, California." A Cooperative Investigation Undertaken by the CA Department of Fish and Game and the Cowley and Hart Ranches.

Davids Engineering, I. (2011a). "Shasta Big Springs Ranch and Nelson Ranch Crop Evapotranspiration Estimates." Unpublished data by Davids Engineering for The Nature Conservancy.

Davids Engineering, I. (2011b). "Shasta Springs Ranch Irrigation Efficiency Study." A Cooperative Investigation Undertaken by the CA Department of Fish and Game and Emmerson Investments.

Davids Engineering, I. (2011c). "Shasta Springs Ranch Irrigation Efficiency Study, Appendix A: Hydrogeologic Assessment." A Cooperative Investigation Undertaken by the CA Department of Fish and Game and Emmerson Investments.
Davids, J. (2012, Personal Comm.). Davids Engineering, Inc. 4/22/2012.
Deas, M. (2009, Pers. comm.). Watercourse Engineering, Inc. 9/17/2009.
Domenico, P. A., and Schwartz, F. W. (1997). *Physical and Chemical Hydrogeology 2nd ed.*, John Wiley & Sons, Inc., New York, NY.
Dong, A. E., Beatty, K. W., and Averett, R. C. (1974). "Limnological Study of Lake Shastina Siskiyou County California." U.S. Geological Survey, Water-Resources Investigations 19-74.
Fairchild, M. G., and McClurg, J. O. (1964). "Bulletin No. 87: Shasta Valley Investigation." Department of Water Resources.
Forsgren Associates, I. (2006). "Water Conservation Study, Big Springs Irrigation District." Shasta Valley Resource Conservation District.
Gannett, M. W., and Lite, K. E. J. (2004). "Simulation of Regional Ground-Water Flow in the Upper Deschutes Basin, Oregon." U. S. G. Survey, ed.
Graf, T., and Therrien, R. (2008). "A method to discretize non-planar fractures for 3D subsurface flow and transport simulations." *International Journal for Numerical Methods in Fluids*, 56(11), 2069-2090.
Graf, T., and Therrien, R. (2009). "Stable-unstable flow of geothermal fluids in fractured rock." *Geofluids*, 9(2), 138-152.
Grenier, C., Bernard-Michel, G., and Benabderrahmane, H. (2009). "Evaluation of retention properties of a semi-synthetic fractured block from modeling at performance assessment time scales (Aspo Hard Rock Laboratory, Sweden)." *Hydrogeology Journal*, 17(5), 1051-1066.
Harbaugh, A. W. (2005). "MODFLOW-2005, The U.S. Geological Survey modular ground-water model -- the Ground-Water Flow Process: U.S. Geological Survey Techniques and Methods 6-A16."
Hoss, A. (2010, Email). "The Nature Conservancy. 1/8/2010."
Hu, B. X., Huang, H., and Zhang, D. X. (2002). "Stochastic analysis of solute transport in heterogeneous, dual-permeability media." *Water Resources Research*, 38(9), 16.
Huntington, J. L., and Niswonger, R. G. (2012). "Role of surface-water and groundwater interactions on projected summertime streamflow in snow dominated regions: An integrated modeling approach." *Water Resources Research*, 48.
James, E. R., and Manga, M. (2000). "Springs in the Oregon Cascades: Where does the water come from? And how old is it?" *Oregon Geology*, 62(4), 87-94.
James, E. R., Manga, M., Rose, T. P., and Hudson, G. B. (2000). "The use of temperature and the isotopes of O, H, C, and noble gases to determine the pattern and spatial extent of groundwater flow." *Journal of Hydrology*, 237, 100-112.
Jefferson, A., Grant, G., and Lewis, S. L. "A river runs underneath it: geological control of spring and channel systems and management implications, Cascade Range, Oregon." *Advancing the Fundamental Sciences: proceedings of the Forest Service national earth sciences conference*, Portland, OR.
Jefferson, A., Grant, G., Lewis, S. L., and Lancaster, S. T. (2010). "Coevolution of hydrology and topography on a basalt landscape in the Oregon Cascade Range, USA." *Earth Surface Processes and Landforms*.
Jefferson, A., Grant, G., and Rose, T. (2006). "Influence of volcanic history on groundwater patterns on the west slope of the Oregon High Cascades." *Water Resources Research*, 42.
Jeffres, C., Dahlgren, R., Kiernan, J., King, A., Lusardi, R., Nichols, A., Null, S., Tanaka, S., and Willis, A. (2009). "Baseline Assessment of Physical and Biological Conditions Within Waterways on Big Springs Ranch, Siskiyou County, California." Report Prepared for: California State Water Resources Control Board.
Kristinof, R., Ranjith, P. G., and Choi, S. K. (2010). "Finite element simulation of fluid flow in fractured rock media." *Environmental Earth Sciences*, 60(4), 765-773.
MacDonald, M. K., Pomeroy, J. W., and Pietroniro, A. (2010). "On the importance of sublimation to an alpine snow mass balance in the Canadian Rocky Mountains." *Hydrology and Earth System Sciences*, 14(7), 1401-1415.
Mack, S. (1960). "Geology and ground-water features of Shasta Valley, Siskiyou County California." California Division of Water Resources.

Manga, M. (1996). "Hydrology of spring-dominated streams in the Oregon Cascades." *Water Resources Research*, 32(8), 2435-2439.
Manga, M. (1997). "A model for discharge in spring-dominated streams and implications for the transmissivity and recharge of quaternary volcanics in the Oregon Cascades." *Water Resources Research*, 33(8), 1813-1822.
Manga, M. (1999). "On the timescalse characterizing groundwater discharge at springs." *Journal of Hydrology*, 219, 56-69.
Manga, M. (2001). "Using Springs to Study Groundwater Flow and Active Geologic Processes." *Annu. Rev. Earth Planet. Sci*, 29, 201-28.
Manga, M., and Kirchner, J. W. (2004). "Interpreting the temperature of water at cold springs and the importance of gravitational potential energy." *Water Resources Research*, 40(5), 8.
McClain, C. (2008). "Provenance and Pathways: A geochemical and isotope analysis of Mt. Shasta groundwater," University of California, Davis.
Molotch, N. P., Blanken, P. D., Williams, M. W., Turnipseed, A. A., Monson, R. K., and Margulis, S. A. (2007). "Estimating sublimation of intercepted and sub-canopy snow using eddy covariance systems." *Hydrological Processes*, 21(12), 1567-1575.
Nakamura, G. (2011, Pers comm.). University of California Cooperative Extension, Specialist Emeritus. 8/11/2011.
Nathenson, M., Thompson, J. M., and White, L. D. (2003). "Slightly thermal springs and non-thermal springs at Mount Shasta, California: Chemistry and recharge elevations." *Journal of Volcanology and Geothermal Research*, 121, 137-153.
Nichols, D. (2012, Personal Comm.). University of California- Davis, Researcher. 10/6/2011.
Ophori, D. U. (2004). "A simulation of large-scale groundwater flow and travel time in a fractured rock environment for waste disposal purposes." *Hydrological Processes*, 18(9), 1579-1593.
Orloff, S. (2011, Pers comm.). University of California Cooperative Extension Farm Advisor. 3/24/2011.
Pomeroy, J. W., Gray, D. M., Shook, K. R., Toth, B., Essery, R. L. H., Pietroniro, A., and Hedstrom, N. (1998a). "An evaluation of snow accumulation and ablation processes for land surface modelling." *Hydrological Processes*, 12(15), 2339-2367.
Pomeroy, J. W., Parviainen, J., Hedstrom, N., and Gray, D. M. (1998b). "Coupled modelling of forest snow interception and sublimation." *Hydrological Processes*, 12(15), 2317-2337.
Powers, R. F. (2011, Pers comm.). PSW Research Station, Emeritus Scientist. 8/12/2011.
PRISM. (2010). "PRISM Climate Group, Oregon State University. http://www.prism.oregonstate.edu/. Accessed 3/2011 and 2/2012."
Rubin, H., Rathfelder, K., Abriola, L. M., Spiller, M., and Kongeter, J. (2004). "Using continuum approach to quantify the remediation of nonaqueous phase liquid contaminated fractured permeable formations." *Journal of Environmental Engineering-Asce*, 130(11), 1345-1356.
Ruud, N., Harter, T., and Naugle, A. (2004). "Estimation of groundwater pumping as closure to the water balance of a semi-arid, irrigated agricultural basin." *Journal of Hydrology*, 297, 51-73.
Saar, M. O., Castro, M. C., Hall, C. M., Manga, M., and Rose, T. P. (2005). "Quantifying magnatic, crustal, and atmospheric helium contributions to volcanic aquifers using all stable noble gases: Implications for magmatism and groundwater flow." *Geochemistry Geophysics Geosystems*, 6(3).
Saar, M. O., and Manga, M. (1999). "Permeability-porosity relationship in vesicular basalts." *Geophysical Research Letters*, 26(1), 111-114.
Scanlon, B. R., Mace, R. E., Barrett, M. E., and Smith, B. (2003). "Can we simulate regional groundwater flow in a karst system using equivalent porous media models? Case study, Barton Springs Edwards aquifer, USA." *Journal of Hydrology*, 276(1-4), 137-158.
Shoemaker, W. B., Kuniansky, E. L., Birk, S., Bauer, S., and Swain, E. D. (2008). "Documentation of a Conduit Flow Prcess (CFP) for MODFLOW-2005." U.S. Geological Survey Techniques and Methods, Book 6, Chapter A24, 50 p.
Snyder, R. L., Orang, M., Bali, K., and Eching, S. (2007). "Basic Irrigation Scheduing (BIS)." Available at http://biomet.ucdavis.edu/irrigation_scheduling/bis/BIS.htm.
Spano, D., Snyder, R. L., Sirca, C., and Duce, P. (2009). "ECOWAT-A model for ecosystem evapotranspiration estimation." *Agricultural and Forest Meteorology*, 149(10), 1584-1596.
Tague, C., Farrell, M., Grant, G., Lewis, S. L., and Rey, S. (2007). "Hydrogeologic controls on summer stream temperatures in the McKenzie River basin, Oregon." *Hydrological Processes*, 21, 3288-3300.

Tague, C., and Grant, G. (2004). "A geological framework for interpreting the low-flow regimes of Cascade streams, Willamette River Basin, Oregon." *Water Resources Research*, 40.
Tague, C., and Grant, G. (2009). "Groundwater dynamics mediate low-flow response to global warming in snow-dominated alpine regions." *Water Resources Research*, 45.
Van der Hoven, S. J., Solomon, D. K., and Moline, G. R. (2002). "Numerical simulation of unsaturated flow along preferential pathways: implications for the use of mass balance calculations for isotope storm hydrograph separation." *Journal of Hydrology*, 268(1-4), 214-233.
Vignola, E., and Deas, M. (2005). "Lake Shastina Limnology." Prepared for the Information Center for the Environment, Dept. of Environmental Science and Policy, UCD and the North Coast Regional Water Qualigy Control Board.
Wang, M. Y., and Kulatilake, P. (2008). "Understanding of hydraulic properties from configurations of stochastically distributed fracture networks." *Hydrological Processes*, 22(8), 1125-1135.
Ward, M. (2011a). "Personal Communication. Michael Ward, Department of Water Resources. April 8, 2011."
Ward, M. (2011b). "Personal Communication. Michael Ward, Department of Water Resources. April 22, 2011."
Ward, M., and Eaves, N. (2008). "Groundwater Data Needs Assessment." California Department of Water Resources.
Willis, A., and Deas, M. (2010). "MWCD Main Canal Conveyance Efficiency Study." Watercourse Engineering, Inc.

Chapter 4: Conjunctive operation of groundwater pumping, surface water diversions, and Lake Shastina releases for stream temperature

Abstract

This work uses optimization to explore coordinated hourly surface and groundwater operations to benefit Shasta River, California stream temperatures between Hole in the Ground pump diversion and the confluence with Parks Creek. The management strategy involves coordinating reservoir releases and diversions to the Shasta Springs Ranch and supplementing river flows with pumped cool groundwater from the Seldom Seen fields well. This modeling organizes the problem, and explores tradeoffs and resulting downstream temperatures of optimized decisions. A basic problem formulation is presented with results, sensitivity analysis, and insights. The problem is also formulated for a larger Shasta River application with multiple stream reaches. Optimized results for a week in July suggest promising reductions to daily maximum and minimum stream temperatures with strategic operation of the water supply portfolio. Yet these temperature benefits have significant costs from reduced irrigation diversions. Increased irrigation efficiency would reduce warm tail water discharges to the river instead of reducing diversions. With increased efficiency, diversions remain and shortage costs decrease. Tradeoffs and sensitivity of model inputs are explored and results discussed.

Introduction

Optimization answers the question, "what's best?" That is, given a particular objective, what is the best decision or combination of decisions within prescribed constraints to reach the objective? With increasing competition between agricultural, urban, and environmental demands for scarce water supplies, the process of optimizing a problem can help organize the problem and bring to the forefront the main issues, influential factors, and promising alternatives. It can also shed light on connections and relationships between factors that were not previously noted. Optimization has been demonstrated as a useful tool for increased understanding of system dynamics, policy evaluation, and influential factors in California water management (Lund et al. 2008; Lund et al. 2007). It has also been widely applied to groundwater-surface water systems for a number of applications with both economic and physical objectives (Barlow et al. 2003; Basagaoglu and Marino 1999; Bazargan-Lari et al. 2009; Bredehoeft and Young 1983; Chiu et al. 2010; Ejaz and Peralta 1995; Peralta et al. 1995; Pulido-Velazquez et al. 2006; Worthington et al. 1985; Yang et al. 2009; Yeh 1992; Yu and Haimes 1974). Conjunctive management of groundwater and surface water resources for surface water temperature has not been widely explored. This research demonstrates the potential benefit to stream temperatures from optimizing the timing and combination of groundwater pumping, diversions and reservoir releases to meet agricultural demands and an in-stream temperature target.

Management models with conjunctive use can be placed in two broad categories depending on whether their objective function is economic or physical. Economic objective functions tend to minimize overall system cost or maximize economic benefits, whereas physically based objective functions commonly maximize aquifer yields and/or have a water quality objective (Barlow et al. 2003; Bazargan-Lari et al. 2009; Louie et al. 1984; Peralta et al. 1995).

There is little literature on formal optimization for stream temperature management, particularly involving groundwater. Bettinger and Johnson (1996) explore several scenarios for forest land management using a heuristic decision-support tool. One goal is to maintain stream temperatures below a threshold for suitable fish habitat, but temperature influences of each solution are evaluated by post-processing. Temperature is not directly built into the decision-support tool. Bogan et al (2004) use a shuffled complex evolution global optimization method to estimate parameters in their model that describe the potential effects of stream channel shading, wind sheltering, and hydrologic sources of heat on observed stream temperatures. Essentially this is the inverse method application for model calibration rather than decision making. Taniguchi et al (1998) also employ this method for a surface and subsurface temperature related problem. In their study, temperature-depth profiles were used to estimate the change in average ground surface temperature 19 years after forest clearing. Optimization was used to estimate surface temperature change due to deforestation by minimizing deviation between observed and calculated

temperatures (Taniguchi et al. 1998). Null (2008) explored environmental water use efficiency and applied optimization to maximize out-migrating smolts from their natal stream. This involved improving fish habitat conditions by better managing surface water quality and quantity, including temperature (Null and Lund 2011).

Another category of temperature related optimization involves reservoir operations for flow and temperature (Carron 2000; Olivares 2008; Rheinheimer 2011). For example, Carron (2000) develops methods for simulation and optimization of reservoir releases to meet location specific temperature targets downstream. He presents multiple formulations with objective functions for different species specific temperature targets. The current research will add to existing work by directly optimizing river temperature while including decision variables for both groundwater and surface water resources. Conjunctive management combined with temperature optimization is a novel contribution to water resources management.

Results will include groundwater pumping rates, surface water diversions, and reservoir operations that minimize pumping and shortage costs while adding a benefit for achieving temperatures less than a specified target temperature established in reaches of interest. This will provide insights on coordinated management of developed surface water and groundwater resources available to the Shasta Springs Ranch along California's Shasta River to maintain environmental temperature targets while meeting agricultural water demands.

Basic problem formulation

The basic problem includes the major components of the system of interest scaled down to a simplified two-node network for a 24 hour period, with hourly time steps. It includes flow released from the reservoir (Q_{in}), a managed cold water source which could be a spring or pumped groundwater (Q_{cold}), warmer tail water returning to the river after irrigating pasture (Q_{hot}), diversions for irrigation (Q_{div}), and flow continuing downstream (Q_{Riv}). The point of interest for temperature is located some distance downstream and estimated heating/cooling is expressed as a change in temperature, ΔT_t, over that distance according to atmospheric conditions, geometry, and shading of the river reach (Figure 29).

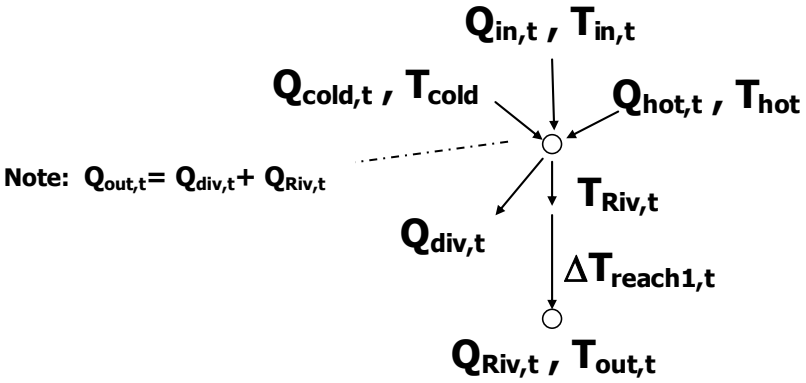

Figure 29. Schematic for basic problem with flows (Q) and temperatures (T)

The central node receives inflow from three main sources (Figure 1) each having different known and potentially varying (hourly) temperatures. T_{in} varies by hour but T_{cold} and T_{hot} are set at a constant temperature for all time (Table 29).

Objective function

The weighted multi-objective function minimizes pumping cost, shortage cost, and/or the outgoing temperature ($T_{out,t}$) by summing differences between calculated outgoing temperature and a temperature target for all time steps. A shortage cost occurs when total diversion volume is less than the agricultural target delivery. A constraint ensures that $T_{out,t}$ is less than the target temperature so anything less than the temperature target benefits (reduces) the objective function value. The constant alpha, below in

Equation 4.1, allows for weighting the influence of the outgoing temperature results on the objective value.

$$\boldsymbol{Min\ Z = (C_{pump} * Lift * Vol_{cold}) + (C_{shortage} * Vol_{shortage}) + \alpha \sum_t (T_{out} - T_{target})}$$

Equation 4.1

Pumping cost (C_{pump}) is specified in dollars per thousand cubic meters (TCM) per meter of lift. Lift is estimated as the difference between the ground surface elevation at the well and the water level elevation during pumping. The total pumping volume is calculated by converting the pumping rate in each time step to a volume and summing over all time. Similarly the volume of shortage ($Vol_{shortage}$) is calculated by summing the volume of diverted water over all time steps and subtracting that from the target delivery for the model time period. The values of given parameters and coefficients are in Table 29.

Table 29. Given model parameters for basic problem

Parameter	Value	Units
alpha	10	n/a
Temperature Target	18	^{o}C
Lift	15.2	m
C_{pump}	0.53	$/(TCM*m)
$C_{shortage}$	81	$/TCM
Ag Target Delivery	6.5	TCM
Eff	34%	n/a
T_{cold}	12.5	^{o}C
T_{hot}	25	^{o}C
T_{in}	Hourly varying	^{o}C
ΔT_t	Hourly varying	^{o}C

Note: TCM is Thousand Cubic Meters

Estimating stream temperature change (ΔT_t)

The hourly varying change in temperature (ΔT_t) is the increase or decrease in temperature over a river reach (from node i to j) in a particular time step due to heating from atmospheric conditions, river geometry, nearby topography and shading, and stream discharge. Three main approaches are often used to model water temperature in streams: regression, stochastic, and deterministic modeling (Caissie 2006). In this section a regression approach is presented to establish a relationship between influential inputs and the change in temperature over a river reach. The main factors considered to influence thermal regime of rivers include atmospheric conditions, topography, streambed processes, and stream discharge (Caissie 2006). Inputs for this regression-based model can use either measured temperature data for specified river reaches or results from a deterministic stream temperature model to provide values for the dependent variable (ΔT_t). The explanatory variables used are hourly flow rate (Q), air temperature (T_{air}), and solar radiation (SR). With these hourly data sets, coefficients from the regression equation below are estimated to explain ΔT_t for a given reach as a function of stream flow rate (decision variable in optimization model) and given atmospheric conditions, as explanatory variables.

$$\Delta T_{reach1,t} = \beta_0 + (\beta_1 * Q_t) + (\beta_2 * Tair_t) + (\beta_3 * SR_t) + \varepsilon_t$$

This change in temperature over the reach is added to the temperature at the upstream node, at a prior time step according to the travel time of the reach ($T_{i,t-r}$), to calculate the stream temperature at the

downstream node of the reach ($T_{j,t}$). The reach's travel time can be estimated from modeling results or measured velocity data.

$$T_{j,t} = T_{i,t-r} + \Delta T_{reach1,t}$$

Where *reach*1 is node i→j and *r* is travel time for *reach*1. For the basic problem, a two hour travel time is assumed.

Constraints

Management decisions (decision variables) are made hourly for a 24 hour period for flow (m^3s^{-1}) released from the reservoir (Q_{in}), cold water input (Q_{cold}), diversions (Q_{div}), and tail water returns (Q_{hot}) subject to the following constraints:

$$T_{Riv,t} = \frac{(Q_{in} * T_{in}) + (Q_{cold} * T_{cold}) + (Q_{hot} * T_{hot})}{Q_{out}}$$ **Heat balance at node**

$$\Delta T_{reach1,t} = \beta_0 + (\beta_1 * Q_t) + (\beta_2 * Tair_t) + (\beta_3 * SR_t) + \varepsilon_t$$ **Regression for ΔT_t**

$$T_{out,t} = T_{Riv,t-2} + \Delta T_{reach1,t}$$ **Mixed temperature + heating downstream**

$$Q_{in,t} + Q_{cold,t} + Q_{hot,t} = Q_{out} \quad for \forall t$$ **Conservation of mass**

$$Q_{out} = constant \ \ for \forall t$$ **Linearization constraint**

$$\left.\begin{array}{l} Q_{Riv,t} = Q_{out} - Q_{div,t} \\ Q_{Riv} \geq 5 \end{array}\right\}$$ **Minimum in-stream flow requirement**

$$Q_{in} \leq 9, \ \ Q_{cold} \leq 5, \ \ Q_{hot} \leq 5, \ \ Q_{div} \leq 9$$ **Capacity constraints, $\forall t$**

$$Vol_{tail\ water} = (1 - Eff) * Target\ Delivery$$ **Tail water return requirement**

$$Vol_{diverted} \leq Target\ Delivery$$ **Water supply constraint**

$$T_{out} \leq T_{target} \ \ \forall t$$ **Temperature constraint for juvenile coho rearing habitat**

Del temperature, ΔT_t, is the change in temperature due to flow and atmospheric conditions for a particular reach at a particular time accounting for the travel time between the location of the node (where mixing occurs) and the location of interest downstream (T_{out}).

Unless forced by a constraint, optimizing the problem will choose a flow rate of zero for 'hot' water (Q_{hot}) release if minimizing stream temperature is heavily weighted in the multi-objective function. Therefore, an estimated total volume of tail water is specified for the model time period based on irrigation efficiency (*Eff*) of the irrigated fields. In this example, the fields have very low efficiency (34%), defined as the volume of applied water used for crop evapotranspiration (ET) over the volume of total applied water. This constraint allows the model to decide when and how much tail water to release and assumes that the only fate for this water is mixing with other inflow sources. Any water not used for ET is assumed to run off into the river.

Nonlinear constraints from the heat balance constraint are avoided by specifying Q_{out} ($Q_{out}=Q_{Riv}+Q_{div}$) as a given and constant number. This results in a linear program solving for Q_{in}, Q_{cold}, Q_{hot}, Q_{div}, Q_{Riv} hourly for a 24 hour period. However, constraining the total node outflow (Figure 29) is not ideal for broadly exploring the variety of management options. Therefore, the nonlinear space can be explored by varying the specified value of Q_{out} and comparing model results. In this case, the range of feasible Q_{out} is 0.23 to 0.42 m^3s^{-1}, due to temperature, capacity, and demand constraints. High shortage occurs when Q_{out} is low because the minimum instream flow constraint requires Q_{Riv} to be at least 0.14 m^3s^{-1}. If Q_{out} is 0.23 m^3s^{-1},

then Q_{div} can only be 0.08 m^3s^{-1}. With this constraint, significant shortage occurs. However, for Q_{out} greater than 0.28 m^3s^{-1}, shortage cost is zero (Figure 30). The sharp decline in shortage cost for increasing outflow from 0.23 to 0.28 m^3s^{-1} leads to a large initial benefit to the optimal objective function value. Total pumping cost oscillates some and is greatest with higher values of Q_{out}. The maximum, minimum, and average temperature for the 24 hour period as a function of changing Q_{out} is shown in Figure 30. Although the maximum temperature remains at 18°C (the upperbound constraint), the minimum temperature ranges from 12.7 to 13.5°C.

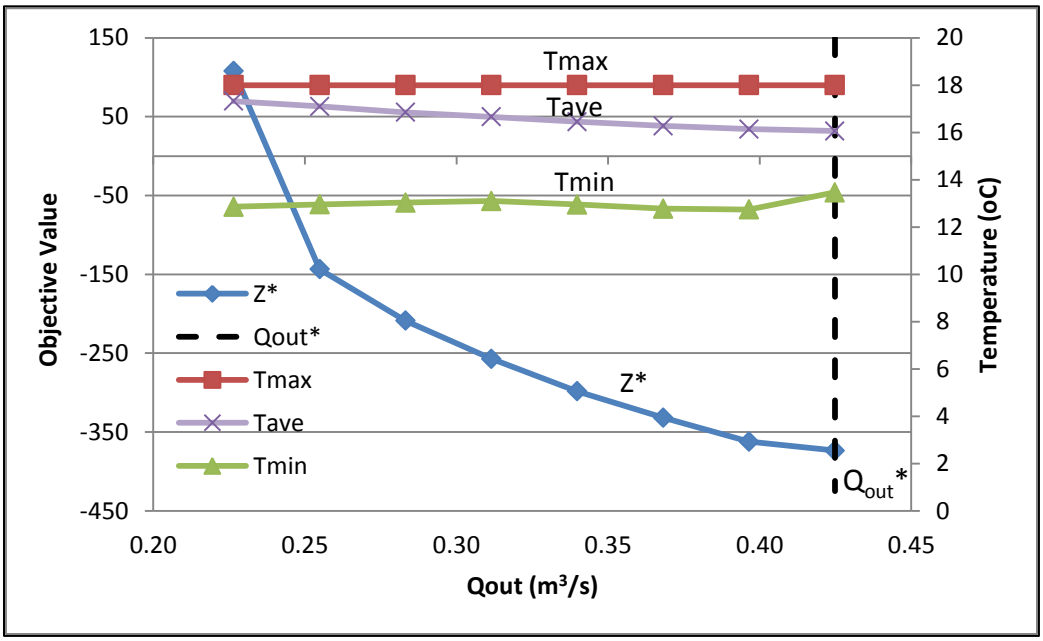

Qout (m^3/s)	0.20	0.23	0.25	0.28	0.31	0.34	0.37	0.40	0.42	0.45
Total Shortage Cost ($)		205	7	0	0	0	0	0	0	
Total Pumping Cost ($)		66	66	67	65	74	82	85	93	
Temp component		-163	-216	-276	-322	-373	-414	-447	-466	
Tmax=		18.0	18.0	18.0	18.0	18.0	18.0	18.0	18.0	
Tmin=		12.9	13.0	13.0	13.1	12.9	12.8	12.7	13.5	
Tave=		17.3	17.1	16.9	16.7	16.4	16.3	16.1	16.1	
Z*	INFEAS	108	-144	-209	-257	-298	-332	-362	-374	INFEAS

Figure 30. Effect of changing q_{out} on objective value, costs, and temperatures for 24 hour period

The average temperature gradually and consistently decreases as Q_{out} increases, with almost a 1°C reduction over the feasible range of Q_{out}. This is because the increased Q_{out} comes, at least in part, from increased cool pumped groundwater. Not only is there a potential tradeoff between costs related to pumping and shortage, a tradeoff can exist between average and minimum temperature for the reach. Carefully defining the temperature objective for a particular problem is complex biologically, but may be significant to model results.

Based on this exploration, a Q_{out} of 0.28 m^3s^{-1} is used for the following sensitivity analysis. This allows some tradeoffs to occur between pumping cost and stream temperature benefits.

Sensitivity analysis

Alpha, α, weights the influence of the temperature component in the objective function on the objective function value. A higher alpha value means minimizing river temperature becomes increasingly valuable in minimizing the overall objective value, Z*. At first, pumping cost increases as alpha increases because

the cold water source becomes increasingly valuable to the objective function (Figure 31). The section of the tradeoff curve with cost less than $90.9 is strictly due to increased pumping and pumping cost (Figure 31A). Q_{cold} occurs at capacity in all but the final two time steps (which have no effect on the objective function value because of the two hour travel time lag) when alpha is 42 $/^{o}C or more, thereby maxing out the pumping cost. Cost remains the same even as alpha increases until alpha exceeds 73 $/^{o}C. With alpha greater than 73 $/^{o}C, the tradeoff curve reflects the tradeoff between average temperature and shortage cost. As minimizing temperature becomes increasingly valuable (driven by higher alpha), agricultural deliveries decrease and shortage cost increases. With α >=107 $/^{o}C, no deliveries occur and total cost remains at $890.91, the sum of maximum pumping cost and shortage cost. Although the increasing alpha inflates the temperature component of the objective function value, it has little value on temperature in real terms. The shortage cost portion of the curve is much steeper but overall has less real benefit to temperature, only a 0.4^{o}C reduction. Therefore, with the given inputs, the tradeoff at play is primarily between pumping cost and river temperature which can reduce average temperature by almost 1^{o}C (Figure 31B). Pumping cold water into the stream has the greatest direct effect on stream temperatures. The greatest marginal improvement to average temperature occurs for alpha around 10 $/^{o}C. Exploring a range of alphas highlights the tradeoffs between the multiple objectives. If minimizing outgoing temperature is all important, alpha should be set to at least 42 $/^{o}C. However, with a value of 10 $/^{o}C, most of the temperature benefit is reached and there is still some room for pumping cost to be considered and influence the optimal objective value. A value of 10 $/^{o}C will be used going forward.

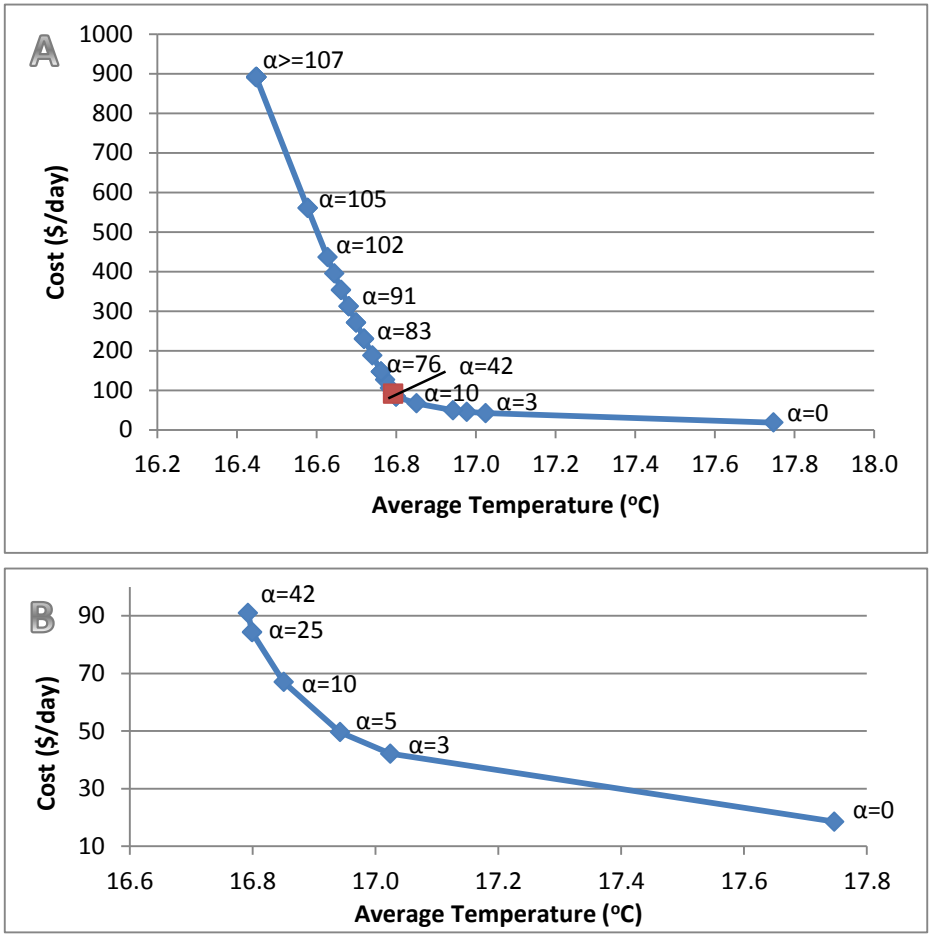

Figure 31. Sensitivity of alpha on objective function components and average temperature

Larger pumping lifts increase total pumping cost and affect the volume of groundwater pumped which affects the daily average stream temperature. Figure 32 shows the tradeoff curve for daily average temperature and pumping cost. With a lift of less than 3.7 meters (lower unit cost for pumping) Q_{cold} is pumped at capacity and the average temperature is at its lowest (16.8°C). The tradeoff curve reveals ranges of lift values that sharply increase cost but with little temperature effect (i.e. lift of 24.4-45.7 meters), and other ranges have a slower cost increase or even decreased cost but have a larger temperature effect (for example, lift of 83.8-121.9 m). A dip in the total pumping cost occurs because the increased marginal pumping cost (driven by increased lift) causes the total volume pumped to drop such that the total pumping cost actually decreases. The volume pumped declines until the minimum level of pumping is reached for the problem to be feasible. Reaching this bound, the total pumping cost again increases as the marginal pumping cost increases with increasing lift. Generally, as lift increases the average daily temperature also increases since less pumping occurs and less cool groundwater is released to the river. For the Shasta River application, pumping lift is estimated to be 12.8 to 17.1 meters. This range in lift translates to a range of about ten dollars for total pumping cost and 0.1°C increase in average temperature (Figure 32). In this narrower range, the tradeoff is negligible. For sensitivity analysis, lift remained at 15.2 meters.

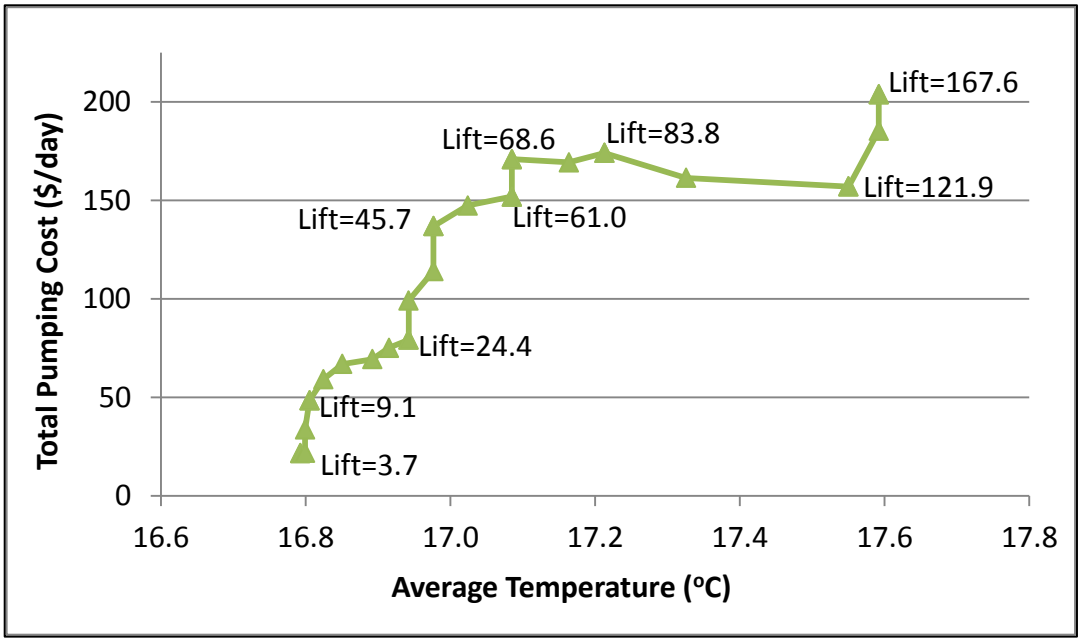

Figure 32. Tradeoff between average temperature and total pumping cost as a function of lift (meters)

Shortage cost occurs when the target irrigation delivery is not met by total diversions. Sensitivity analysis on shortage cost ($/TCM) indicates that if the marginal shortage cost exceeds 11.4 $/TCM, no shortage occurs and the target delivery is always met (Figure 33). Pumping is less expensive than shortage. Without a penalty for shorting deliveries (Cs=0), none of the 9.9 TCM demanded are delivered. The effect on average temperature is low, only a 0.4°C decrease when maximum shortage occurs (16.5 to 16.9°C). This further reinforces the minimal tradeoff between deliveries and river temperature with the given scenario, although the timing of diversions is strategic as shown below (Figure 35). Based on penalty functions used for region 1 in CALVIN (Draper et al. 2003), a statewide economic-engineering optimization model, $81/TCM ($100/AF) is used for marginal shortage cost in this application.

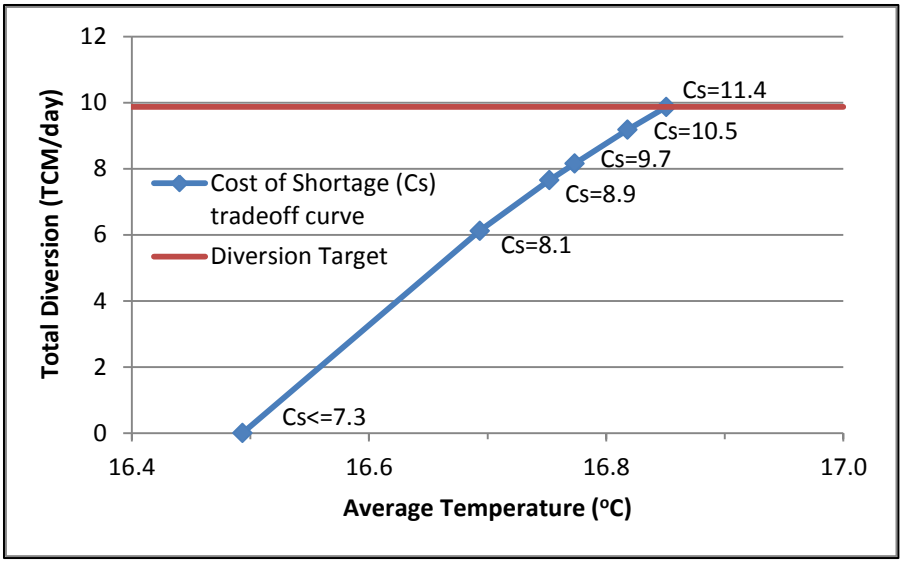

Figure 33. Total diversion (TCM) and daily average temperature tradeoff curve for varied marginal shortage cost ($/TCM)

Results and insights from the basic problem

The optimization model provides hourly decisions for flow rates Q_{in}, Q_{cold}, Q_{hot}, and Q_{div} given an 18°C temperature constraint, agricultural demand, and specified tail water return (as a function of delivery target). With the given inputs, constraints and parameters, the problem is feasible, no agricultural shortage occurs and downstream temperatures (T_{out}) are maintained below 18°C. This shows strategic management of a cold water source, hot water input (tail water), diversions, and upstream releases can change and potentially improve temperature conditions.

For this basic problem, better temperature conditions come from releasing water at full capacity from the reservoir from 3-8 am when reservoir release temperatures are at their coolest (Figure 35). The system takes advantage of this free cool water and does not pump groundwater during those hours. As the reservoir release temperatures begin to warm, releases taper off (Q_{in}) and relatively cool groundwater is pumped at capacity during the following hours to minimize downstream temperatures and meet the minimum in-stream flow requirement, specified as 0.14 m^3s^{-1}. Q_{in} and Q_{hot} are inversely related (Figure 34). Somewhat surprisingly, Q_{hot} is mostly released increasingly throughout the afternoon and diversions are at their lowest at that time, while cold water input is at its maximum. Since diversions affect stream temperatures by reducing the flow and therefore increasing the rate of heating (ΔT_t), they occur in all but the time of day when ΔT_t is at its highest. When the marginal cost of shortage is zero, diversions do not occur, which decreases average temperature only about 0.4 °C (as described previously).

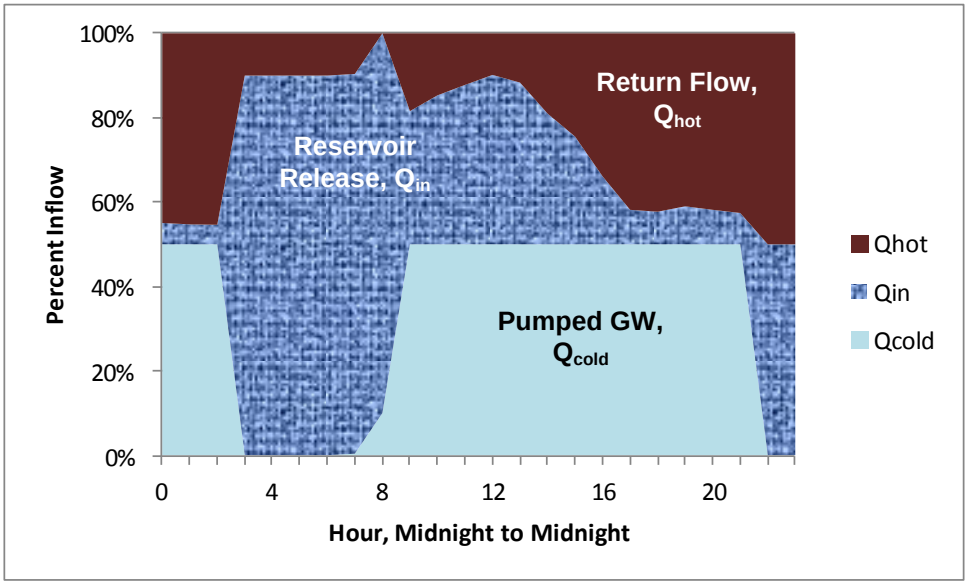

Figure 34. Fractions of source waters for the 24 hour period

Figure 35 also shows T_{out} under a non-optimized scenario where diversions (Q_{div}=0.11 m^3s^{-1}) and tail water (Q_{hot}=0.08 m^3s^{-1}) occur steadily over the 24 hour period, Q_{in} is released at capacity (0.25 m^3s^{-1}) 10am-4pm and there is no groundwater input to the river (Q_{cold}=0). This increases temperatures to over 20^{o}C from 12 pm-6 pm. The average temperature is only 13.9^{o}C but the peak temperature reaches 21.8^{o}C. This demonstrates that managing the timing of these different water sources can have a significant and important effect on river temperature and can reduce the peak stream temperature, albeit perhaps elongating it. For example in this case, the non-optimized peak stream temperature is over 21^{o}C for six hours whereas the optimized T_{out} maintains temperature at or below 18^{o}C but its peak temperature remains a binding constraint for 13 hours, from 11 am until midnight. Increasing cool groundwater input or decreased return flow (Q_{hot}) could decrease the number of hours the upper bound constraint would be binding.

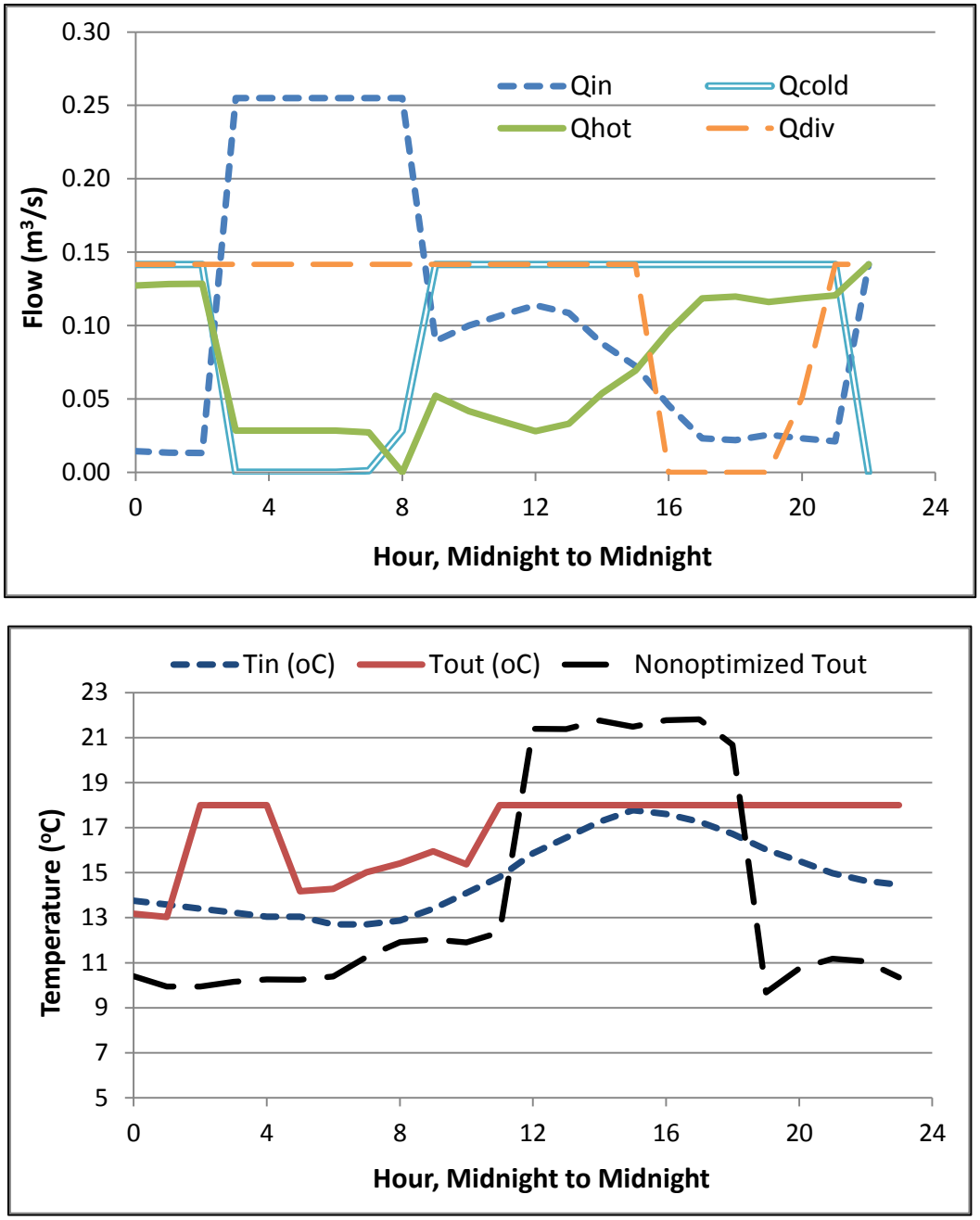

Figure 35. Hourly flow decisions with specified and calculated temperatures for 24 hour period

Sensitivity to input temperatures

With the current inputs for ΔT_t and T_{in}, the cold water source cannot exceed 15.0°C for the problem to be feasible. As T_{cold} increases above 11.8°C, pumping becomes less effective in cooling T_{out} and therefore less valuable so the total volume pumped decreases. The minimum temperature increases from 11.4 to 13.9°C when T_{cold} increases from 10.0 to 15.0°C. Conversely, minimum and average temperatures are reduced when the cold water source is colder (Figure 36). The temperature of the cold water source is an important input and directly affects the potential benefit of optimal operations.

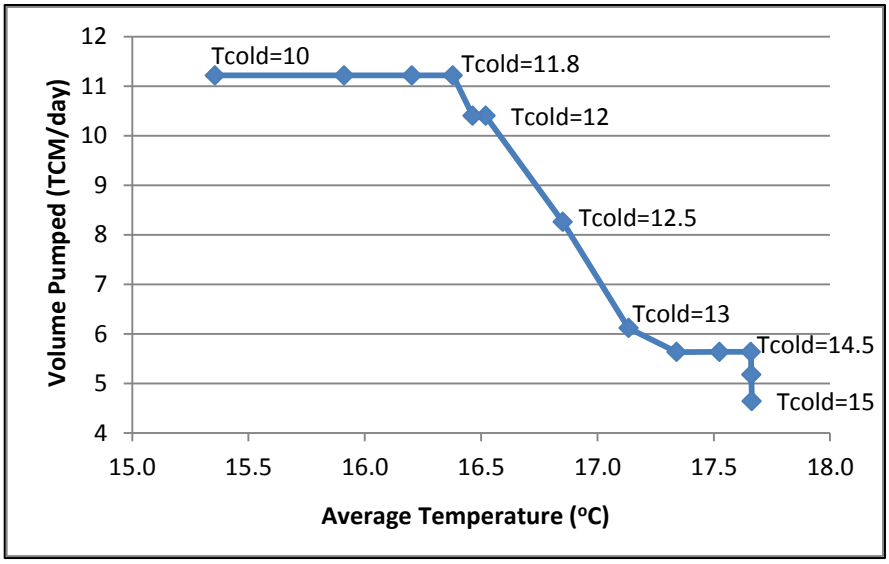

Figure 36. Effect of T_{cold} on average downstream temperature (T_{ave}, T_{min}) and volume of cold water pumped over 24 hours

The hot tail water return flow input temperature also affects operations and downstream temperatures. T_{hot} must be less than 30.0°C for the problem to be feasible with given inputs (Table 29). The volume of cold groundwater pumped is not affected by T_{hot} until it exceeds 24°C at which point pumping decreases until it must increase again to maintain feasibility. This basic problem formulation makes the simplifying assumption that T_{hot} enters the river at a known and constant temperature regardless of the time of day. In this respect, this is a conservative case since T_{hot} should cool some during the night and could potentially become a small source of cold water input. This could be further explored if the relationship between the timing of diversions (irrigation application) and tail water return were established and incorporated into the model.

Improved irrigation efficiency

Improving irrigation efficiency decreases the volume of tail water that enters as Q_{hot} thereby lowering downstream temperatures. Though not modeled as such in the basic problem, it would also decrease the total target diversion (Q_{div}). An increase in efficiency from 34% to 90% drops the average temperature 2.2°C, from 16.9 to 14.6°C. With low efficiency, the 18°C temperature constraint is binding for about sixteen hours, however with efficiency increased to 90% it is a non-binding constraint and the maximum temperature drops to 17.1°C. Increased irrigation efficiency can effectively reduce downstream temperatures.

This basic problem demonstrates the potential benefits of optimizing water sources and supplies (inputs and diversions) for river temperature. It shows that timing matters and understanding the temperature sources and travel times and adjusting operations accordingly can change stream temperature and potentially provide benefits to stream temperature conditions. This approach also highlights some tradeoffs in this type of system.

Case study- Shasta River application

The Shasta Springs Ranch is located along reaches of Parks Creek and the Shasta River between Dwinnell Dam and Big Springs Creek confluence. The river reach between the dam and Shasta River's confluence with Big Springs Creek often has high temperatures and low flows during the irrigation season making it ill-suited for coho during the summer (Jeffres 2012, Pers Comm.). Releases from Lake Shastina satisfy requests for downstream diversions for irrigation and generally introduce warm flows to the river. Warm tail water return from flooded pasture also contributes warm flows to the river. Additionally, Parks Creek joins the Shasta River bringing with it sometimes significant, but often warm flow. In contrast, Clear Springs introduces about 0.10 m^3s^{-1} of consistently cool flow directly to the river

(Figure 37). Introducing cool pumped groundwater to the river at strategic times could provide another cool water source, albeit costly. With adequate flow and temperature, the reach downstream of Clear Springs and upstream of Parks Creek confluence could provide additional rearing habitat for juvenile coho which over summer in the river. To be suitable habitat, its temperatures would ideally be consistently less than 18^{o}C and flow should be 0.14 m^3s^{-1} or more (Jeffres 2012, Pers Comm.). These characteristics become constraints in the management model.

Current operations

Shasta Springs Ranch currently pumps groundwater from the Seldom Seen (SLD) well (Figure 37) to irrigate approximately 60 hectares of pasture (referred to as Seldom Seen Fields) west of the Shasta River (Davids Engineering 2011a). During the 2010 irrigation season, the well was pumped at an approximate rate of 0.08 m^3s^{-1} half of the time (12 hours on, 12 hours off). An aquifer test in 2010, suggests the well could produce water at a higher frequency and likely at a higher rate (Davids Engineering 2011b). This pumped groundwater could serve as a source of cold water to the Shasta River at strategic times to maintain downstream temperatures below a temperature target set for coho rearing habitat. Downstream, a gravity diversion structure (HIGGVdiv) sends water from the river into a ditch on the east side of the river to flood irrigate about 53 hectares (referred to as Hole in the Ground Gravity Fields). Further downstream, water is pumped from the river (HIGPMPdiv) to irrigate 51 hectares on the west side of the river that drains tail water to the Shasta River and another 138 hectares drain to Parks Creek (Hole in the Ground Pump Fields). Between the two diversion points, Clear Springs provides 0.07-0.10 m^3s^{-1} of 13.55^{o}C flow during the 2010 irrigation season (Davids Engineering 2011b).

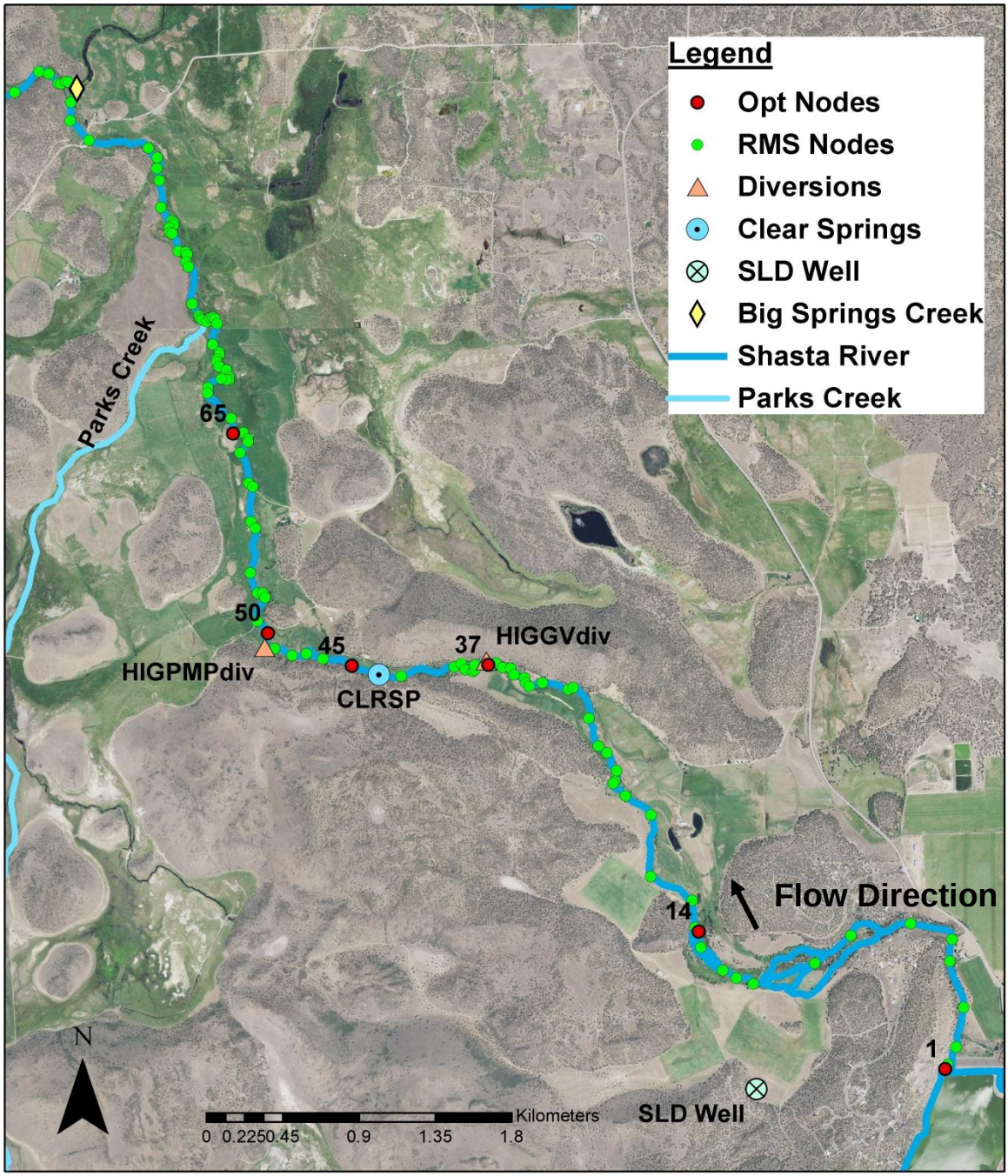

Figure 37. Overview map with nodes defining optimization model reaches and key inflow and diversion points along the Shasta River

Water balance analysis based on estimates of evapotranspiration of applied water (ETAW) and measured stream flows calculated the return flow of tail water to the river as the closure term, for the 2010 irrigation season (Davids Engineering 2011a). Water not used for ET from the HIGGV and HIGPMP fields was assumed to run off. This amounts to about 259 TCM and 185 TCM returning to the Shasta River from these fields in July and August, respectively. The Seldom Seen fields do not have tail water return flow to the Shasta River; water not used for crop ET becomes deep percolation to groundwater (Davids Engineering 2011a). The fields' irrigation efficiency (Table 30) is defined as the fraction of applied water used for crop ET. One minus this fraction is the return flow fraction. Total applied water can be

calculated as the ETAW divided by the irrigation efficiency. This approach is used for inputs of target delivery and required return flow for the optimization model.

Table 30. Evapotranspiration of Applied Water (ETAW) for July and August as estimated in 2010 (TCM) and irrigation efficiency for the three fields (Davids Engineering 2011a)

Month	SLD (TCM)	HIGGV (TCM)	HIGPMP (TCM)
July	78	132	365
August	63	104	261
Daily Average (TCM/day)			
July	2.51	4.26	11.78
August	2.03	3.34	8.44
Irrig Eff.	47%	34%	89%

The Shasta Springs ranch has senior Shasta River water rights established prior to the construction of Dwinnell Dam. As a result, they have rights to call for the release of water from Shastina for diversion at either Hole in the Ground Gravity diversion (HIGGVdiv) or Hole in the Ground Pump diversion (HIGPMPdiv). However, with releases from Shastina, Shasta River flow is dominated by warm water from the reservoir in this reach and then mixes with the cooler Cold Springs source before being diverted at HIGPMPdiv.

Davids Engineering, Inc. performed an irrigation efficiency study including water balance analysis for sub-units of the Shasta Springs Ranch. As a management strategy for improving in-stream fishery conditions by reducing stream water temperature and sustaining agricultural production, they suggest two alternatives: 1) divert warm water released from Lake Shastina to supply irrigation for the Seldom Seen fields and pump an equal amount to discharge into the Shasta River, or 2) increase the Seldom Seen (SLD) well production for discharge into the Shasta River for downstream diversion at HIGGV or HIGPMP diversion locations (Davids Engineering 2011b).

This location and situation provides a testing ground for coordinating surface and groundwater resources for managing stream temperatures. With potential for reservoir releases, groundwater, and rights to surface water diversion, ranch managers have a variety of sources from which to use and manage supplies for irrigation. An optimization model for this system explores if these sources can be operated so that downstream temperatures, at node 65 on Figure 37, can be kept below 18^{o}C.

The optimization model uses hourly river temperatures and atmospheric conditions from an RMS model of the Shasta River developed by Null et al (2010) for January-December 2001. In that study, the Tennessee Valley Authority's Modeling System (TVA-RMS v.4) was used to simulate flow and temperature from Dwinnell Dam to the confluence with the Klamath River with an hourly time step. RMS is a one-dimensional longitudinal, physically-based model with a hydrodynamics module and a water quality module (Hauser and Schohl 2002). Needed inputs for the optimization model include hourly temperature for releases from Shastina, hourly air temperature and solar radiation, and temperature changes and travel times between select nodes to develop an equation describing ΔT_t for each defined river reach.

Problem formulation

The management model for the Shasta River application consists of releases from Lake Shastina (Q_{DWIN}), Clear Springs inflow (Q_{CLRSP}), releases from the SLD well to the Shasta River (Q_{SLDrel}), diversion at Hole in the Ground Gravity diversion (Q_{div1}), diversion at Hole in the Ground Pump station (Q_{div2}), and calculated flow at each river node ($Q_{i,j}$) including outgoing river flow (Q_{Riv}). Input temperatures include hourly temperature for Shastina releases (T_{DWIN}), pumped groundwater from the SLD well (T_{SLDrel}), and Clear Springs (T_{CLRSP}). Temperatures are otherwise calculated at each node using heat balance for mixing and regression analysis for warming across each river reach. The final downstream temperature, T_{out}, is of greatest interest and included in the objective function (Figure 38).

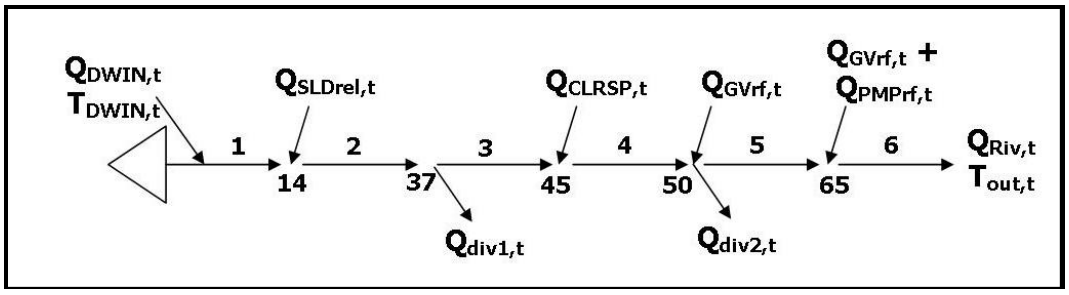

Figure 38. Shasta River application schematic with RMS node numbering

Objective function and inputs

The objective function minimizes the sum of pumping cost, shortage cost resulting from unmet water demand, and a benefit for reducing T_{out} below the target temperature, scaled by alpha as shown in Equation 4.2.

$$\boldsymbol{Min\ Z = \left(C_{pump} * Lift * Vol_{cold}\right) + \left(C_{shortage} * Vol_{shortage}\right) + \alpha \sum_{t} \left(T_{out} - T_{target}\right)}$$

Equation 4.2

Pumping cost (C_{pump}) is specified in dollars per thousand cubic meters (TCM) per meter of lift. Lift is estimated as the difference between the ground surface elevation at the well and the water level elevation during pumping. A groundwater pumping lift of 15.2 meters is chosen based on available data for the SLD well from 2010 (Davids Engineering 2011b). Pumping cost per TCM per meter of lift is based on pumping costs used in CALVIN (Draper et al. 2003) and specified as 0.53 $/TCM/m. Total pumping volume is calculated by converting the pumping rate in each time step to a volume and summing over all time. Therefore, total pumping cost is the marginal cost per TCM multiplied by the total volume pumped and the lift. The volume of shortage ($Vol_{shortage}$) is calculated by summing the volume of diverted water over all time steps and subtracting that from the target delivery for the model time period. Marginal cost of shortage is 81 $/TCM based on penalty functions for region 1 in CALVIN (Draper et al. 2003), a statewide economic-engineering model of California's water supply network. A marginal cost range of 62 to 148 $/TCM will be evaluated during sensitivity analysis. The initial model parameter values and coefficients are reported in Table 31.

The temperature target is the upper bound constraint for T_{out}. For over summering juvenile coho in the Shasta River, ideally, maximum river temperature is 18^{o}C. Improving temperature conditions for coho habitat requires consistently good conditions so that fish are not attracted by temporarily cool river temperatures and then caught in areas that may heat up and become deadly (Jeffres 2012, Pers Comm.; Jeffres and Moyle 2012). Managing flows and temperatures with fish in mind requires careful consideration of what species and what life stage(s) the habitat is intended to support.

The temperature of the SLD pumped groundwater and Clear Springs is based on temperatures reported by Davids Engineering, Inc. (Davids Engineering 2011b). The flow and temperature of Clear Springs has little variation and is set to 13.55^{o}C. Groundwater temperature from the SLD well is likewise assumed to be constant. Boundary condition input data for the 2001 Shasta River RMS model developed by Dr. Sarah Null provides the time varying temperature of Lake Shastina releases. This approach assumes 2001 reservoir release temperatures are generally representative and contain the range and variability likely to occur during the irrigation season or model time period.

Table 31. Shasta River model parameters

Parameter	Value	Units
alpha	100	n/a
Temp Target	18	^{o}C
Lift	15.2	m
C_{pump}	0.53	$/TCM/m
$C_{shortage}$	81	$/TCM
T_{SLDrel}	12.5	^{o}C
T_{CLRSP}	13.55	^{o}C
T_{DWIN}	Hourly varying	^{o}C
ΔT_t	Hourly varying	^{o}C

The agricultural target delivery is calculated as a function of irrigation efficiency and ETAW (Table 30). The appropriate daily ETAW rate is multiplied by the number of days in the modeled time period and divided by the irrigation efficiency, for each field. The total combined volume delivered from both diversions is compared to the combined delivery target and the difference is multiplied by the shortage cost. This leaves the optimization model to decide the timing and delivery volume in each time step.

Estimating temperature change for the Shasta River

An approach is needed to estimate change in temperature, heating or cooling, that occurs over specified reaches in the optimization model. Stream temperature research indicates atmospheric conditions are mainly responsible for heat exchange processes at the water surface (Caissie 2006). Simple regression models have been used to predict water temperature using only air temperature as the input parameter, mostly for weekly and/or monthly time steps. Caissie et al (2006) describes several studies using this approach. Others have used multivariate regression models to predict river temperature. Other explanatory variables include river discharge, time lag data, solar radiation, depth of water, among others (Caissie 2006). For this study, flow rate, air temperature, and solar radiation are used to predict change in temperature over a specified river reach.

The 2001 Shasta River RMS model simulates hourly stream temperatures using a heat budget approach estimating heat fluxes for net solar radiation adjusted by a shading factor, atmospheric long-wave radiation, channel bed heat flux, back radiation from the river, evaporative heat loss, and conductive heat transfer (Hauser and Schohl 2002). Meteorological input data includes dry bulb temperature, atmospheric pressure, wind speed, solar radiation and relative humidity. For the regression, an hourly time series of ΔT_t for July-August (when stream temperatures tend to be the highest) was calculated from RMS model temperature outputs. To control for flow rate, the 2001 RMS model was run several times with different levels of constant flow for the upstream boundary condition flow rate. This required seven model runs for the odd flow rates from 0.14-0.48 m^3s^{-1}, considered to be a reasonable range for the Shasta River upstream of Parks Creek. With current operations, flow rates are often less than 0.14 m^3s^{-1} during the irrigation season so additional model runs were needed to produce ΔT_t calculations for the flow range of interest for the optimization problem. Hourly air temperature and solar radiation inputs for the 2001 RMS model as well as flow rate were used as input variables for the regression model. The result is the linear regression equation:

$$\Delta T_{reachX,t} = \beta_0 + (\beta_1 * Q_t) + (\beta_2 * Tair_t) + (\beta_3 * SR_t) + \varepsilon_t$$

Where the betas are coefficients estimated from the linear regression analysis. This was done for five reaches (Table 32) using ordinary least squares. Regression results indicate the explanatory variables are significant (p-value < 0.05) and explain 63-80% of the variation in ΔT_t (depending on the reach, Table 32). Results also highlight the marginal effect of flow rate on ΔT_t. Generally, an increased flow is expected to decrease the ΔT_t occurring over the given reach since higher flow means more mass which heats/cools more slowly. This is reflected by the negative sign on the coefficient for flow (β1) for most of

the reaches (1-4). On average, an increase in flow of 0.3 m^3s^{-1} decreases ΔT_t by 0.003-0.08^oC, depending on the reach (Table 32).

Table 32. Regression coefficients for July-August estimate of ΔT_t (^oC)

Reach	1	2	3	4	5
node i	1	14	37	45	50
node j	14	37	45	50	65
Constant, β	0	0	0	0	-0.087** (0.017)
Flow, β1	-0.078** (0.0014)	-0.044** (0.0012)	-0.009** (0.00062)	-0.003** (0.00069)	0.002* (0.00085)
Air Temp, β2	0.029** (0.00080)	0.009** (0.00068)	-0.006** (0.00036)	-0.014** (0.00040)	-0.011** (0.00065)
Solar Radiation, β3	0.004** (0.00003)	0.003** (0.00002)	0.002** (0.00001)	0.002** (0.00001)	0.002** (0.00002)
Adjusted R-sqd.	0.8078	0.7824	0.7505	0.7069	0.6351
Travel Time (hr)	2	2	1	1	1

** p value < 0.05, ** p values < 0.01, Standard error in parenthesis*

The regression model results in reasonable estimation of hourly temperatures at the downstream node, RMS 65 (Figure 39). The spreadsheet simulation model uses temperature input data for Shastina releases from the 2001 RMS model as the upstream boundary condition and then estimates the ΔT_t for each reach using the reach's corresponding regression equation. This ΔT_t is added to the temperature leaving the upstream node (*i*) in a previous time step, determined by the estimated travel time of the reach (Table 32), to estimate temperature at the downstream node (*j*):

$$T_{i\rightarrow j,t} = T_{i,t-r} + \Delta T_{i\rightarrow j,t} = T_{i,t-r} + \Delta T_{reachX,t}$$ where r is the travel time for reach i to j.

In this way, the spreadsheet model simulates hourly temperature at each node. The target temperature is set for the furthest downstream node (RMS 65) in the optimization model. Since this is the location of interest, temperature results from the spreadsheet model are compared to 2001 RMS results at this node (Figure 39).

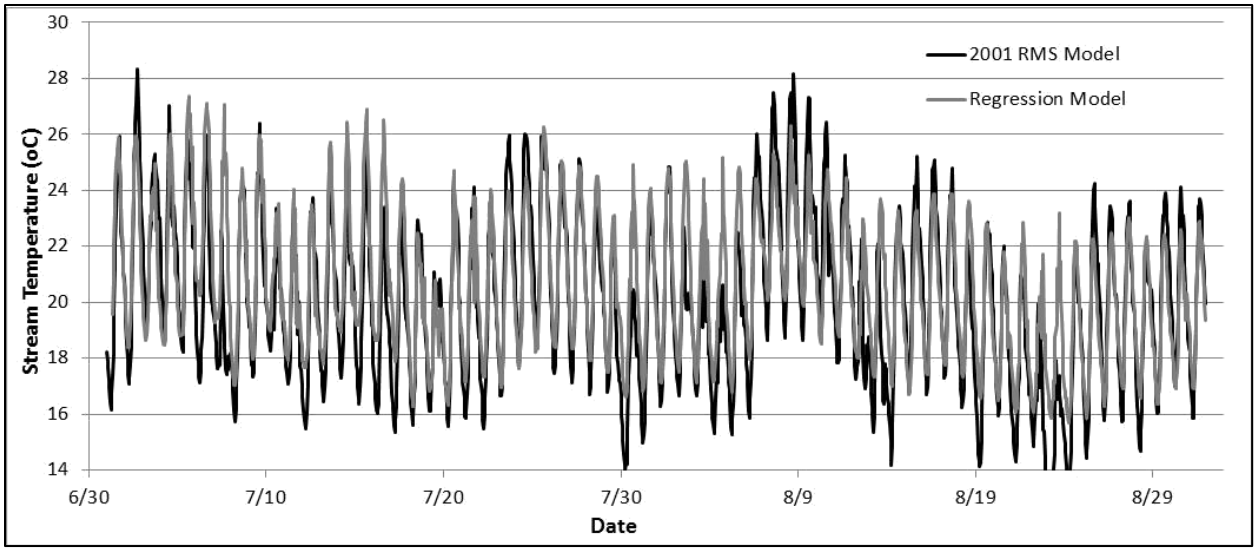

Figure 39. Stream temperature at node 65 from 2001 RMS model and spreadsheet model using regression, July-August

The root mean square error (RMSE) for RMS node 65 is 1.62^{o}C. The regression model overestimates daily maximum and minimum temperatures more than it underestimates them. For the July to August period, the maximum overestimation of maximum daily temperature is 5.24^{o}C and the maximum overestimation of minimum daily temperature is 4.20^{o}C. In contrast, the maximum underestimate of daily maximum temperature is 2.38^{o}C and only 0.57^{o}C maximum underestimate of daily minimum temperature. Therefore, the regression model generally tends to overestimate temperatures, making it conservative for optimizing stream temperatures for habitat suitability. This trend of overestimation is true on the weekly time scale as well, but overall the regression-based spreadsheet model provides reasonable approximation of simulating Shasta River temperatures in this reach of interest.

Table 33. Mean Weekly Maximum and Mean Weekly Minimum Temperatures for weeks July-August from the 2001 RMS and spreadsheet regression-based model for RMS node 65

	MWMaxT (^{o}C)			MWMinT (^{o}C)		
Week	**Regression**	**2001 RMS**	**Difference**	**Regression**	**2001 RMS**	**Difference**
1	26.4	25.8	0.6	19.0	17.9	1.0
2	24.8	24.6	0.3	18.0	16.8	1.2
3	24.2	23.5	0.7	17.5	15.8	1.6
4	24.7	24.9	-0.1	17.8	17.1	0.7
5	24.5	22.3	2.2	17.1	15.8	1.3
6	25.0	26.2	-1.1	18.9	17.7	1.1
7	23.5	23.6	-0.1	17.4	16.2	1.2
8	22.4	21.4	1.0	16.1	13.9	2.2
9	22.6	23.5	-0.8	16.6	15.8	0.8
Average	**24.3**	**24.0**	**0.3**	**17.6**	**16.4**	**1.2**

Constraints

Management decisions (decision variables) are made hourly for flow rates (m^3s^{-1}) released from the reservoir (Q_{DWIN}), diversions ($Q_{div1,}$ Q_{div2}), return flows (Q_{GVRFup}, $Q_{GVRFlwr}$, Q_{PMPRF}), and groundwater releases to the Shasta River (Q_{SLDrel}) subject to several constraints (Figure 38).

Temperature at each node where mixing water sources of different temperatures occurs (nodes 14, 45, 50, and 65) uses a heat balance approach where the sum of incoming flows multiplied by their respective temperatures equals the sum of outgoing flow multiplied by its respective temperature. This nonlinear equation is used to solve for the outgoing river temperature. For example, the outgoing temperature from node 14 ($T_{14,t}$) is a function of flow from the upstream node and the incoming flow from pumped groundwater:

$$T_{14,t} = \frac{Q_{1,t-r} * T_{1-14,t} + Q_{SLDrel,t} * T_{SLDrel}}{Q_{1,t-r} + Q_{SLDrel,t}}$$ **Heat balance**

$r_{i-j,t}$ is travel time between node i and j at time t.

The incoming temperature to each node ($T_{i->j,t}$) is the temperature at the upstream node in a prior time step (according to travel time) adjusted by ΔT_t:

$$T_{1\rightarrow 14,t} = T_{1,t-r} + \Delta T_{1\rightarrow 14,t}$$ **Downstream heating/cooling**

ΔT is defined by regression analysis as described previously.

$$\Delta T_{1\rightarrow 14,t} = \beta_0 + (\beta_1 * Q_{1,t-r}) + (\beta_2 * Tair_t) + (\beta_3 * SR_t) + \varepsilon_t$$ **Regression equation for** ΔT_t

Conservation of mass equations define the flow at each node. Continuing the example for reach 1->14:

$$Q_{14,t} = Q_{1,t-r} + Q_{SLDrel,t}$$ **Conservation of mass, inflows=outflows**

At nodes where diversions take place (node 37 and 50, Figure 38), a minimum in-stream flow requirement constrains flow to be greater than 0.14 m^3s^{-1}.

$$Q_{37,t}, Q_{50,t} \geq 0.14$$ **Minimum in-stream flow requirement**

Several capacity constraints limit rates of reservoir releases, groundwater pumping, diversions, and return flows in any given time (Table 34). They are constant for all time in the modeled period.

Table 34. Capacity constraint for Lake Shastina releases, pumping rate from SLD well, diversions HGGV and HGPMP, and all three return flows

	Flow (m^3s^{-1})
Q_{DWIN} >	0.02
Q_{DWIN} <	0.34
Q_{SLDrel} <	0.14
Q_{div1} <	0.21
Q_{div2} <	0.14
Q_{RFs}<	0.08

Water supply constraints for the sum of deliveries from HIGGV and HIGPMP ensure that no more than the delivery target is diverted for each of these fields.

$$Delivery\ Target\ (HIGGV) \geq Total\ Delivered\ (div1)$$

Water supply constraints

$$Delivery\ Target\ (HIGPMP) \geq Total\ Delivered\ (div2)$$

Constraints define relationships for diversions and their resulting return flows. Return flow is driven by irrigation efficiency and the volume of diversions (based on decision variables). According to descriptions in the Shasta Springs Ranch Irrigation Efficiency Study (Davids Engineering 2011a), return flows from the HIGGV fields partially return to the Shasta River above the HIGPMP diversion (upper reach) and partially in the stretch between the pump diversion and the confluence with Parks Creek (lower reach). About 59% of this lower reach is modeled here (up to node 65). The split between these two reaches is 16% and 84% to the upper and lower reaches, respectively. The volume of return flows to the lower reach is reduced by 41% to account for the stretch of river not included in the optimization model. Similarly, return flow to the lower reach results from diversions from HIGPMP that irrigate fields on the west side of the river. This is also reduced by 41%. These constraints ensure the total volume of return flows reflect the irrigation efficiency and diversions made, but allows the optimization model to choose the timing and magnitude of these return flows:

$$\sum_t Q_{GVrf\_upper} = 0.16 * (1 - Irrig\ Eff) * \sum_t Q_{div1}$$

$$\sum_t Q_{GVrf\_lwr} = 0.59 * 0.84 * (1 - Irrig\ Eff) * \sum_t Q_{div1}$$

Return flow constraints

$$\sum_t Q_{PMPrf} = 0.59 * (1 - Irrig\ Eff) * \sum_t Q_{div2}$$

Finally, a constraint also ensures that outgoing temperatures from node 65 are less than or equal to the set temperature target, ideally 18°C.

$$T_{out,t} \leq T_{target}$$

Temperature constraint for juvenile coho rearing habitat

These constraints, as labeled, force the optimization model to follow the problem's physics (conservation of mass and heat) and engineering (capacity constraints). They also include constraints that can be explored further (minimum in-stream flow requirement and temperature target) through sensitivity analysis to understand what is binding and what tradeoffs are at play in the system.

Solver

The optimization problem is solved using What's*Best*! Nonlinear solver version 3.0 which uses a generalized reduced gradient (GRG) algorithm. The default nonlinear solver options are employed which includes successive linear programming (SLP) to compute new search directions, the presolve option that identifies and removes extraneous variables and constraints from the formulation, and selective constraint evaluation which causes the solver to only evaluate constraints on an as needed basis.

Results

Optimization model results for the Shasta River application provide hourly operations of reservoir releases, SLD pumping, diversions, and tail water return flows to maintain river temperatures at node 65 below the target temperature. Results for a 'current operations' scenario are presented and compared to optimized results for the week of July 1-7 using 2001 atmospheric conditions from the 2001 RMS stream temperature model and constraints and deliveries from 2010 water balance data collected by Davids Engineering as part of their water efficiency study on the Shasta Springs Ranch. Sensitivity analysis results for the optimization model are also presented and discussed.

Current operations

The spreadsheet model is set up as a simulation model to provide a 'current operations' baseline of hourly temperature at node 65 for July through August. Time series of irrigation diversions and Clear

Springs flow measured in 2010 by Davids Engineering, Inc (Davids 2012, Email) is input for Q_{div1}, Q_{div2}, and Q_{CLRSP}. The 2001 RMS model provides temperature of Lake Shastina releases and atmospheric conditions (air temperature and solar radiation) for ΔT_t calculations. Shastina releases (Q_{DWIN}) were estimated by setting flow at the end of the line (node 65) to measured hourly flow data (also provided by Davids Engineering) for the Shasta River just upstream of Parks Creek confluence and back calculating Q_{DWIN}. Return flows were set to average flow rates reported in the Shasta Springs Ranch efficiency study (Davids Engineering 2011a); 0.01, 0.08, 0.003 m^3s^{-1} for Q_{GVrf_upper}, Q_{GVref_lwr}, and Q_{PMPrf}, respectively. The temperature of return flow is set at 25°C for all time. Additional data on the timing and temperature of return flow would improve representation of this important component.

Resulting modeled temperature at node 65 for the two month period is summarized by mean weekly maximum temperature (MWMaxT) and mean weekly minimum temperature (MWMinT) for the July-August period (weeks 1-9). These results are in line with the reality that this reach of the river maintains unacceptably high maximum and minimum temperatures for juvenile coho rearing.

Table 35. Mean Weekly Maximum Temperature and Mean Weekly Minimum Temperature (°C) for the nine weeks spanning July-August for temperatures at node 65 simulated with the spreadsheet-based model

Week	MWMaxT	MWMinT
1	24.4	20.3
2	23.5	19.3
3	23.1	18.9
4	23.3	18.9
5	23.4	19.0
6	23.3	19.1
7	21.9	17.6
8	21.5	17.5
9	21.9	18.6
Average	22.9	18.8

Optimization results

The week of July 1-July 7 is optimized within the described formulation and given constraints. This first week of July had the highest maximum and minimum temperatures of the July-August period (Table 35) and thus serves as a worst case timeframe and demonstrates the promising potential for reducing stream temperature in the Shasta River upstream of Parks Creek confluence with strategic operation of inflows and tail water. A temperature target of 18°C was infeasible, however, 18.1°C was feasible. The resulting time series of decision variables successfully reduced maximum temperatures while also maintaining cooler nighttime temperatures. The MWMaxT with optimized results became 18.1°C and the MWMinT is 13.1°C. Figure 40 shows the hourly temperatures with current operations, optimized operations, and boundary condition temperatures from Shastina releases. The reduction in temperature is promising, yet comes at a cost. Table 36 summarizes costs and temperatures (maximum, minimum, and average) for the Current Operations and Optimized results.

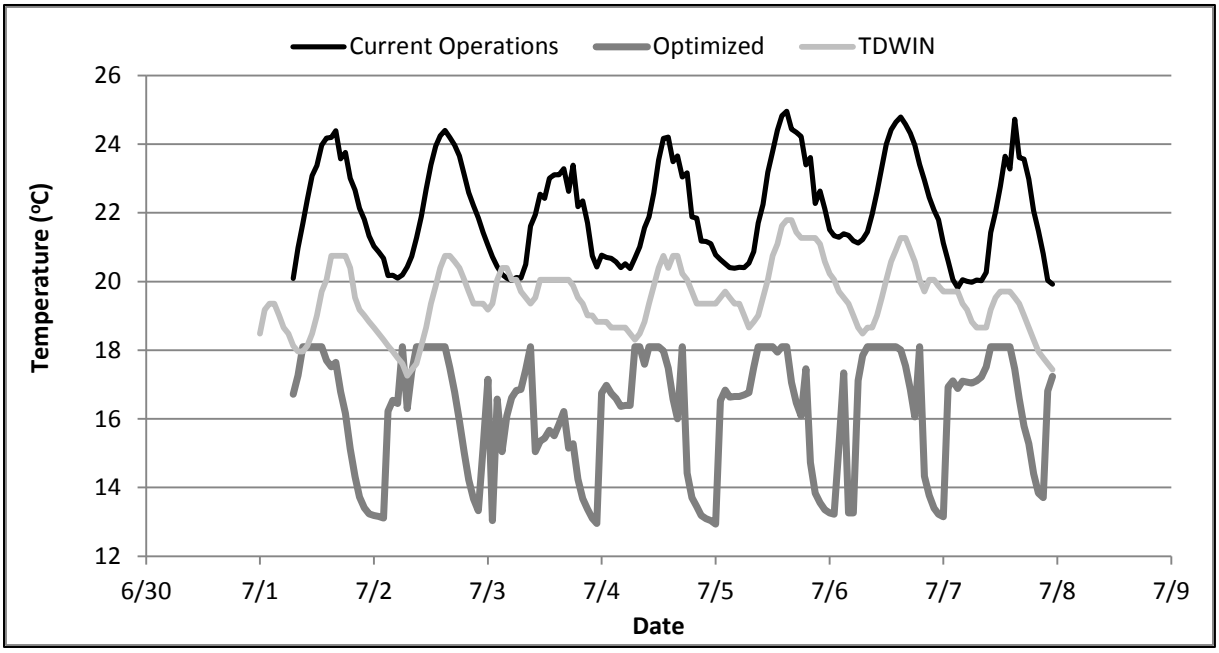

Figure 40. Optimized Shasta River temperature at node 65 compared to Current Operations and Input temperature from Shastina releases

Table 36. Comparison of weekly costs ($) and temperatures (^{o}C) at node 65 for Current Operations and Optimized results

Run	Total Cost ($)	Pumping Cost ($)	Shortage Cost ($)	Tmax (^{o}C)	Tmin (^{o}C)	Tave (^{o}C)
Current Operations	1,780	0	1,780	25	19.8	22.1
Optimized	11,125	350	10,775	18.1	12.9	16.2

Since the HIGGV diversion has low irrigation efficiency (34%), it brings high levels of warm (set at 25^{o}C) return flow to the river. Therefore, with optimized conditions, essentially no water is diverted from HIGGV for irrigating the Gravity diversion fields. This leads to a shortage of about 88 TCM for this diversion. A fraction of the PMP diversion also becomes a source of warm tail water return flow. Shortage for the PMP fields amounts to almost 46 TCM compared to the delivery target of 93 TCM for the week. The total shortage cost therefore is $10,775 for this one week of operation (Table 36).

To achieve these optimal temperature conditions, the SLD well releases about 0.11 m^3s^{-1} of cool water to the river for about 12 (+/- 3) hours each day from morning to evening (Figure 41A). A high flow Shastina release tends to be in the evening and/or close to midnight. Moderate flows continue through the night when Shastina temperatures are coolest and then releases drop in the early morning, between 5 and 7 am. Diversions at HIGPMP are fairly continuous at 0.08 m^3s^{-1} with occasional peaks up to 0.14 m^3s^{-1} (its upper bound constraint) often around midnight, and sometimes down to zero m^3s^{-1} (Figure 41B). Managed tail water is released to the Shasta River at capacity (0.08 m^3s^{-1}) during nine different hours over the seven day period. The timing of these releases are in the evening or early morning. This suggests concentrated return flow releases at strategic times provide the least harm to river temperatures.

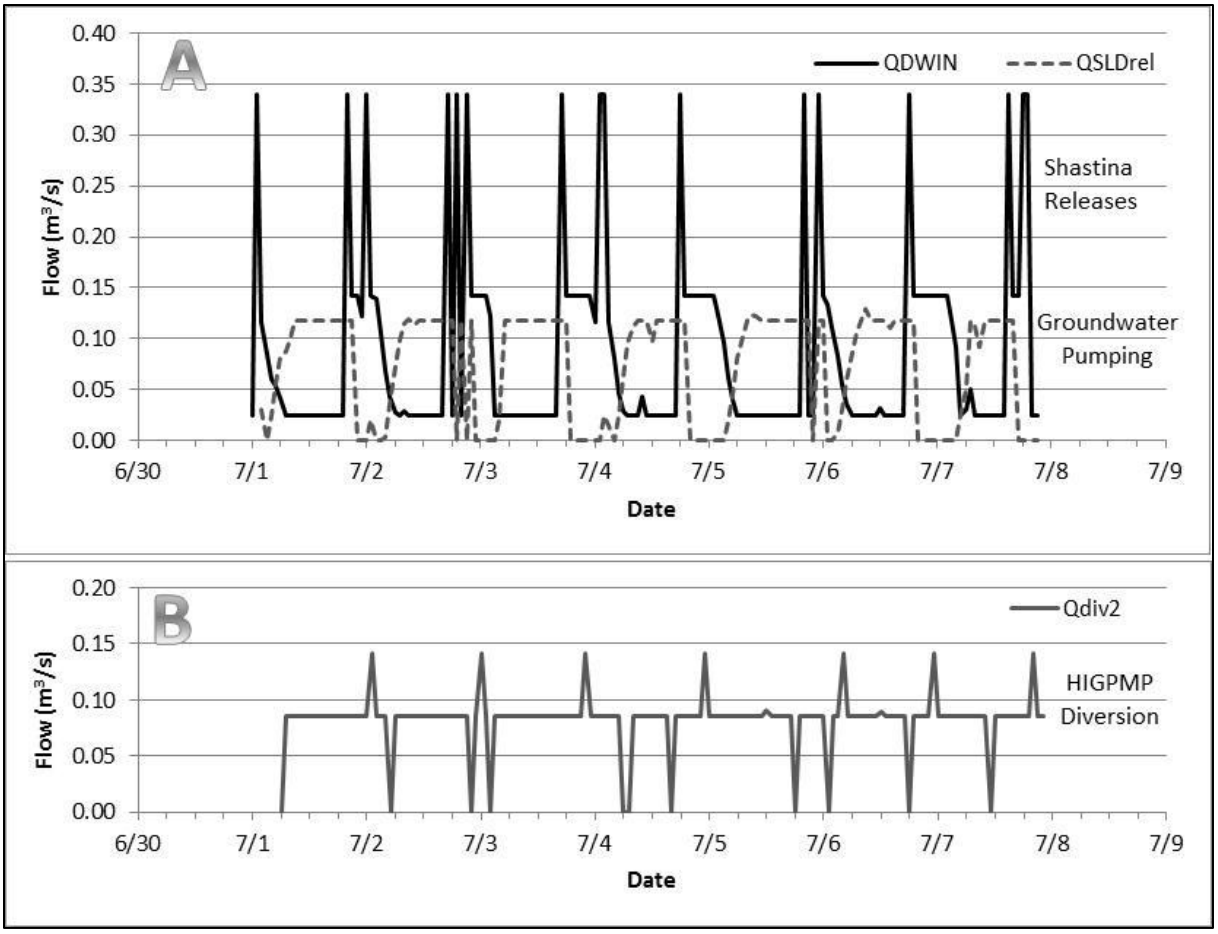

Figure 41. Optimized flows for Shastina releases, SLD well releases, and diversions at HIGPMP

This operation results in an objective function value of -18,850 resulting from a total shortage cost of $10,775, pumping cost of $350, and a temperature component of -29,975. The average temperature over the seven day period is 16.2°C.

Sensitivity analysis

Sensitivity analysis for the July 1-July 7 model was conducted on the temperature target, alpha, shortage cost, and irrigation efficiency. The temperature target, in the range of 18.1-24°C, has no significant effect on shortage, and little effect on the minimum and average temperature. In all cases, groundwater is pumped at capacity from the SLD well.

Alpha influences the value to the objective function of maintaining temperatures below the target temperature. The temperature constraint ensures that maximum temperatures do not exceed the target temperature, but the temperature component of the objective function and therefore alpha, drives the model to achieve temperatures as much below the temperature target as possible. This is important because cool temperatures at night are also crucial for fish. Heating during the day can be acceptable if it also cools sufficiently at night (Jeffres 2012, Pers Comm.). Alpha provides the driver for maintaining cool nighttime temperatures in the optimization. Without the temperature component in the objective function, 18.1°C is maintained during all time steps over the seven day period. This satisfies the temperature target constraint but would not be suitable for fish. Figure 42 shows the tradeoff curve between average temperature and total cost (pumping and shortage cost) for different values of alpha. Since pumping occurs at capacity for all values of alpha, the tradeoff really is between shortage and temperature. Some shortage cost occurs just to maintain feasibility, but it increases quickly to achieve cooler temperatures. An alpha of 100 captures most of the temperature benefit at a total cost of $11,125.

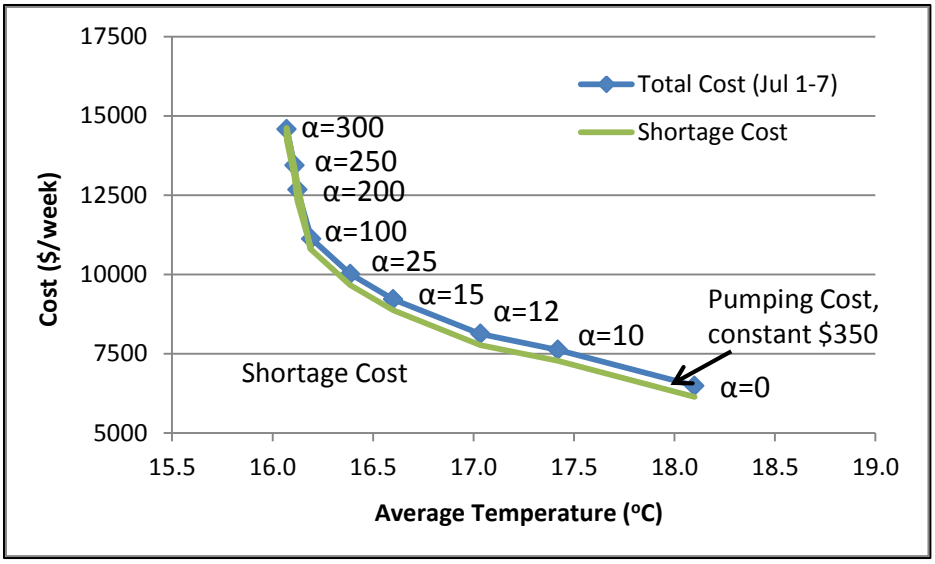

Figure 42. Tradeoff curve between average temperature and cost (alpha in $/°C)

The initial marginal shortage cost used is 81 $/TCM as described. However a range of $41-$97/TCM is reasonable for irrigated pasture in Northern California. Within this range, optimization results for average temperature do not vary significantly and remain at about 16.2°C. Shortage responds slightly with 143 TCM when marginal cost is 41 $/TCM down to 133 TCM when marginal cost is 61 $/TCM. This amounts to a difference of about $2,300 in shortage cost. Marginal costs above 61 $/TCM have essentially no effect on shortage or temperature results. Generally, the model is relatively insensitive to the marginal shortage cost.

Irrigation efficiency is important and has a prominent effect on shortage and shortage cost. Increased irrigation efficiency, particularly for the HIGGV fields directly and significantly reduces warm tail water returns to the system at nodes 50 and 65 when diversions are made at node 37 (Q_{div1}). Improved efficiency allows more diversions without a significant temperature effect which in turn reduces shortage cost. If irrigation efficiency of the HIGGV fields could be improved to 75%, shortage cost would drop to $6,706 from $10,775. If it could further be improved to 90%, shortage cost would be $3,879 for the seven day period, almost a third of the cost with original efficiencies of 34 and 89% (Table 37). Irrigation efficiency is an important and effective means of benefiting stream temperatures and maintaining higher deliveries to irrigated agriculture.

Table 37. Irrigation efficiency effects on shortage cost, pumping cost and the temperature component of the objective function

HIGGV Efficiency	**0.34**	**0.50**	**0.75**	**0.90**	**0.90**	**0.95**	**0.34**
HIGPMP Efficiency	**0.89**	**0.89**	**0.89**	**0.89**	**0.90**	**0.95**	**0.95**
Total Shortage Cost ($)	10775	8331	6706	3879	3650	3003	10119
Total Pumping Cost ($)	350	350	350	350	350	350	350
Temp component	-29975	-29623	-29986	-30346	-30431	-31617	-31275

Discussion

The optimization model organizes the problem and its components in a way that allows alternatives and tradeoffs to be explored. The spreadsheet model is solved by a commercial solver, *What's Best!*. It includes input data, constraint sets, and mathematical relationships to minimize the value of the objective function. Model results include time series (hourly) decisions for Lake Shastina releases, SLD pumping for release, two HIG diversions, and tail water return flows. Hourly temperature at the downstream location (node 65) and each model node is also an output. The nonlinear model is run for July 1-7 based

on 2001 atmospheric conditions (reservoir release temperatures, air temperature, and solar radiation based on the 2001 RMS Shasta River model), and 2010 operations/demands since the most comprehensive data for demand and releases is available for this irrigation season. This particularly hot week (simulated stream temperatures with current operations have high daily maximums and minimums) provides a good testing ground for the optimization model and its results reveal trends in operations that effectively reduce stream temperatures at the downstream location, node 65. Since the primary objective is to create habitat for juvenile coho rearing during the summer, the temperature target is left firmly at 18^{o}C (or as close to it as is feasible, 18.1^{o}C in this case) and other constraints explored. Model results illuminate which constraints are binding, how much cold water it takes and when to keep in-stream temperatures below the target, how costly it is, and what the tradeoffs are between maintaining acceptable river temperatures and supplying water to irrigate. The different assumptions and chosen inputs can easily be changed and ranges explored to assess their sensitivity and influence on river temperatures and agricultural deliveries. This tool allows this management strategy regarding pumping, release, and diversion decisions to be explored and evaluated in relation to water supply and habitat conditions. This work provides a technical evaluation of the proposed management strategy to use the SLD well as a cool water source and demonstrates that it has potential in practice. However, it also suggests that managing the cold water source and reservoir releases alone would not be sufficient. Reducing warm water sources (i.e. tail water) is necessary to effectively improve temperature conditions in the river. In addition, managing the timing of those return flows is also important. Tail water can be effectively reduced either by decreasing diversions, which is costly, or by increasing irrigation efficiency, or a combination of the two.

This modeling has several limitations and assumptions that should be further explored if the management approach is to be considered. No hydrogeologic connection between pumping from the SLD well and Shasta River flow is represented in the spreadsheet model. This warrants further investigation and would require additional field work to test and observe the effects of pumping on stream flow. Any coordinated management of surface and groundwater resources should acknowledge and emphasize understanding the interconnectedness of surface and groundwater resources. A pump test with measured stream flow data could be used to develop a relationship between pumping and stream flow that could be incorporated into the optimization model. This aspect is currently not included in the model.

Different types of irrigation technology with varying irrigation efficiencies could be represented in the model by using multiple links between adjacent nodes. Each link would represent a different irrigation technology and have a corresponding cost. This would allow for the evaluation of the costs, benefits and tradeoffs of different irrigation technologies (flood, solid set sprinklers, etc.).

The formulation also assumes that irrigation of the SLD fields could be met either by additional releases from Lake Shastina or by additional pumping from the SLD well. Currently, the SLD well provides water to irrigate these fields. A seasonal water balance with optimal operations is needed to evaluate how much water is required from Lake Shastina to meet these temperature targets and whether it is in the range of the Shasta Springs Ranch water rights. Additionally, the production constraints of the SLD well should be firmly established through additional pump tests and model inputs adjusted to reflect them.

Conclusions

Results from the basic problem reveal the tradeoffs between pumping cost and river temperatures. Including a hot water source (i.e. tail water) in the basic problem allows the exploration of the effect of timing of tail water returns to the river and reservoir releases and how to minimize their detrimental impact on peak river temperatures. Improving irrigation efficiency and thereby reducing the amount of hot water input to the river is an effective way of improving stream temperatures. In general, releasing water from the reservoir during the night and early morning when release temperatures are coolest is best. Supplementing with cool water from another source (i.e. groundwater) during the other hours helps mitigate warm inflows and warming in-stream temperatures. The basic problem results demonstrate that intentional timing of releases and understanding travel times can improve downstream temperatures while still meeting water demand targets.

The Shasta River application likewise reveals tradeoffs between stream temperatures and irrigation deliveries, primarily due to low irrigation efficiencies which return a large portion of diverted water to the river at higher temperatures. Improving irrigation efficiency allows increased deliveries for irrigation with less warm water input from tail water that significantly degrades river temperature conditions. Additional data collection should explore the stream-aquifer interaction and investigate pumping effects on stream flow from the SLD well. Data describing the flow and temperature of tail water return flow would also further improve the optimization model's accuracy in identifying the best timing and magnitude of the various water supply sources.

This work presents a novel approach to managing surface and groundwater resources conjunctively for stream temperatures and develops a management tool to explore potential benefits of strategically operating releases, pumping, and diversions. It demonstrates the effectiveness of using a regression-based stream temperature model to explicitly include temperature aspects in the optimization problem itself. Coordinated management of groundwater and surface water to decrease thermal loading and maintain sufficiently lower stream temperatures may be a promising approach for restoration and environmental management of Shasta River's water supply and quality above the Parks Creek confluence. This approach is applicable to other systems and demonstrates that timing matters when water sources of varying temperature in space and time are part of the supply portfolio.

References

Barlow, P. M., Ahlfeld, D. P., ASCE, M., and Dickerman, D. C. (2003). "Conjunctive-Management Models for Sustained Yield of Stream-Aquifer Systems." *Journal of Water Resources Planning and Management*, 129(1), 35-48.

Basagaoglu, H., and Marino, M. A. (1999). "Joint management of surface and ground water supplies." *Ground Water*, 37(2), 214-222.

Bazargan-Lari, M. R., Kerachian, R., and Mansoori, A. (2009). "A Conflict-Resolution Model for the Conjunctive Use of Surface and Groundwater Resources that Considers Water-Quality Issues: A Case Study." *Environmental Management*, 43(3), 470-482.

Bettinger, P., Johnson, K. N., and Sessions, J. (1996). "Forest planning in an Oregon case study: Defining the problem and attempting to meet goals with a spatial-analysis technique." *Environmental Management*, 20(4), 565-577.

Bogan, T., Stefan, H. G., and Mohseni, O. (2004). "Imprints of secondary heat sources on the stream temperature/equilibrium temperature relationship." *Water Resources Research*, 40(12), 16.

Bredehoeft, J. D., and Young, R. A. (1983). "Conjunctive use of Groundwater and Surface-Water for Irrigated Agriculture - Risk-Aversion." *Water Resources Research*, 19(5), 1111-1121.

Caissie, D. (2006). "The thermal regime of rivers: a review." *Freshwater Biology*, 51, 1389-1406.

Carron, J. C. (2000). "Simulation and Optimization of Unsteady Flow and Water Temperature in Reservoir Regulated Rivers," University of Colorado.

Chiu, Y. C., Nishikawa, T., and Yeh, W. W. G. (2010). "Optimal Pump and Recharge Management Model for Nitrate Removal in the Warren Groundwater Basin, California." *Journal of Water Resources Planning and Management-Asce*, 136(3), 299-308.

Davids Engineering, I. (2011a). "Shasta Springs Ranch Irrigation Efficiency Study." A Cooperative Investigation Undertaken by the CA Department of Fish and Game and Emmerson Investments.

Davids Engineering, I. (2011b). "Shasta Springs Ranch Irrigation Efficiency Study, Appendix A: Hydrogeologic Assessment." A Cooperative Investigation Undertaken by the CA Department of Fish and Game and Emmerson Investments.

Davids, J. (2012, Email). Davids Engineering, Inc. 5/23/2012.

Draper, A. J., Jenkins, M. W., Kirby, K. W., Lund, J. R., and Howitt, R. E. (2003). "Economic-engineering optimization for California water management." *Journal Of Water Resources Planning And Management*, 129(3), 155-164.

Ejaz, M. S., and Peralta, R. C. (1995). "Maximizing Conjunctive Use of Surface and Ground-water Under Surface-Water Quality Constraints." *Advances in Water Resources*, 18(2), 67-75.

Hauser, G. E., and Schohl, G. A. (2002). "River Modeling System v4 - User Guide and Technical Reference." Report No. WR28-1-590-164; TVA River System Operations and Environment, Norris, Tennessee; May.

Jeffres, C. (2012, Pers Comm.). UC Davis Center for Watershed Sciences, Staff Research Associate. 5/29/2012.
Jeffres, C., and Moyle, P. (2012). "When Good Fish Make Bad Decisions: Coho Salmon in an Ecological Trap." *North American Journal of Fisheries Management*, 32, 87-92.
Louie, P. W. F., Yeh, W. W. G., and Hsu, N. S. (1984). "Multiobjective Water-Resources Management Planning." *Journal of Water Resources Planning and Management-Asce*, 110(1), 39-56.
Lund, J. R., Hanak, E., Fleenor, W., Bennett, W., Howitt, R., and Moyle, P. (2008). "Comparing Futures for the Sacramento-San Joaquin Delta." Public Policy Institute of California.
Lund, J. R., Hanak, E., Fleenor, W., Howitt, R., Mount, J., and Moyle, P. (2007). "Envisioning Futures for the Sacramento-San Joaquin River Delta." Public Policy Institute of California, San Francisco, California.
Null, S. (2008). "Improving Managed Environmental Water Use: Shasta River Flow and Temperature Modeling," University of California, Davis.
Null, S. E., Deas, M. L., and Lund, J. R. (2010). "Flow and Water Temperature Simulation for Habitat Restoration in the Shasta River, California." *River Research and Applications*, 26(6), 663-681.
Null, S. E., and Lund, J. R. (2011). "Fish Habitat Optimization to Prioritize River Restoration Decisions." *River Research and Applications*, 28(9), 1378-1393.
Olivares, M. A. (2008). "Optimal Hydropower Reservoir Operation with Environmental Requirements," University of California, Davis, Davis.
Peralta, R. C., Cantiller, R. R. A., and Terry, J. E. (1995). "Optimal Large-Scale Conjunctive Water-Use Planning - Case-Study." *Journal of Water Resources Planning and Management-Asce*, 121(6), 471-478.
Pulido-Velazquez, M., Andreu, J., and Sahuquillo, A. (2006). "Economic optimization of conjunctive use of surface water and groundwater at the basin scale." *Journal of Water Resources Planning and Management-Asce*, 132(6), 454-467.
Rheinheimer, D. E. (2011). "Modeling Multi-Reservoir Hydropower Systems in the Sierra Nevada with Environmental Requirements and Climate Warming," University of California, Davis, Davis.
Taniguchi, M., Williamson, D. R., and Peck, A. J. (1998). "Estimations of surface temperature and subsurface heat flux following forest removal in the south-west of Western Australia." *Hydrological Processes*, 12(13-14), 2205-2216.
Worthington, V. E., Burt, O. R., and Brustkern, R. L. (1985). "Optimal Management of a Confined Groundwater System." *Journal of Environmental Economics and Management*, 12, 229-245.
Yang, C. C., Chang, L. C., Chen, C. S., and Yeh, M. S. (2009). "Multi-objective Planning for Conjunctive Use of Surface and Subsurface Water Using Genetic Algorithm and Dynamics Programming." *Water Resources Management*, 23(3), 417-437.
Yeh, W. W. G. (1992). "Systems-Analysis in Groundwater Planning and Management." *Journal of Water Resources Planning and Management-Asce*, 118(3), 224-237.
Yu, W., and Haimes, Y. Y. (1974). "Multilevel Optimization for Conjunctive use of Groundwater and Surface Water." *Water Resources Research*, 10(4), 625-636.

Chapter 5: Conclusions

Creative management strategies are needed to stretch limited water resources among agricultural, urban, and increasingly complex environmental demands. Although treated as separate supplies by California water law, groundwater and surface water should often be managed for both human needs and the environment as an interconnected and interrelated resource. A change in one system often affects the other, in predictable or sometimes unforeseen ways. Modeling approaches that include surface water and groundwater supplies and dynamics support comprehensive resource management. Likewise, when managing water resources for ecosystem health and environmental purposes, incorporating flow and temperature into modeling and objectives is important. More fully incorporating all these aspects into management models strengthens the analysis and provides a more complete framework from which to evaluate alternatives and assess tradeoffs.

Simulation and optimization modeling for this research is applied to the Shasta Valley in Northern California, dominated by a largely unexplored volcanic, spring aquifer system characteristic of Cascade hydrogeology. Outcomes of the study include 1) a recalibrated stream temperature model using Distributed Temperature Sensing (DTS) data, 2) a numerical groundwater simulation model of the Pluto's Cave basalt and Parks Creek valley areas, and 3) a management model optimizing stream temperatures for salmon habitat while penalizing water shortages to agriculture and meeting physical constraints.

Several methodological and case study-specific conclusions result from this research:

Methodological conclusions

- River temperature datasets using DTS technology have high value for improving model performance and development by providing high resolution data for calibration and helping to identify mixing zones and in-stream thermal complexities to aide node placement and frequency.
- DTS data can be used to post-process existing modeled stream temperature results to capture a more realistic range of variability in stream temperature.
- High resolution DTS data reveals strengths and weaknesses of the heat budget approach in stream temperature modeling and can help refine our understanding of processes governing stream temperature heat budgets. Future work should further explore representation of solar radiation and air temperature in physically-based temperature models.
- Developing a groundwater model, even using a continuous porous media approach in a complex fracture flow system, helps organize and quantify the conceptual model and major flow paths providing a valuable framework for resource management discussions and advancing the understanding of system dynamics.
- In a largely unexplored and un-modeled system, groundwater modeling provides more details and insights than aquifer mass balance analysis since system interconnectedness can be evaluated and assumptions tested or adjusted.
- A novel approach to managing surface and groundwater resources conjunctively for stream temperatures is developed and tradeoffs explored.
- Minimizing the difference between calculated stream temperature and a target temperature such that the difference is negative and benefits the objective function is effective in reducing night time temperatures. An upper bound constraint on temperature ensures that maximum temperatures are below the target temperature.
- A regression-based model with inputs of flow, air temperature, and solar radiation captures hourly downstream heating/cooling well and is easily incorporated into an optimization framework to explicitly optimize stream temperature and build it into the objective function. This approach could have wide application.
- When sources in a supply portfolio have varying temperatures, their timing of use or release can significantly affect stream temperature. Strategic and optimized operations can effectively reduce stream temperature conditions in some cases.

Case study conclusions

- DTS data from the Shasta River is useful for identifying and measuring temperature effects of unmapped and un-quantified inflows (either tail water or groundwater springs/seeps).
- Small groundwater seeps along the mainstem Shasta River in the reach between Parks Creek and Big Springs Creek confluence have relatively constant temperature (14.4 and 15.2^{o}C for the two measured), but do not contribute enough flow to significantly affect mainstem temperatures.
- Parks Creek Overflow, thought to be mostly tail water from irrigation, creates a mixing zone in the mainstem with greater thermal variability and complexity.
- The steady state groundwater model advances the understanding of Shasta Valley hydrogeology and groundwater dynamics.
- Optimization results suggest stream temperatures in the Shasta River just above its confluence with Parks Creek could be significantly improved by reoperation of reservoir releases and use of groundwater pumping as a cool water input.
- Improved Shasta River temperature occurs at the cost of irrigation deliveries because a high fraction of water diverted returns to the river as warm tail water (low irrigation efficiency). The shortage cost can be significantly reduced by improving irrigation efficiency and strategically managing warm tail water returns to the river.
- If there is landowner interest and support for reoperation and improved irrigation efficiency efforts to benefit stream temperatures, additional investigation should assess the connection between groundwater pumping and river flow. Improved understanding of tail water timing and temperature from the Hole in the Ground fields should also be incorporated into the optimization.

Appendix A

This appendix follows up on some ideas and feedback received at a discussion at UC Davis in October 2012 with several people who have done considerable work (hydrology, geology, and/or biology related) in the Shasta Valley system. A general consensus revolved around the model boundary conditions: recharge from Mount Shasta seemed low, flux across the northern boundary for the MODERATE model realization seemed too large and likely some of the flow across the northern border in the MODERATE scenario is more likely to come from the east side instead. This appendix therefore evaluates PRISM data for additional zones around the southern and eastern areas of the model domain to estimate potential for additional recharge and changes the northern and eastern borders to fixed flux boundaries. Initial model calibration and results are presented.

Additional recharge estimated

Additional zones were delineated in ArcMap to the south and east of the model domain as a means of estimating potential additional recharge across these model boundaries. Figure 43 shows these zones with the associated estimate of potential recharge volume (MCM). It appears that even just a portion of zone 2 to the west of the original Mount Shasta recharge zone could contribute significant additional flow to the groundwater system represented in the model domain. Recharge estimates were made using a similar method as described in Chapter 3. PRISM data was used to estimate precipitation in these areas and GAP data was used to assign percentage of ground cover to different ecosystem types in order to assign native vegetation evapotranspiration (ET) rates from ECOWAT results. Total recharge was then estimated as the difference between the precipitation volume and ET volume (Table 38). Unlike the Mount Shasta recharge estimation (zone 0), sublimation was not accounted for in these additional zones since much of this area may receive precipitation primarily as rain rather than snow. Future analysis could delineate predominant snowfall areas from rainfall areas to tighten the estimation, but this analysis was done as a preliminary look at the potential for additional recharge from these surrounding areas. Results suggest that it could be significant.

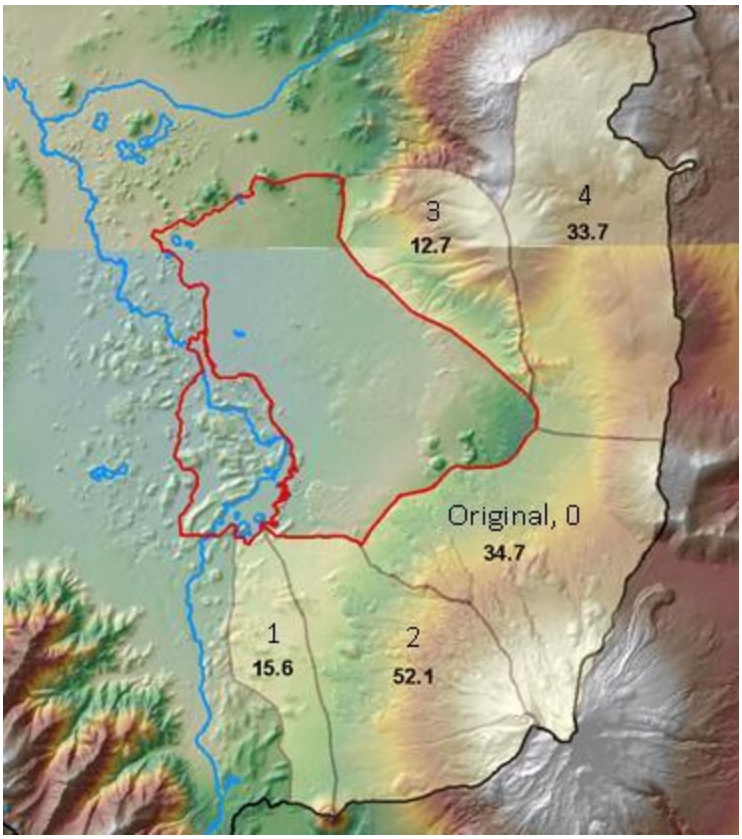

Figure 43. Additional recharge zones (1-4) with labeled estimated recharge volume (MCM) for 2008.

Table 38. Estimated precipitation, evapotranspiration (ET) and resulting recharge from additional recharge zones in million cubic meters (MCM)

Recharge Zone	PPT Vol (MCM)				ET Vol (MCM)				Recharge Vol (MCM)			
	2008	2009	2010	2011	2008	2009	2010	2011	2008	2009	2010	2011
Original - 0	98.6	110.9	128.8	151.2	32.5	31.7	35.6	37.3	34.7	43.2	52.2	66.7
1	23.6	26.0	30.2	35.9	8.0	8.2	8.9	9.1	15.6	17.8	21.3	26.8
2	82.1	99.2	121.0	130.8	30.0	29.7	33.0	34.5	52.1	69.6	88.1	96.2
3	32.7	28.6	30.1	43.2	20.0	20.1	22.1	22.8	12.7	8.5	8.0	20.4
4	76.1	65.6	70.4	100.2	42.5	41.5	46.5	49.1	33.7	24.1	24.0	51.1

Northern boundary revisited

Instead of a general head boundary, the northern model boundary was changed to be a fixed flux boundary. The flux was estimated for each model element along the boundary using the following equation:

$$Q\left(\frac{m^3}{yr}\right) = b\ (m) * w(m) * K\left(\frac{m}{yr}\right) * grad\ h\ (\frac{m}{m}) \quad \text{Equation A.1}$$

where **Q** is the volume flow rate (model input)

b is the aquifer thickness calculated as the difference between the model's bottom elevation and resulting head from the MODERATE model realization

w is the width of the model element (100 meters)

K is the effective hydraulic conductivity
grad h is a gradient estimated from Mack (1960) wells north and south of the boundary

Gradients from three well pairs were assigned to model elements. These gradients ranged from -0.002 to -0.004 m/m across the northern portion of the boundary and 0.003 m/m for the short segment along the western border in the far northwest corner of the model domain. This calculation results in almost 16.04 MCM inflow across the northern boundary and 16.41 MCM outflow to the west. This magnitude and net outflow is likely more realistic than the 49.34 MCM northern boundary flow in the MODERATE realization results.

Also noteworthy is an apparent groundwater divide between the model's northern boundary and the Little Shasta River. The northern boundary remains a considerable source of uncertainty. Additional groundwater level data from this area would be useful for better understanding and representing groundwater dynamics.

Eastern boundary revisited

Originally the eastern boundary was assumed to be a no flow boundary. From the subsequent discussion of results, the northern boundary was deemed unlikely to provide the high inflows (49.34 MCM magnitude) seemingly required by the model for calibration and to produce reasonable spring flow volumes from the Big Springs complex. As a result, recharge from the eastern boundary is a more reasonable source of this boundary inflow. Evaluation of PRISM data and estimated ET suggests that about 46.4 MCM could potentially recharge from the eastern side (water year 2008).

Flow across this boundary was also estimated using a similar approach as was done for the fixed flux northern boundary (Equation A.1). A range of gradients were estimated from the dashed contour lines on Mack's (1960) contour map, -0.03 to 0.008 m/m. A gradient of 0.007 m/m was used with the aquifer thickness, again calculated using the bottom elevation and MODERATE model head results for elements along the border. The calculated inflow (m^3/yr) volume from all elements along this border using calibrated K values from the MODERATE realization amounts to about 191.19 MCM. This recharge inflow is significantly greater than the PRISM estimate. It seems unlikely that the flow from the east would be that large, however additional data and investigation should be conducted to better clarify the role of this boundary. For additional groundwater modeling, an 'injection' rate corresponding to the PRISM estimate (46.4 MCM) was used as input for the new eastern fixed flux boundary.

Additional modeling, initial calibration, and results

New boundary conditions (fixed flux) for the northern and eastern borders of the model domain were input to the MODERATE realization version of the groundwater model. Also the southern fixed flux boundary representing Mount Shasta recharge was extended to the west (increased to 198 boundary wells from 154) and the total volume of Mount Shasta recharge was increased to 61.67 MCM to reflect feedback from the expert discussion suggesting this recharge source should be closer to 75% of the total Big Springs complex volume (73-95 MCM). Recharge estimates for areas west of the originally defined Mount Shasta recharge zone (Figure 43) suggest this increase is reasonable for initial exploration and recalibration.

The model was run with these new boundary conditions but the same MODERATE calibrated values for the K zones. This model results in reasonable spring flows (Table 41) but lots of flooding in the southeast area of the model domain (Figure 44A). Adjustments were then made to the K zone values to improve calibration of groundwater elevations with their target water surface elevation. The resulting Ks are compared to MODERATE realization K values in Table 39.

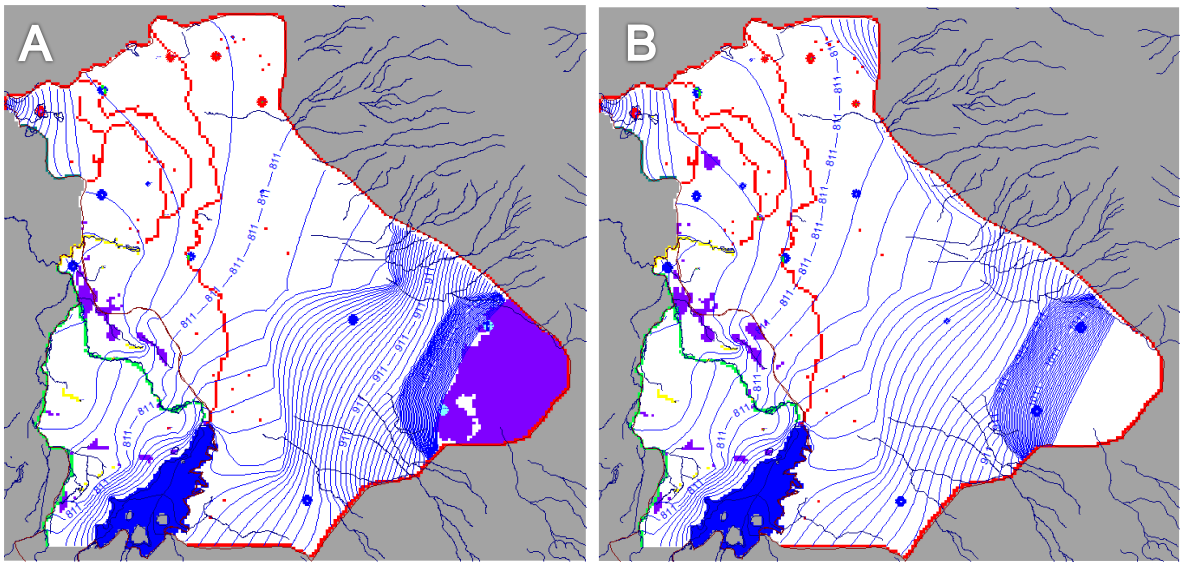

Figure 44. Same K zones as original calibration (Figure 20). New fixed flux boundaries on the northern and eastern boundaries and increased flux from the Mount Shasta Recharge zone (southern boundary, also extended). Figure A shows results with calibrated K values from the MODERATE realization; B results from newly calibrated K values. Purple cells are flooded, i.e. head is above the ground surface elevation. Blue and Red circles are targets, color and size indicative of residual.

Table 39. Hydraulic Conductivity (K) in meters per day for new model runs

Zone	Geology	MODERATE Ks	New Ks
1	Tertiary Volcanic (Debris flow)	1.6	1.6
2	Recent Volcanic (Pluto's)	178	123
3	Alluvium	49	49
4	S.W. debris/alluv	16	16
5	S.E. Pluto's North	4.1	9.6
6	N.W. Pluto's	8.2	8.2
7	S.E. Pluto's South	0.41	0.68
8	N.E. Volcanic	205	4.1

This preliminary calibration also results in reduced residuals and improved calibration statistics (Table 40). The root mean square error of the calibrated new model run is 14 compared to 35 meters.

Table 40. Calibration statistics and residuals for new runs (meters)

Target (m)	MODERATE Ks	New Ks
44N05W21H001M	-12	-14
Big Springs Lake	0	0
M43N04W26	-114	-36
M43N04W16	-18	-6
M43N04W13	-97	-13
43N05W11A001M	-8	-11
43N05W02C002M	-2	-4
44N05W34H001M	-4	-6

44N05W14M002M	0	-3
M42N04W05	-22	-14
M44N04W19	12	7
M44N04W31	-3	-8
M44N05W14	10	7
M44N05W13	15	11
Seldom Seen Well	0	0
NW springfed lake	12	11
TNC Border Field M	-28	-29
TNC Rock House	-26	-26
Little Springs	1	1
Calibration Statistics (m)		
RMS Error	35	14
Residual Mean	-14	-6
Res. Std. Dev.	32	12
Sum of Squares	25,503	4,005
Abs. Res. Mean	18	10
Min. Residual	-114	-36
Max. Residual	15	11
Range	253	253

The calibrated model has improved residuals and calibration statistics, and the spring flow results of the two new model runs are similar (Table 41). The major difference is a reduction in flow from Big Springs Creek in the calibrated model compared to the un-calibrated new model run: about 52.6 MCM compared to 65.5 MCM. This results primarily from the reduced K value for zone 2, the Pluto's Cave basalt.

Table 41. Annual spring flow results for new model runs (MCM)

	WY 2008 Flow Volume (MCM)		
Target Name	**Target**	**MODERATE Ks**	**New Ks**
Big Springs Lake	-37.0	-26.0	-26.1
Big Springs Creek	-58.0	-65.5	-52.6
Alcove Springs		0.0	0.0
Little Springs	-6.2	0.0	0.0
Hole in the Ground	-4.9	-4.3	-4.7
Clear Spring	-1.9	-0.8	-0.8
Hidden Valley Spring	-1.1	-5.2	-5.6
Kettle Springs	-6.2	-3.7	-3.7
Black Meadow Springs	-0.7	-0.9	-0.9
Bridge Field Springs, N. and S	-2.8	-3.1	-3.1
NW Springfed Lakes	< 1.2	0.0	0.0
Mack Spring	0.0	-2.6	-2.6

After initial calibration of the new model, the adjusted K values were used in Equation A.1 to re-estimate flow across the eastern boundary. Summing across the entire border amounts to 28.1 MCM, compared

to 191.2 MCM as originally estimated with MODERATE model Ks. This new estimate is much closer to the estimate made using PRISM data, 46.4 MCM. The greatest factor in this change was the reduction of K zone 7 from 205 m/d to 4 m/d. This K value could be further calibrated to yield boundary flows closer to the PRISM estimates. This approach is useful for exploring the reasonable range of K values for these zones.

This additional modeling with initial calibration and results demonstrates that these new boundary conditions produce reasonable results for spring flow and groundwater levels. However, additional recharge from Mount Shasta raises the head south of Lake Shastina and results in reduced lake leakage, 11.4 MCM compared to its target of 37.0 MCM. Additional data and calibration could further improve this representation. Even so, recalibrated K values better reflect reasonable flows estimated as a function of head gradients across the eastern boundary. Using Equation A.1 as a means for estimating boundary flows is a useful approach for better quantifying flows across borders that have significant uncertainty associated with them and testing the reasonableness of calibrated K values.

Additional work remains to further develop this groundwater model. However, the development thus far provides a tool for testing and adjusting our conceptual model of the system and exploring groundwater dynamics. This was evident in the discussion in Davis in October 2012 and the subsequent analysis presented here.

References

Mack, S. (1960). "Geology and ground-water features of Shasta Valley, Siskiyou County California." California Division of Water Resources.